STRIKE COMPARISON OF THE COMPOSITIONAL VARIATIONS OF THE LOWER GROUP AND MIDDLE GROUP CHROMITITE SEAMS OF THE CRITICAL ZONE, WESTERN BUSHVELD COMPLEX.

by

H. L. Doig B.Sc. (Hons.) (Rhodes)

Thesis is submitted in partial fulfilment of the requirements for the degree of

MASTER OF SCIENCE
(Economic Geology)

Department of Geology
Rhodes University
P O Box 94
Grahamstown 6140
South Africa

2000

ABSTRACT

The variations in the composition, specifically the Cr_2O_3 content and the Cr:Fe ratio, and the morphology of the Lower Group (LG) and Middle Group (MG) chromitite seams of the Critical Zone (CZ) across the western Bushveld Complex, including the Ruighoek and Brits sections, is investigated by means of whole-rock chemical data, both major and trace elements analysis, XRD and electron microprobe data. As a result of the paucity of exposed or developed LG1 - LG5 chromitite seams in the western Bushveld Complex, this study is confined to the investigation of the compositional variations of the LG6 to MG4 chromitite seams. In only one section, the Ruighoek section, was the entire succession of chromitite seams, from the LG1 - MG4, exposed.

The silicate host rocks from the LG6 pyroxenite footwall to the collar of the CC2 drillcore (lower uCZ) in the Rustenburg section were sampled. This study reviews the compositional trends of the silicate host rocks, as the compositional variations of the chromitite seams reflect the chemical evolution of the host cumulate environment and, to a lesser degree, the composition of the interstitial mineral phases in the chromitite seams.

The compositional variations of the LG and MG chromitite seams are attributed to the compositional contrast between the replenishing magma and the resident magma. The chemical trends of the LG and MG chromitite layers and the host cumulate rocks do not support the existence of two compositionally dissimilar magmas in the CZ, rather the cyclic layering of the CZ and the chemical variations of the chromitite seams are attributed to the mixing of primitive magma with the resident magma, both of which have essentially similar compositions. The compositional variations of the LG and MG chromitite seams along strike away from the supposed feeder site (Union section) to the distal facies (Brits section) are attributed to the advanced compositional contrast between the resident magma and the replenishing primitive magma pulses.

The CZ is characterized by reversals in fractionation trends and this is attributed to the compositional evolution of the parental magma and not to the replenishment of the resident magma by influxes of grossly dissimilar magma compositions.

The Cr_2O_3 content and the Cr:Fe ratio of the MG chromitite layers increase from the Ruighoek (near proximal) section to the Brits section (distal facies). This is attributed to the advanced compositional contrasts between the resident magma and the replenishing primitive magma. In contrast, the Cr_2O_3 content and Cr:Fe ratios of the LG6 and LG6a chromitite seams decreases eastwards from the Ruighoek section. The average Cr:Fe ratio for the western Bushveld Complex is between 1.5 and 2.0, nonetheless, a progressively lower Cr:Fe ratio is noted from the LG1 chromitite up through to the MG4 chromitite seam in the Ruighoek section. In the LG2 - LG4 chromitite interval a deviation to higher ratios is encountered.

A progressive substitution of Cr by Al and Fe in the Cr-spinel crystal lattice characterizes the chromitite succession from the LG1 seam up through the chromitite succession to MG4. The petrogenesis of the chromitite seams of the CZ is attributed to magma mixing and fractional crystallization of a single magma type.

ACKNOWLEDGEMENTS

The author would like to thank the Council for Geoscience for the assistance, laboratory work and financial support over the period that the thesis was completed in. I would like to express my sincere gratitude to L.W. Schürmann and M.G.C. Wilson for their time spent editing the thesis. Grateful thanks to Prof. J.M. Moore and Prof. H.V. Eales for their review of the thesis and their assistance. I wish to thank Dr. M. du Toit and my colleagues at the Council for their time and inputs into this thesis. Gratitude is extended to the mining companies involved who allowed access to sample their mines and quarries. Finally, I would like to thank M. Prinsloo and R. Oosterhuis for the draughting of the maps and the figures.

DECLARATION

I January 2000

All work in this thesis is the original work of the writer except where specific acknowledgement is made to the work of others.

Signed: . . . . . .
H. L. Doig

Address: P O Box 8
Boksburg East
1478

CONTENTS

List of Figures

Tables

Appendices

1. Introduction

The Bushveld Complex, the largest layered mafic-ultramafic intrusion known, intruded the Kaapvaal Craton at ~ 2.06 - 2.05 Ga (Von Gruenewaldt *et al.*, 1985). The Complex is conventionally subdivided into the eastern, the western, the far western, the Bethal and the Potgietersrus lobes. The Bushveld Complex is host to extensive reserves and resources of chromium, platinum group metals, titanium and vanadium, to name the more important commodities. The chrome industry exploiting the western Bushveld Complex lobe is currently active and dynamic and it is for this reason that the geochemical characteristics of the chromitite seams of the Critical Zone (CZ) in this area are investigated. Regional sampling was undertaken in an effort to provide a representative database for the Lower Group (LG) and Middle Group (MG) chromitite seams in the western Bushveld Complex, and to search for a geochemical fingerprint for the identification of each seam. The petrogenesis and compositional variations of the chromitite seams across the western Bushveld Complex, specifically the Cr_2O_3 content and the Cr:Fe ratio, are investigated with the aim of identifying and correlating the compositional variations of the seams. The silicate host rocks of the CZ are reviewed, as an understanding of their chemical evolution will aid in the interpretation of the compositional variations found in the chromitite seams.

1.1. Location

The study area extends from the southwestern perimeter of the Pilanesberg Alkaline Complex through Rustenburg and further east towards Brits (fig. 1). The area has moderate relief and is rimmed by ridges of Magaliesberg and Rayton Formations and the prominent Pilanesberg Alkaline Complex has intruded in the north of the study area. The western Bushveld Complex was previously subdivided into various sections by Hatton and Von Gruenewaldt (1985) and their subdivisions will be retained in this study. The five sections are the Brits section in the east, followed by the Marikana, Rustenburg, Boshoek and, finally, the Ruighoek sections to the west. In this study, the Brits section extends from east of the Brits Graben (De Kroon 444 JQ) to Wolhuterskop (fig. 1); the Marikana section from Wolhuterskop westwards to the Spruitfontein Upfold; the Rustenburg section from the western margin of the Spruitfontein Upfold to the farm

Boekomhoutfontein 260 JQ; from where the Boshoek section extends to the Mahobieskraal Fault. The Ruighoek section falls between the Mahobieskraal Fault and the northwestern margin of the Pilanesberg Alkaline Complex.

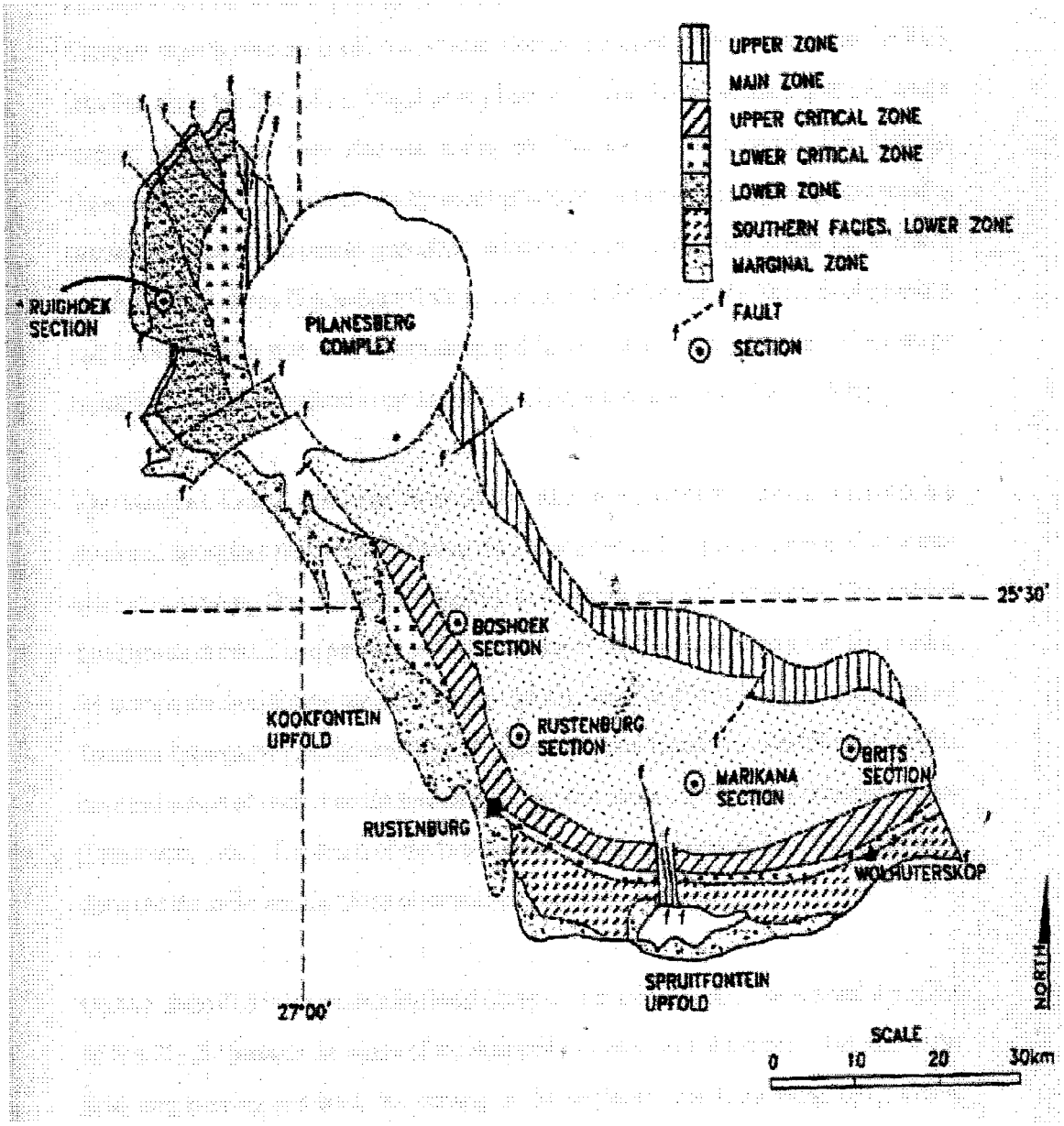

Fig. 1. The western lobe of the Bushveld Complex (modified after Hatton and Von Gruenewaldt, 1985, p 44).

1.2. Regional Geology

The Rustenburg Layered Suite (RLS), Lebowa Granite Suite and Rashoop Granophyre Suite comprise the Bushveld Complex which, in this study area, intruded the early Proterozoic Transvaal Supergroup volcanic and sedimentary rocks between the levels of the Magaliesberg Formation and the Rooiberg Group (SACS, 1980). The level at which the western Bushveld Complex actually intruded is still contentious. Cheney and Twist (1991) propose that the RLS intruded along the level of the Magaliesberg Formation, but that all indications of this gentle angular unconformity were removed during the injection of the magmas. The Rashoop Granophyre Suite, composed of homogeneous granophyre with associated granophyric granite, granophyre porphyry and pseudo-granophyre, is intrusive into the Rooiberg felsites and is in turn intruded by the Lebowa Granite Suite (LGS). The LGS is divided into the Nebo, Bobbejaankop and Lease Granites, with the Bobbejaankop and Lease Granites being the result of late-stage crystallization of differentiated magmas (SACS, 1980; SADC Excursion Guide, 1995).

The Marginal, Critical and Main Zones of the RLS in the western Bushveld Complex are developed throughout the Complex, whereas the Lower Zone (LZ) is poorly developed or absent west of Rustenburg (fig. 1), but developed in the Ruighoek area and northwards. The variable development of the LZ is in part due to the upwarping of the Transvaal Supergroup floor rocks, for example the Spruitfontein and Kookfontein Upfolds. The Complex is locally characterized by Transvaal Supergroup quartzite xenoliths and inliers. The Spruitfontein and Kookfontein Upfolds have had a marked control on the formation of the RLS zones and hence the chromitite seams (Schürmann, 1991). The origin of the two upfolds is poorly understood, but clearly they have disrupted the strike and dip of the chromitite and cumulate succession.

Outcrop of the RLS in the western Bushveld Complex is extremely poor. The regional dip of the RLS is 8° - 20° towards the centre of the Bushveld Complex, with the strike of the RLS in the Brits area trending east-west, but curving to the northwest near Rustenburg, being almost northwest - southeast between Rustenburg and the Pilanesberg Alkaline Complex. In general, the dips flatten with depth and are on average 2°steeper at surface. This is believed to be the result of unburdening (Schürmann, pers. comm.) The strike and dip of the layering varies in the vicinity

of the upfolds. The LG and MG chromitite seams often display a gentle warping, not dissimilar to a sinusoidal wave, formed during the crystallization of the RLS.

Pre-Bushveld sills, related to subsidence of the Transvaal Basin, intruded the Transvaal Supergroup and are now largely altered to amphibolitic compositions. The syn-Bushveld unaltered mafic sills are thought to represent offshoots of the parental magma and have compositions varying from peridotites to quenched micropyroxenites (LZ and CZ) and gabbros (upper Critical Zone and Main Zone). Prominent syenitic dykes radiate from the Pilanesberg Alkaline Complex and dykes of related composition and age cross-cut the RLS in the entire western Bushveld Complex (Von Gruenewaldt *et al.*, 1985). Transgressive iron rich pegmatoidal bodies occur in both the eastern and western lobes of the Bushveld Complex. These postcumulus bodies do not usually contain economic mineralization, an exception being the Kennedy's Vale body in the Eastern Bushveld lobe, but introduce problems in mining the laterally otherwise consistent orebodies (SADC Excursion Guide, 1995).

1.3 Emplacement of the Bushveld Igneous Complex

The Bushveld Complex has previously been suggested by Hall (1932) and Irvine *et al*, (1983) to have intruded as a lopolith and by Molengraff (1901) and Mellor (1906) to have intruded as a laccolith or a series of small laccoliths (Eales *et al.*, 1993b). The lopolith and laccolith models are no longer subscribed to, as there is a lack of geophysical evidence to support such theories. Such theories as a meteorite impact (Hamilton, 1977), the result of an underlying hot spot, that the Bushveld Complex overlies a spreading centre (Van Biljon, 1979), and rising mantle diapirism (Sharpe *et al.*, 1981; Hartzer, 1994) have been suggested to explain the emplacement of the Bushveld Complex. The factors which resulted in the intrusion of the Bushveld Complex, the stratigraphic position and, the laterally persistent silicate, chromitite and platinum-bearing layers is still highly hypothesized.

Sharpe and Snyman (1980) propose the multiple intrusion of the magmas into more than one compartment and the overlapping of three conical chambers. An elaboration of this model is presented in Sharpe *et al*, (1981), and the pertinent facts are summarized below.

Sharpe *et al,* (1981) propose that the Bushveld Complex feeder zones and satellite intrusive bodies, for example the Uitkomst Complex, are located along two concentric elliptical traces (fig.2), the product of large-scale conical fractures. Seven feeder sites, indicated by seven high Bouger anomalies, are proposed, with two postulated feeder zones in both the western and eastern Bushveld lobes. The ellipses were controlled by the regional strain of the basement rocks and are located along the Bushveld-Great Dyke lineament and are suggested to approximate the original extent of the Transvaal Basin.

The fractures acted as the magma conduits to the shallow, inverted, right conical magma chambers that lay at their apices (Sharpe *et al.*, 1981). Rising mantle diapirism at the base of the crust is the proposed mechanism for the fracturing of the crust into elliptical fracture traces. Upward migrating diapirism could result in high pore fluid pressure and confining pressure. The subsequent release of volatiles could have resulted in shock fronts, forming conical fractures which filled with magma. A schematic representation of the mantle diapirism and formation of the Bushveld magma chambers is shown in fig. 3.

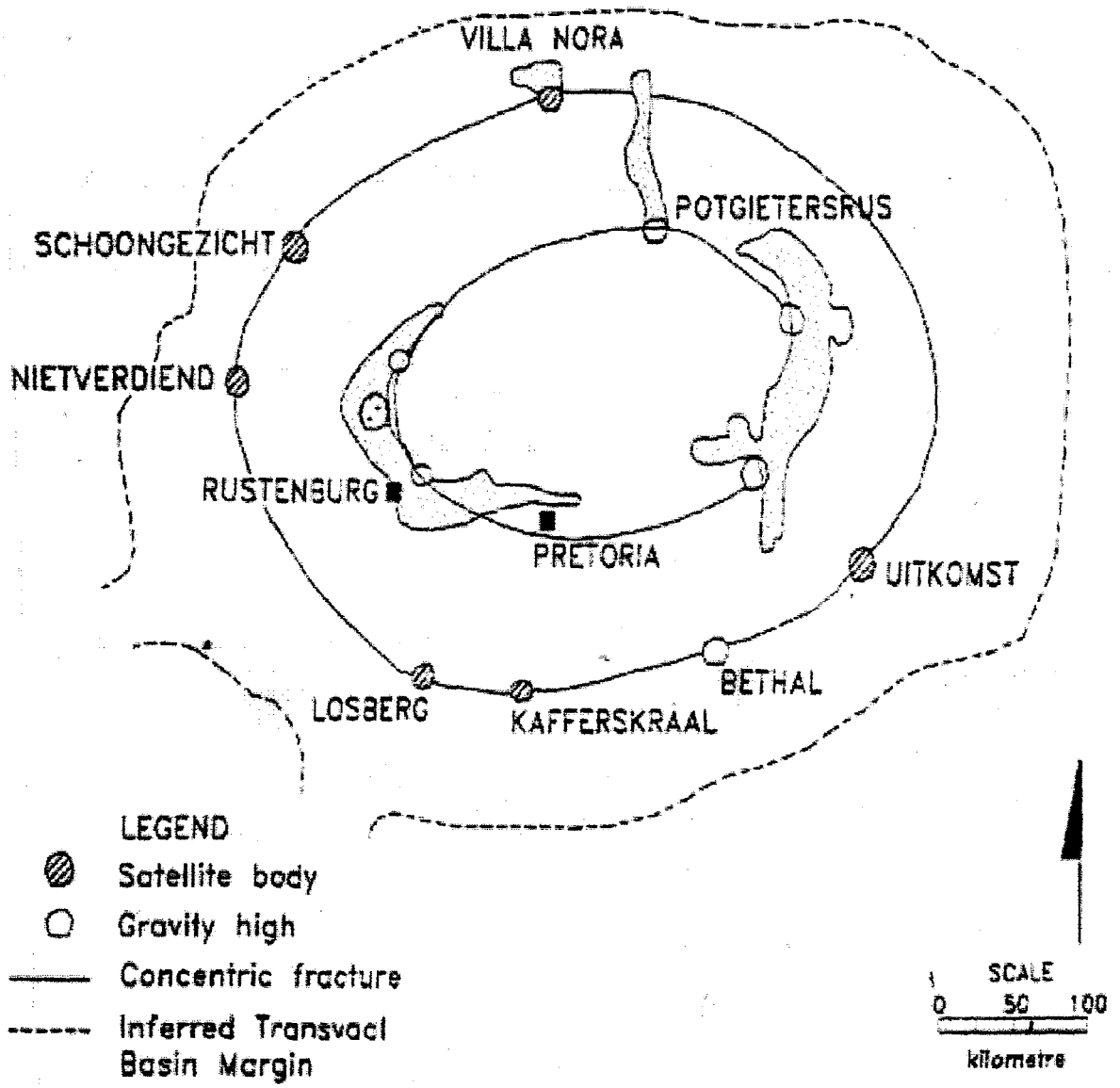

Fig. 2. The concentric elliptical traces, position of the Bushveld lobes and satellite intrusions, and the inferred original extent of the Transvaal Basin (after Sharpe *et al.*, 1981, p 241).

Intrusion of the pre-Bushveld mafic sills and the emplacement of the basaltic (Dullstroom) and acidic (Rooiberg) volcanics at the close of the Transvaal Basin sedimentation, were the precursor indications of the pending intrusion of the Bushveld Complex (Vermaak and Von Gruenewaldt, 1981). The mechanisms which resulted in the intrusion of the Bushveld magmas were elevated geothermal gradients, fluid pore pressures and confining pressures (Sharpe *et al.*, 1981).

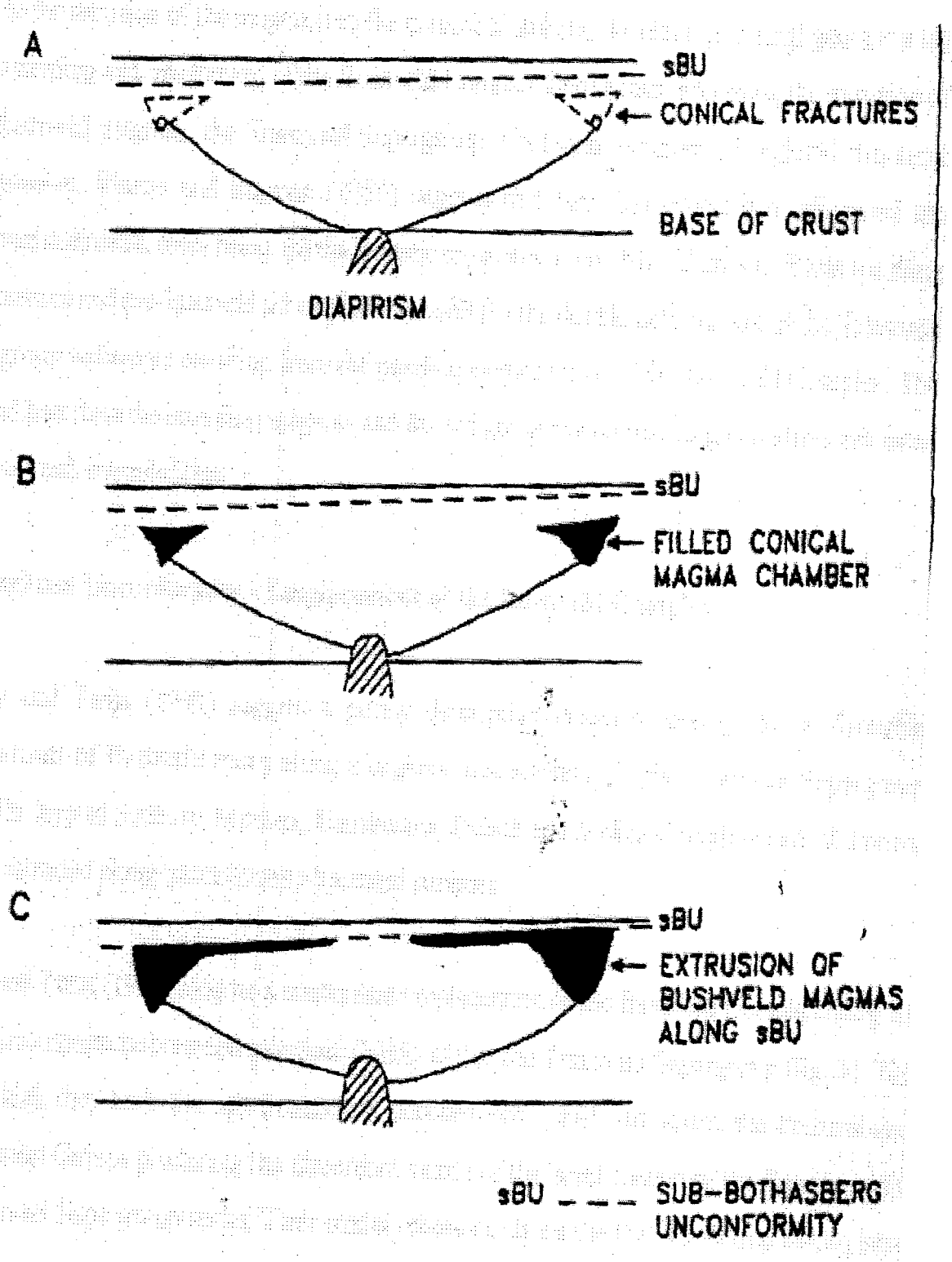

Fig. 3. Proposed mechanism for the genesis of the Bushveld Igneous Complex (modified after Sharpe *et al.*, 1981, p 243).

Vermaak and Von Gruenewaldt (1981) propose that the feeder zones resulted in the formation of three large magma chambers, these being the western, the eastern, and the northern Bushveld lobes and the continuous supply of heat from successive magma influxes resulted in continual replenishment of heat lost to the country rocks.

Prior to the intrusion of the magma into the conical chambers, the elevated crustal geotherm led to the warping and up-doming of the Bushveld Complex floor rocks. Preceding the intrusion of the Bushveld magmas, the Transvaal Supergroup lithologies experienced regional structural deformation. Sharpe and Snyman (1980) suggest that two fold events had influenced the Transvaal sediments, these being: (a) the isostatic re-equilibration of the Transvaal Basin resulting in subsidence and pre-Bushveld sill emplacement and (b) the ductile deformation of the Transvaal Supergroup sediments resulting from the pending emplacement of the Bushveld Complex. The elevated heat from the intruding magmas and the weight of the crystallizing cumulates enhanced the floor-rock irregularities.

1.4. Regional Unconformity - Emplacement of the Bushveld Complex

Cheney and Twist (1991) suggest a purely descriptive model proposing the conformable emplacement of Bushveld rocks along a regional unconformity in the Transvaal Supergroup rocks. The layered Sudbury, Muskox, Usushwana, Duluth and Mellen Complexes are all known to have intruded along unconformity-bounded surfaces.

Cheney and Twist (1991) propose a concordant emplacement of the Bushveld Complex along an angular unconformity-bounded sequence (UBS) within the Transvaal Supergroup (fig. 3). The UBS, which they term the sub-Bothasberg unconformity (sBU), truncated the Pretoria and Chuniespoort Groups producing the discordant nature of the basal contact of the Complex with the Transvaal Supergroup rocks. Their model relies heavily on the Pretoria Group having been laterally more persistent on a regional scale, than it is at present. Cheney and Twist (1991) suggest that as a result of the sBU, the northern, southern and western Bushveld magmas intruded at stratigraphically lower levels than in the eastern Bushveld Complex.

1.5. Stratigraphic Subdivision of the Rustenburg Layered Suite

1.5.1. The Marginal Zone

The Marginal Zone, or Kolobeng Norite, represents the basal or chilled margin of the RLS in the western Bushveld Complex and comprises orthopyroxene, plagioclase, ample clinopyroxene, quartz, and accessory biotite and magnetite (SACS, 1980). Worst (1993) reports that the Marginal Zone is well developed in the area between Mooinooi village and Huttenhof and extends approximately 7 km north from the Magaliesberg Quartzite and bulges northwards from the Magaliesberg Quartzite contact in the vicinity of Buffelspoort Dam. The strike of the remainder of the RLS curves around the bulge. Between the town of Rustenburg and the area south of the Pilanesberg Alkaline Complex, the Kolobeng Norite is suggested to have incorporated numerous quartzite xenoliths of the Magaliesberg Formation. Assimilation of the country rock quartzite contaminated the magma resulting in the crystallization of a quartz-noritic rock. The quartz-norite is fine-grained with sub-ophitic textures and is composed chiefly of plagioclase, orthopyroxene, clinopyroxene, quartz and amphibole. Quartz constitutes approximately 20 % of the mode, as does amphibole, whereas clinopyroxene and biotite are accessory (Worst, 1993). The composition of the quartz-norite is not homogeneously developed throughout the Marginal Zone, but varies between quartz-norite to pyroxene-rich norite to quartz-gabbro. It is not developed everywhere and may locally lie in direct contact with the ICZ (Worst, 1993).

1.5.2. The Lower Zone

The Lower Zone (LZ), comprised of the Eerlyk Bronzite, Makgope Bronzite, Groenfontein Harzburgite and the Tweelaagte Bronzite Formations (fig. 4), consists of alternating pyroxenite, bronzite and harzburgite layers with a total thickness of 940 metres (SACS, 1980). The LZ is not developed throughout the entire study area - for example, west of Rustenburg it is either poorly exposed, absent or does not outcrop. It is the most inconsistently developed zone of the Bushveld Complex due mainly to the irregular floor topography of the complex. Numerous xenoliths of the Rayton and Magaliesberg Formations occur in the LZ and a northward bulge of the Marginal Zone norites interrupts the LZ between the farms Kafferskraal 342 JQ and Zuurplaats 341 JQ in the Rustenburg and Marikana sections (Worst, 1993).

1.5.3. The Critical Zone

The Critical Zone (CZ) concordantly overlies the LZ lithologies. In type section the CZ is 850 - 1000 metres thick and subdivided into the Ruighoek Pyroxenite and the Mathlagame Norite-Anorthosite units (fig. 4) (SACS, 1980). Informally, the CZ is subdivided into the lower CZ (lCZ) and the upper CZ (uCZ), with the boundary between the two zones being located between the MG2 and MG3 chromitite seams, at the base of an anorthosite marker which is, however, not developed throughout the western Bushveld Complex. The Ruighoek Pyroxenite, or lCZ, consists of feldspathic pyroxenite with numerous chromitite layers. The Mathlagame Norite-Anorthosite comprises alternating melanorites and leuconorites, spotted and mottled anorthosite, pyroxenite, and chromitite. The mineralogical boundary between the two units of the CZ does not apply to the eastern portion of the western Bushveld Complex, where abundant cumulus plagioclase crystallized in the lCZ. The well-known MG4, UG1, UG2 seams and the Merensky Reef are found in the Mathlagame unit and the giant mottled anorthosite of the Bastard cyclic unit forms the top of this unit (SACS, 1980).

The lCZ contains on average twelve chromitite seams, the LG1 to LG7 chromitite seams and the MG0 to MG3 chromitite seams. The chromitite seams of the lCZ are typically hosted by feldspathic pyroxenites and have either sharp or gradational contacts with the pyroxenite. The uCZ contains five to six chromitite layers, the MG4 and UG chromitite seams. No norite inclusions have been reported in the anorthositic units of the uCZ and the anorthosite grades into norite with the upward increase in pyroxene content (Worst, 1993).

The CZ chromitite layers thicken/thin, bifurcate, coalesce and vary in composition, specifically Cr_2O_3 and Al_2O_3 content and Cr:Fe ratio both along strike and up the stratigraphic column. The individual chromitite layers vary in thickness from a few centimetres to over 1.5 metres. Thin chromitite layers and stringers, usually in the order of a few millimetres, are often hosted by the hanging wall lithologies and, to a lesser extent, in the footwall lithologies of the chromitite seams.

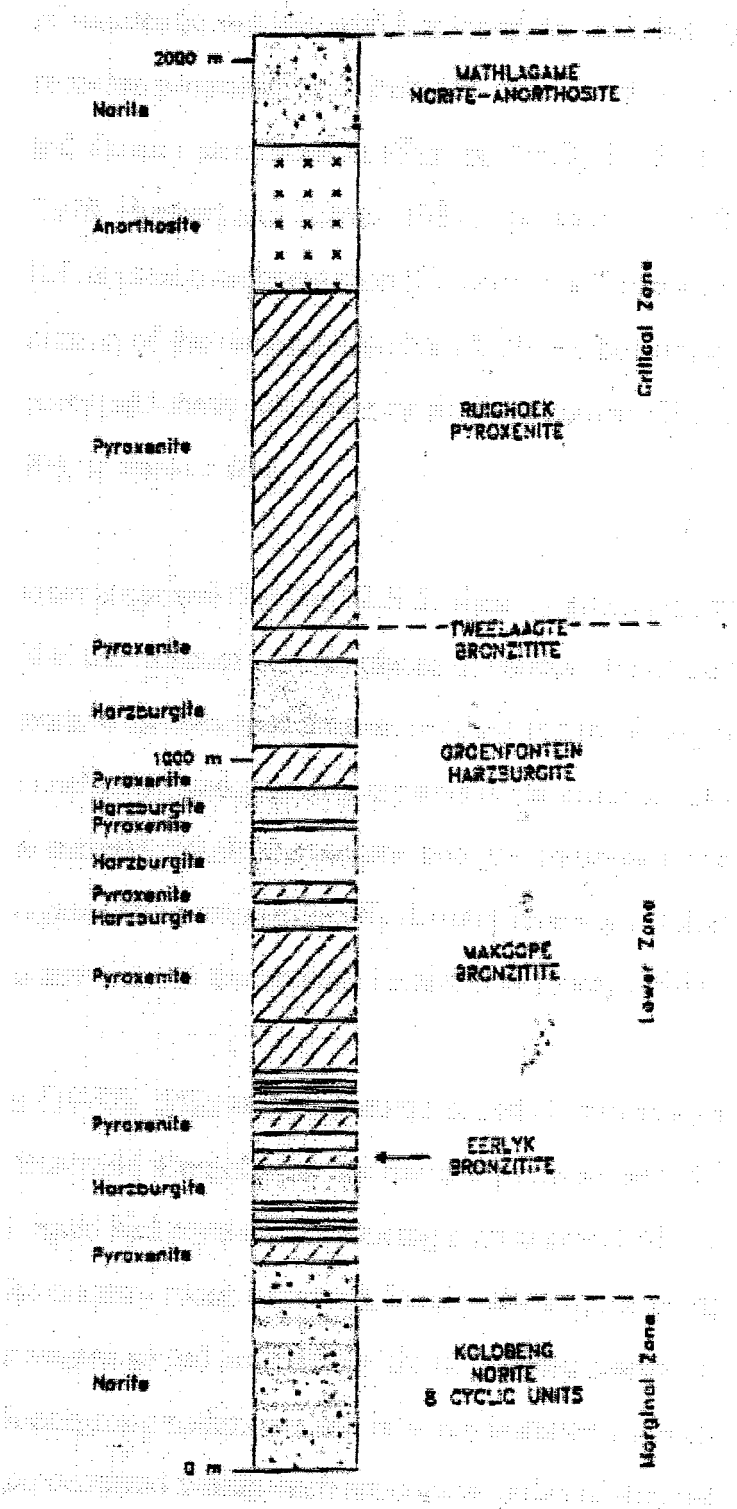

Fig. 4. Lithostratigraphy of the lower portion of the RLS, western Bushveld Complex (SACS, 1980, p 241).

1.6. Literature Review - Magmatic Models

The origin of the cyclic layering and associated wealth of mineralization in the Bushveld Complex has led to a number of magmatic models which attempt to decipher the petrogenesis of the Bushveld Complex. Processes proposed have included differentiation (Wagner, 1924), double-diffusive convection and density stratification (Turner, 1973, 1985; Turner and Chen, 1974; Turner and Gustafson, 1978; Huppert and Turner, 1981; Sparks *et al.*, 1984), magmatic currents combined with differential magmatic sedimentation (Cameron and Emerson, 1959), crystal settling resulting in the differentiation of the magma (Lombaard, 1934), bottom growth (Jackson, 1961, 1970), and mixing of compositionally dissimilar or similar magmas (Hatton, 1988, Irvine *et al.*, 1983; Eales *et al.*, 1990), to name a few.

In 1968, Wager and Brown proposed that the RLS formed by gravity-controlled crystal settling. They further proposed that the magmas were emplaced at various stages during the crystallization of the RLS and the successive intrusions of magma resulted in the mixing of resident magma and primitive magma. The nucleating and growing crystals in the magma sank to the floor aided by convection and density currents within the magma and gravitational forces which exceeded the yield strength of the magma. The compositionally distinct layering resulted from the differences in the densities, shapes and sizes of the crystals (Maier and Eales, 1997).

According to Coertze (1970), differentiation commenced during magma generation prior to emplacement of the Bushveld Complex at its current position and differentiation was only complete when the last liquid had crystallized. During emplacement of the differentiated magma some assimilation of the country rocks occurred, locally altering the composition of the liquids. With emplacement, the magma spread horizontally along bedding planes or unconformities of the overlying Transvaal Supergroup sediments and in some instances, the magma transgressed the layering. Differentiation occurred within each successive pulse of magma and crystallization of separate lithological units occurred under more-or-less similar conditions (Coertze, 1970).

Irvine (1975) proposed that the chromitite layers of large layered ultramafic intrusions, such as the Muskox and Bushveld intrusions, formed as a result of extensive contamination of the parental

basic magma by granitic melt derived from sialic roof rocks. The composition of the basic magma would have been sufficiently modified to evolve from olivine to clinopyroxene crystallization. Subsequent work by Irvine (1977) revealed that the contamination factor would have to have been unacceptably large to induce the crystallization change. Furthermore the Bushveld magma differentiated towards an iron enrichment, which he postulated was only possible in tholeiitic magmas that are poor in alkalies and thus the Bushveld Complex parental magma experienced little contamination.

A popular group of models for the origin of the Bushveld Complex proposes the mixing of several mafic magma types (Hatton, 1988; Irvine *et al.*, 1983; Irvine, 1977; Campbell, 1986; Naldrett *et al.*, 1987). In their model, Irvine *et al*, (1983) hypothesize the mixing of Mg-basaltic primitive magma with a more evolved derivative magma, or U-type (ultramafic) and A-type (anorthositic) magmas, respectively. Mixing of the two magma types is believed to have resulted in the formation of the chromitite layers. The U-type magma has a crystallization order of olivine, orthopyroxene, plagioclase. The A-type magma crystallizes plagioclase, olivine, clinopyroxene, and finally orthopyroxene. The bulk mixing of the two dissimilar magmas would result in the new liquid lying in the primary phase field of chromite.

The U-type magmas are primarily boninitic in composition, rich in SiO_2 (52 - 56 %), MgO (12 - 16 %), Cr_2O_3 (800 - 2000 ppm), and incompatible elements (20 - 50 ppm Rb, 150 - 400 ppm Zr), with strontium initial isotope ratio (R_O) in the range of 0.703 - 0.705 (Sharpe and Irvine, 1983). The A-type magma has a similar composition to tholeiitic basalts, with 48 - 50 % SiO_2 and 8 - 10 % MgO, and low incompatible elements and Cr values, with a R_O range between 0.707-0.708. Sharpe and Irvine (1983) propose that the LZ crystallized from U-type magma and the formation of the lower CZ (lCZ) was influenced by an increasing influx of A-type magma, until at the transition stage from lCZ to upper CZ (uCZ), where A-type magma accounted for the principal volume of the magma present. The Main Zone (MZ) is believed to have crystallized from an essentially A-type liquid, based on an increase in R_O at the Merensky Reef level (Von Gruenewaldt *et al.*, 1985).

Hatton (1988) proposes that three parental magma types, B1, B2 and B3, were responsible for

the formation of the LZ and CZ rock types. In his model, the B1 magma is compositionally similar to the U-type magma of Irvine *et al,* (1983) and is the parental liquid responsible for the formation of the LZ. The B2 and B3 liquids formed the CZ and are similar to the A-type magma. B1 is considered to be boninitic, whereas B2 and B3 are of tholeiitic origin. B1 is hypothesised to be less dense than B2 and B3 and has a higher liquidus temperature (1280 - 1290°C versus 1190°C of B2 and B3). The mixing of B1 and B2/B3 magmas led to the precipitation of large volumes of chromite (Hatton and Von Gruenewaldt, 1985; Schürmann, 1991; Maier and Eales, 1997).

Currently popular models for the origin of the cyclic layering in the CZ propose repeated injection of magma into the chamber and the mixing of compositionally similar magma types, as proposed by Eales *et al,* (1990) and Teigler *et al,* (1992). Both propose that the cyclic layering resulted from the mixing of two magma types of essentially similar composition and point out that the compositional variations of the cumulate rocks of the CZ do not support the existence of two compositionally dissimilar magmas. Scoon and Teigler (1994) propose that the magma influxes intruded as basal flows or as fountains. In light of the compositional variations in the CZ silicate and chromitite units (chapters 6 and 7), this study subscribes to the presently favoured model that the Bushveld Complex formed by multiple magma injections and mixing of compositionally similar magmas.

The chromitite seams of the Bushveld Complex were classified as early as 1923 by Wagner and by Kuperburger *et al,* (1937). Coertze (1958) observed the intrusive relationships of the RLS and subdivided the Bushveld Complex lithologically into eight constituent rock types; viz. pyroxenite, chromitite, anorthosite, norite, porphyritic pyroxenite, pegmatitic pyroxenite, gabbro, ferrogabbro, dunite and magnetitite. He proposed that each type was separately emplaced. Cousins and Feringa (1964) observed that the chromitite seams are strike continuous for considerable distances. Based on the correlation and strike-continuous relationships between the seams, they formulated the current subdivision of the chromitite intervals into three groups, namely the Lower, Middle and Upper Groups. They assigned suffixes to denote the individual seams in each group - for example, the Lower Group (LG) consists of the LG1 to LG7 layers and the Middle Group (MG) comprises at least five seams, the MG1 to MG4a layers.

2. Tectonic Aspects of the Western Bushveld Complex

2.1. Folding and Upwarping of the Floor Rocks

At least two phases of folding affected the western Bushveld Complex and its Transvaal Supergroup floor rocks. The first phase resulted from a compressional stress regime believed to have been induced by isostatic subsidence related to the Transvaal Supergroup sedimentation and the emplacement of pre-Bushveld sills (Sharpe and Snyman, 1980). The second phase of folding resulted from the ductile deformation of the floor rocks during the emplacement of the Bushveld Complex, culminating in down-warping and upwarping of the Bushveld Complex floor. The fold axes of the first and second phases of folding/warping are normal to each other.

The Spruitfontein (fig. 5 and 6) and Kookfontein Upfolds influenced, to a large degree, the manner of emplacement of the RLS and hence development of the LZ and the CZ (fig. 6) in the eastern portion of the western Bushveld Complex. The Spruitfontein Upfold is thought to have developed during the period of LZ formation, and has resulted in lithologically dissimilar LZ stratigraphy in the Rustenburg and Marikana sections. The Kookfontein Upfold is thought to have formed concurrently with the crystallization of the lCZ. The Kookfontein Upfold was accompanied by Bushveld folding, in which the Bushveld rocks were affected to a lesser degree than those of the Pretoria Group (Schürmann, 1991).

In the vicinity of the Spruitfontein Upfold variably dipping Magaliesberg Formation floor rocks outcrop and are surrounded and overlain by Marginal Zone norites. Associated with the upwarping, the RLS experienced minor tectonism, such as that on the farm Rooikoppies 297 JQ, Marikana, where faulting led to the formation of a small graben structure (Davey, 1992).

2.2. Faulting

Considerable post-Bushveld faulting has affected the area - for example, the strike-slip and dip-slip faults which radiate away from the Pilanesberg Alkaline Complex are believed to have been a direct result of its emplacement; the Rustenburg right-lateral strike-slip fault trends northwesterly, from southeast of Rustenburg to Boshoek; the radial faulting related to the Pilanesberg Alkaline Complex has resulted in the local juxtaposition of the LG and MG chromitite

seams in the vicinity of the Pilanesberg Alkaline Complex. Structural differences in the Pretoria Group rocks occur on the eastern and western sides of the Rustenburg Fault. Westwards from the fault, the Pretoria Group rocks are generally not folded, striking parallel to the edge of the Bushveld Complex (Coertze, 1962). Seismic modelling of the area south of the Crocodile River fragment, revealed that pre-Bushveld faulting had a direct influence on the emplacement of the Bushveld Complex (Du Plessis and Walraven, 1990).

To the south of the town of Brits the structural setting of the area is dominated by a major graben with associated sub-graben blocks, the whole structure being referred to as the Brits Graben. The graben is bounded by two northwesterly striking faults, with displacements in the order of 600m or less. Smaller scale faulting is present within and outside the main graben. The strike/dip of the pseudo stratification varies within the graben and the graben hosts transgressive syenitic and doleritic dykes of post-graben age (Teigler *et al.*, 1992).

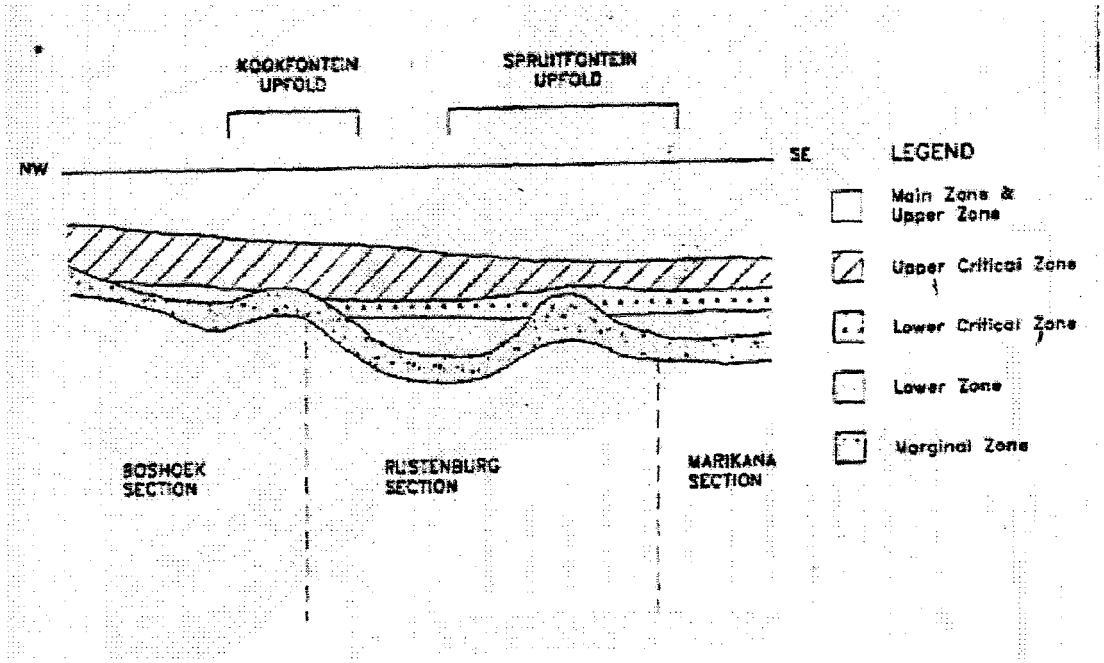

Fig. 5. Simplified structural model explaining the relationship between the Lower and Critical Zones of the southwestern Bushveld Complex and the floor rocks (after Schürmann, 1991, p 9).

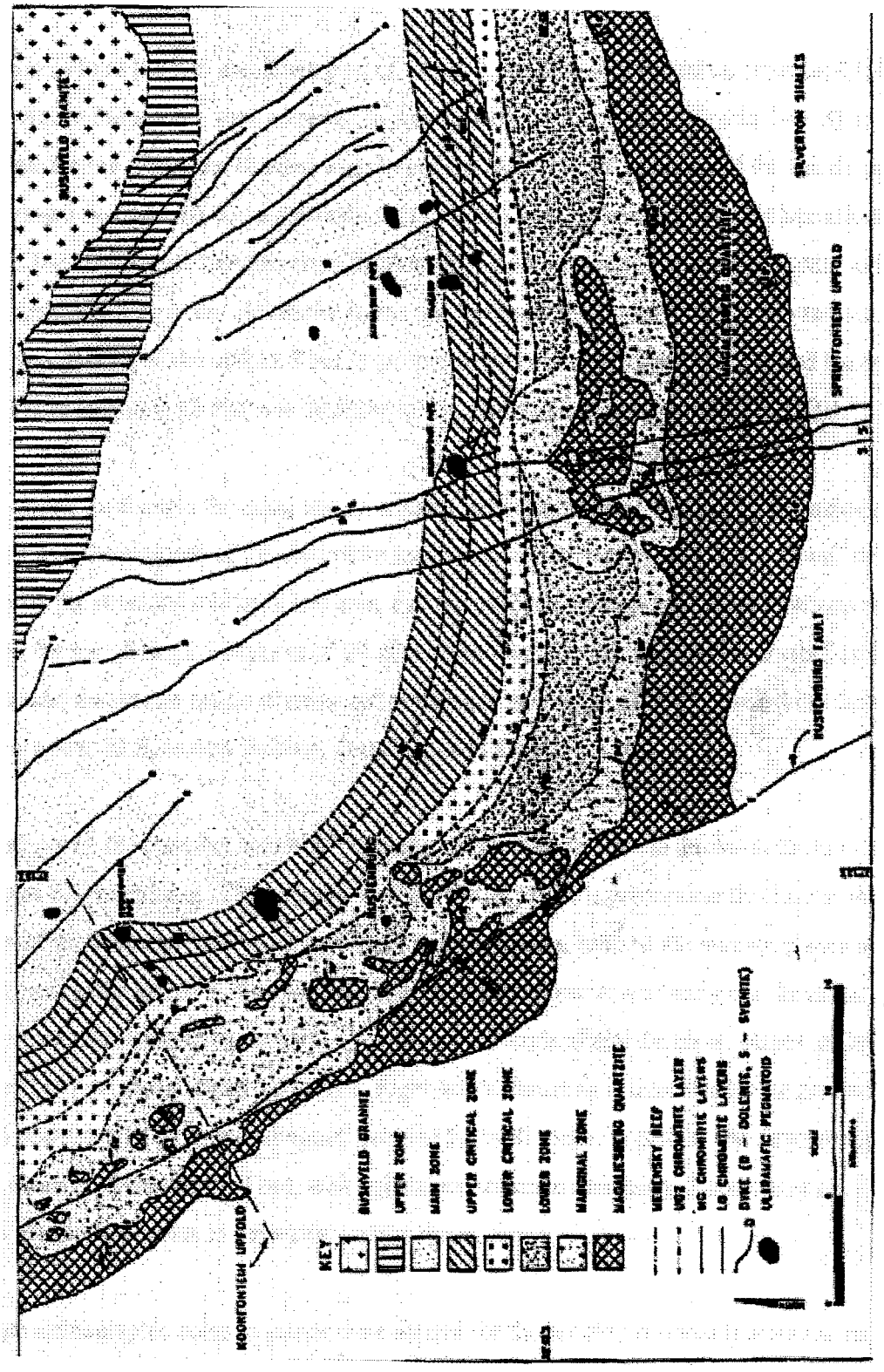

Fig. 6. The Spruitfontein Upfold (from Davey, 1992, p 142).

2.3. Structural Interpretation of a Section Adjacent to the Spruitfontein Upfold

A portion of both the lCZ and lower part of the uCZ, specifically the interval from the LG4 to MG4a chromitite seams, were exposed in trenches on the farm Spruitfontein 341 JQ in the Marikana section. From the detailed mapping of the trenches (see appendix H for trench logs), it is proposed that post-RLS, out-of-basin thrusting occurred in the vicinity of the Spruitfontein Upfold. The north-south trenches were excavated by a private mining company in order to find the strike extensions of the chromitite seams for purposes of exploiting the seams and not for exposing a portion of the upfold. Thus, exposure in two trenches (one 90 metres and the other 60 metres in length) is all that was available to be examined in this portion of the upfold.

Right-lateral, low angle thrusting and to a lesser extent left-lateral thrusting, with associated stacking and shearing out of the chromitite seams and related hanging wall and footwall strata, summarize the structural setting of this area. For the purposes of mapping, distinction was made between the morphological features of the chromitite seams that formed during crystallization - for example, the sinuous nature of seams and presence of pyroxenite xenoliths - and those features which are post-RLS, namely faulting, thrusting, and tilting of the strata.

Due mainly to the complex nature of the duplication of the strata, the throw on the low-angle faults was not determined. The orientation of the thrust planes is predominantly close to that of the dip of the strata and the thrusting has, in most instances, utilized the contact planes of the hanging wall and footwall strata. In some cases, however, shear zones transgress the strata with no apparent relationship to the contacts. The dips of the strata above the thrust planes are locally affected by movements along the thrusts. Right-lateral thrusting is indicated by the presence of folded strata, which have been dragged over the footwall rocks. In places, the strata along the thrust planes have been sheared out, with only minor tectonite remaining. S-structures are found within the footwall strata in the vicinity of the thrust planes.

Average stereographic poles to planes were plotted for the bedding surfaces (chromitite seams) (fig. 7). The average strike/dip for the thrust planes is 090 / 39 N and for the bedding planes is roughly 090 / 44 N and thus it can be seen that the thrusting is nearly parallel to the bedding

planes. The thrusting was therefore accommodated by differences in rheology between the chromitite seams and the hanging and footwall rocks.

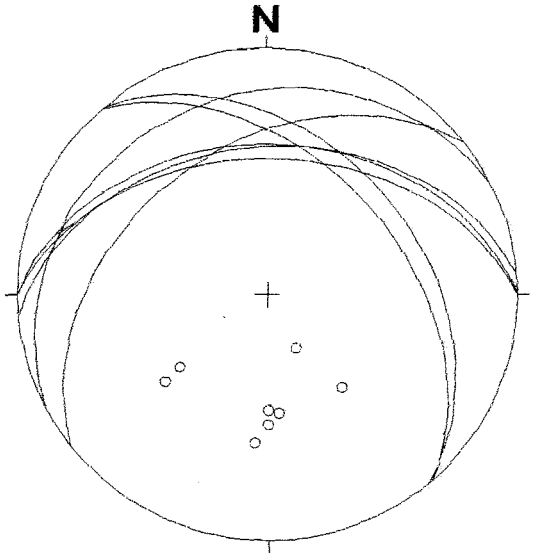

Poles to planes

180	46 Average for the chromitite seams
180	51 Average for the thrust planes
142	50 LG5
153	70 LG4
175	50 MG1
185	39 MG2
229	45 MG3
230	52 MG4

Average strike/dip for thrust planes

090/39 N

Chromitite seams

LG4	063/20 N	MG2	095/51 N
LG5	052/40 N	MG3	139/45N
MG1	085/40 N	MG4	140/3 N

Fig. 7. Stereographic plot of poles to planes of the thrust planes and bedding planes (chromitite seams), in the western Bushveld Complex, Marikana section.

Prominent jointing utilized the contacts, with a second set roughly perpendicular to the contacts. The material in the joint planes consists of amorphous remobilised host rock, clay, talc, and magnesite. The orientation of the fractures is parallel to subparallel to the direction of thrusting and, secondary foliation, related to the deformational events, is concordant with the direction of thrusting.

A single fold structure is exposed in one of the trenches, with the axial plane of the fold trending 240° and plunging at 50°. The fold is either pre- or post-thrusting but this could not be ascertained with any certainty owing to the presence of a shear zone which has pervasively altered the pyroxenites and chromitite seams (LG6 & LG6a). The LG6 seam has been thrust and multiply stacked and portions of the seam are ramped up on itself. Roll structures and folding of the seam both indicate a right-lateral thrust direction.

As indicated in the cross-section (appendix H), the LG4 and LG5 seams are poorly developed, forming thin seams of the order of 10 - 25 centimetres thick. The silicate middling between the LG4 (with a dip of 12° to 20°N) and LG5 (dipping at 30° to 40°N) chromitite seams thins down dip and it is assumed that the LG4 and LG5 chromitite seams will be stacked one on top of another forming a 'single seam' further down dip. A massive shear zone occupies the pyroxenite middling between these two seams. Westwards from the trenches the dip and morphology of the seams return to their normal habit, with dips of 14° to 16° N, striking east-west.

In summary, the thrusting is possibly related to out-of-basin thrusting, itself believed to be the result of volume accommodation in the RLS due to progressive unburdening and tilting of the Bushveld Complex lithologies towards the centre of the Complex during isostatic re-equilibration of the Transvaal and Bushveld lithologies. Erosion of the Bushveld lithologies would have unburdened the Bushveld Complex allowing for volume accommodation to occur, possibly being expressed as out-of-basin thrusting.

The right-lateral thrusting observed on Spruitfontein 341 JQ may be related to the Spruitfontein upfold to the south, but could also be associated with the regional post-Bushveld tectonism that affected both the Transvaal sediments and the Bushveld Complex lithologies. It is not known whether the structures observed in the trenches are a local phenomenon or whether they characterize the entire upfold area. Further field work needs to be undertaken on the Spruitfontein Upfold to determine if the observed structures are related to the Upfold or post-Bushveld Complex tectonism.

A translocated pyroxenite xenolith, measuring one metre by 0.6 metres, is hosted by the MG4 and MG4a chromitite seams in the 60 metre trench. The elliptical pyroxenite xenolith provides evidence for the dynamic processes in the crystallizing magma chamber, in that the ensuing magma pulses were able to rip up crystallized cumulates from the lower portion of the cumulate mass.

3. Lithostratigraphy and Description of the Chromitite Seams

Cousins and Feringa (1964) classified the chromitite seams into three groups, the Lower, Middle and Upper Groups, based on their host cumulate environment and their stratigraphic position within the CZ. The Lower Group (LG) chromitite seams form the basal members of the ultramafic cyclic units (see section 7.8) which constitute the lCZ. The Middle (MG) and Upper (UG) Group chromitites are hosted by the ultramafic to leucocratic lithologies of the uCZ. The LG and MG1 chromitite seams are restricted to the lCZ, whereas the MG2 - MG3 chromitite seams straddle the boundary between the lCZ and the uCZ and the MG4 chromitite seam is hosted by the uCZ. The boundary between the lCZ and the uCZ is defined by the first appearance of cumulus plagioclase-bearing rocks.

It is typical for the chromitite seams to form the basal members of cyclic units, but this is not always the case as thin chromitite layers and stringers are frequently hosted within cyclic units. Throughout the thesis reference is made to the term massive chromitite or simply chromitite - this terminology refers to a rock in which chromite is the only cumulus phase (Teigler, 1990).

3.1. Stratigraphy

3.1.1. The Lower Group Chromitite Seams

At least seven chromitite layers constitute the Lower Group, from the LG1 near the base of the lCZ to the LG7 towards the top of the lCZ (fig. 8). In the type area for the LG seams, **Ruighoek**, the four lower seams (LG1 - LG4) each have an approximate thickness which rarely exceeds 0.30 m. The LG5 seam is a composite seam of five or more thin chromitite layers which bifurcate and coalesce but which has an average thickness of one metre. The economic viability of the LG5 chromitite seam is affected by contamination resulting from the intervening silicate units (Hatton and Von Gruenewaldt, 1985). Generally, the LG6 chromitite layer is the most economically viable chromitite layer due to its high Cr_2O_3 content, high Cr:Fe ratio (see section 7.4) and average thickness of 0.80 m. The LG6 is overlain by a thin chromitite layer known as the LG6a or LG6 Leader seam, which has an approximate thickness of 0.30 m. The intervening cumulates

separating the two seams are up to 9 metres thick.

Cousins and Feringa (1964) recorded a complete succession of LG seams in the **Boshoek** section. Nonetheless, exploration drilling on the farms Stellite 255 JQ, Boekenhoutfontein 260 JQ, Bultfontein 259 JQ and Turffontein 462 JQ in the Boshoek section indicate that the Lower Zone and LG seams are poorly developed in this section and, where developed, the LG seams display lateral variations in both composition and morphology.

In contrast, the LG chromitites are well developed in the **Rustenburg** section, though the thickness of the host cumulate package is reduced to one-sixth of the thickness elsewhere in the western Bushveld Complex. The thickness of the LG chromitite seams in the Rustenburg section is equivalent to that of the LG seams in the other sections. The LG6 and LG6a chromitite seams are currently exploited in this section (Hatton and Von Gruenewaldt, 1985).

Seven thin and variably developed chromitite layers are present below the MG seams in the **Marikana** and **Brits** sections, but correlation with LG seams elsewhere in the western Bushveld Complex is tenuous (Hatton and Von Gruenewaldt, 1985). On the farm Spruitfontein 341 JQ, in the Marikana section, the LG6a is 0.3 m - 0.4 m thick and the LG6 is 0.7 m - 1.20 m thick, but the latter thins in places to 0.4 m. The thickness of both the LG6 seam and the middling between the LG6 and LG6a, decreases from west to east across the western Bushveld Complex. The LG6 seam forms a thin layer in the Brits section and several chromitite layers below the LG6 are tentatively correlated with the LG1 - LG5 seams to the west, on the basis of compositional trends. The LZ in the Brits section is ill-developed and the Marginal Zone is unusually thick. Moreover, the cumulate succession of the CZ is more leucocratic in the Brits area than in the northwestern portion of the western Bushveld Complex (Hatton and Von Gruenewaldt, 1985; Scoon and Teigler, 1994).

3.1.2. The Middle Group Chromitite Seams

The **Marikana** section is the type area for the MG chromitite seams (fig. 8). The five MG seams, totalling 8 m in thickness, are developed over a stratigraphic zone approximately 50 m in

thickness. The MG1 seam is hosted by the lCZ cumulates while the MG2 - MG3 seams straddle the boundary between the lCZ and uCZ and the MG4 seam is hosted by the more leucocratic uCZ cumulates.

The MG1 seam is, on average, one metre thick with two thinner chromitite seams developed below it. The MG2 chromitite seam averages one metre in thickness but thinner chromitite layers are developed both above and below it. The MG2 layer is underlain by pyroxenite and overlain by anorthosite which, in turn, forms the footwall to the MG3 chromitite. The MG3 is a single chromitite layer whilst the MG4 is a composite seam consisting of two chromitite layers, the MG4 and MG4a, each approximately one metre thick. Additional thinner chromitite layers are often associated with the MG4 chromitite seam (Hatton and Von Gruenewaldt, 1985). Norite overlies the MG3 seam and pyroxenite occupies the interval between the MG4 and MG4a layers and usually persists for 1.50 m above the MG4a, before grading into norite.

The thickness of the MG1 seam in the **Brits** section varies locally but is usually 1.00 to 1.40 m. The MG2 comprises up to three layers. In this section two chromitite layers constitute the MG4 seam and these are known as the MG4 (~ 1.8 m thick) and MG4a (~ 1.4 m thick). A fifth MG chromitite layer, the MG0 chromitite seam, is developed in both the Brits and Marikana sections below the MG1 seam but is either poorly developed or absent in the Rustenburg section and further west.

In the **Rustenburg** section, the MG1 seam is on average 0.40 - 0.60 m thick and only one MG2 layer has developed, in contrast to the three MG2 layers (each ~ 45 cm thick) encountered in both the Marikana and Brits sections. The MG3 is, on average, 0.70 - 0.80 m thick. The MG4 is a composite layer and often comprises three sub-layers, the upper two layers being approximately one metre thick whilst the lowest layer is only 0.20 - 0.30 m thick. The stratigraphic interval between the upper LG chromitites and the MG4 in the Rustenburg section is less than in the Ruighoek section, where the MG and LG chromitites are separated by several tens of metres of silicate rock.

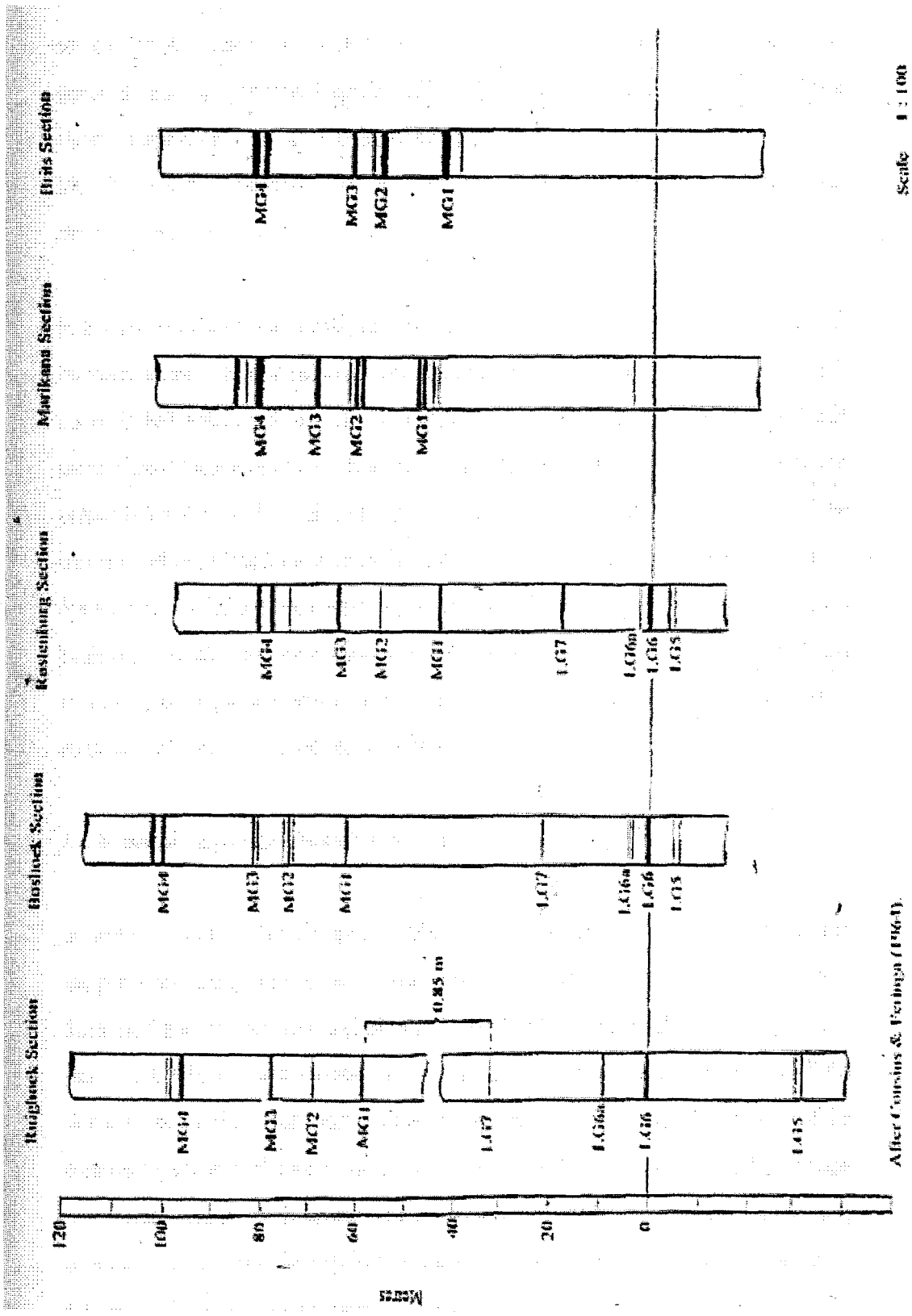

Fig. 8. Stratigraphic logs of the LG and MG chromitite seams of the CZ, from Brits to Ruighoek (after Cousins and Feringa, 1964, p 189).

In the **Ruighoek** section five chromitite seams correlate with the MG1 to MG4a seams of the type section. Complex radial faulting related to the intrusion of the Pilanesberg Alkaline Complex has disrupted the stratigraphy of the Ruighoek section, often resulting in the juxtaposition of different chromitite seams. This lends itself to the increased economic viability of mining both the LG and MG chromitites in this section, as the depth of the mining operations to exploit the lower chromitite seams is reduced.

Hatton and Von Gruenewaldt (1985) state that notable differences exist between the LG and MG chromitite seams to the west and to the east of the Spruitfontein Upfold respectively. East of the upfold, in the Marikana section, the MG chromitite seams are well developed, with the result that the Marikana-Mooinooi area is the type area for the MG chromitites. Thin chromitite seams are present below the MG, but their correlation with the LG chromitites from other sections of the western Bushveld Complex is tenuous. In contrast, the LG chromitite seams to the west of the Spruitfontein Upfold are well-developed, and the LG6 chromitite seam is 0.90 m thick and the LG6a is 0.3 m thick at Kroondal (Rustenburg section) (Davey, 1992). The decrease in thickness of the intervening package between the LG6 and MG2 seams in the Marikana and Rustenburg sections is believed to have been caused by the Spruitfontein Upfold (fig. 8).

3.2. Regional Map of the Chromitite Seams

In spite of the vast number of maps available portraying the economically important chromitite and platinum-bearing layers of the western Bushveld Complex, no regional map of the western Bushveld Complex has been compiled recently which indicates the localities of the chromitite seams (LG, MG, UG, and Merensky Reef). Due mainly to the economic importance of the chromitite seams, the author undertook the compilation of a regional map (Appendix D) of the economically important chromitite seams. The map was compiled from geological and mine maps and literature research. Field mapping of the chromitite seams was out of the scope of this project, so it must be noted that the map must be used with some caution. It is mainly for the use of determining the position of the seams in a regional context.

3.3. Compositional Variations within the Chromitite Layers and the Effect of the Host Cumulate Environment on the Composition of the Chromitite Layers

Compositional variability within individual chromitite seams is characteristic of the LG, MG, and UG layers. The scale of this investigation, however, did not permit the sampling of individual seams to establish within-seam compositional variation.

Teigler and Eales (1993) investigated the compositional variations across two chromitite seams, the LG6 and MG4 chromitites, on the farm Nooitgedacht in the Union section. The eight samples representing the LG6 seam indicate that the highest Cr:Fe ratios are attained in the middle of the seam and that the Cr:Fe ratio at the top of the seam is greater than at the base of the chromitite seam. They found a similar Cr:Fe trend for the MG4 chromitite but interpretation of the across-seam compositional variation is restricted for the MG4 chromitite by the pyroxenite middling between the MG4 and MG4a seams. The systematic compositional variations across individual seams appear to be largely limited to but not exclusively Cr, Mg, Al, Fe^{2+}, Fe^{3+}, and Ti (Teigler and Eales, 1993). Variations within an individual chromitite seam reflect the chemical evolution of the host silicate cumulates. The reader is referred to chapter 7 for factors influencing the precipitation and composition of chromite.

The composition of the chromite grains at the contact with the pyroxene and/or plagioclase cumulus material differs slightly from that of the chromite within a monomineralic chromitite seam. At the contact with the silicate minerals the chromite has a higher proportion of silicate inclusions than the chromite within the seam (McDonald, 1967). The Mg, Al, Fe^{2+} and Fe^{3+} variability is ascribed by De Waal (1975) and Roeder and Campbell (1985) as a function of the host-cumulate environment and the composition of the intercumulus minerals (or co-precipitating minerals) within a seam. Eales *et al,* (1988) established that, in olivine-rich cumulate environments, the chromitites have elevated Al compositions resulting from the co-precipitation of olivine and, in plagioclase-rich cumulate environments, co-precipitation of intercumulus plagioclase depletes the liquid in Al. In pyroxene-rich cumulus environments the chromitites have intermediate Al contents due to the greater compatibility of Al with respect to orthopyroxene than olivine. However, it should be noted that after the first appearance of cumulus plagioclase at the

lCZ - uCZ boundary, the Al content of the chromitites does not decrease as would be expected, but rather the chromitites display a steady Al level.

In the cumulus orthopyroxene environment, variable MgO contents across a chromitite seam may in part represent the waning of cumulate orthopyroxene precipitation in favour of cumulate chromite precipitation.

Within the UG2 layer, which is essentially a massive chromitite seam, McLaren and De Villiers (1982) reported a general upward increase in Fe^{2+}, Fe^{3+}, Cr, and Fe^{3+}/Fe^{2+} from the bottom to the top of the seam along with a decrease in the Mg, Al, Cr:Fe and Cr/Al values. They ascribe this to the greater stability of the end-member spinel $Fe^{2+}(Cr, Fe^{3+})_2O_4$ toward the top, and of the $MgAl_2O_4$ end member toward the bottom of the UG2 layer.

The whole rock analyses of the chromitite seams in part reflect the composition of the cumulate host environment. In other words, across-seam compositional variations of the chromitites reflect the activity limits and ratios of MgO, FeO, Fe_2O_3, Cr_2O_3 and Al_2O_3 of the host cumulate environment and magma (Thayer, 1970).

3.4. Proximal and Distal Facies Model for the Western Bushveld Complex

Eales *et al,* (1988) formulated a model of the uCZ which proposed a proximal (Union section) and a distal facies (Brits section) (fig. 9). Teigler *et al,* (1992) extended this theory to include the lCZ. The proximal-distal facies model can account for the variations in chemistry and morphology of the RLS sequence along strike. The CZ in the Union section, or proximal facies, is represented by olivine-rich and compositionally more primitive cumulates, in which the lithologies are depleted in cumulus plagioclase. The Brits section, or distal facies, is characterized by an increase in the proportion of leucocratic cumulates and cryptic variations towards lower-temperature phases. These characteristics support the model that the Union section represents the proximal facies and the Brits section the distal facies. Both facies are represented by the crystallization sequence chromite → olivine → orthopyroxene → (minor accessory clinopyroxene) → plagioclase but the distal facies is more plagioclase-rich (Teigler *et al.,* 1992).

Teigler *et al,* (1992) outline several facts that support the proximal-distal facies model for the lCZ, based on their investigation of diamond drill hole SF-7, drilled on the farm Sandfontein 447 JQ in the Brits section. These include the limited development of pyroxenites and the putative LG chromitites, the development of only two olivine units below the MG1 chromitite seam (60 and 90 m below), the evolved nature of the ferromagnesian phases and ultramafic units, and a reversed fractionation trend of the lower portion in the cumulate succession, up to the uppermost olivine-bearing unit.

The primitive liquid evolved along strike away from the supposed feeder site, due mainly to the progressive crystallization of ferromagnesian phases accompanying loss of heat. The liquid composition thus evolved closer toward the plagioclase-orthopyroxene cotectic (Teigler *et al.*, 1992). Therefore, Teigler *et al,* (1992) conclude that the CZ was not derived from two compositionally different magmas, but rather from a primitive magma which evolved along strike and was rejuvenated periodically by the influx of fresh magma.

The proximal-distal model is based upon the observation of fractionation within basal flows along strike away from the supposed feeder site at Union section. Fractionation appears to have been the dominant process in the upper part of the lCZ, resulting in the accumulation of cumulus plagioclase at the lCZ - uCZ boundary. The same stratigraphic interval in the distal facies (Sandfontein) has well-developed MG and UG chromitite seams due to the upfolds no longer inhibiting the magma advance. The greater thickness of the MG chromitite seams in the distal facies may be the result of advanced compositional contrast between supernatant and replenishing liquid in the distal facies, intensifying chromite nucleation from the parent magma during magma mixing (Teigler *et al.*, 1992).

The boundary between the lCZ and the uCZ is represented by an anorthosite layer between the MG2 and MG3 chromitite seams which constitutes the first appearance of cumulus plagioclase-bearing rocks. This anorthositic layer is not, however, developed across the entire western Bushveld Complex. In the distal facies, cumulus plagioclase occurs below what is generally accepted as the boundary between the lCZ and uCZ. This can be explained by the liquid composition having evolved closer toward the plagioclase-orthopyroxene cotectic in the distal

facies.

The model can also explain the variations in thickness of the cumulate succession in part of the CZ from the proximal to the distal sectors. As noted in Table I below, the vertical distance from the UG1 chromitite seam to the MG2 chromitite seam and the MG2 to the LG6 chromitite seams decrease respectively from the proximal facies toward the distal facies. Furthermore, the thickness of the silicate units between the UG1 and LG6 is reduced in the distal facies compared with the same units in the proximal facies. Eales *et al,* (1988) propose that these thickness variations are the result of thermal erosion and/or cessation of crystallization of plagioclase-rich lithologies. The facies change across the western Bushveld Complex is gradational as exemplified by the gradual decrease in thickness of the cumulate thickness of the CZ as seen in the table below.

From To	Merensky Reef UG1 (metres)	UG1 MG2 (metres)	MG2 LG6 (metres)	Merensky Reef LG6 (metres)
Union	55	347	286	688
Boshoek	196	204	106	506
Rustenburg	212	199	67	478
Marikana	238	139	53*	430*
Brits	360	180	68*	608*

* uppermost chromitite layer below the MG1 chromitite

Table I. Vertical distances between chromitite marker layers (from Teigler *et al.*, 1992, p 17).

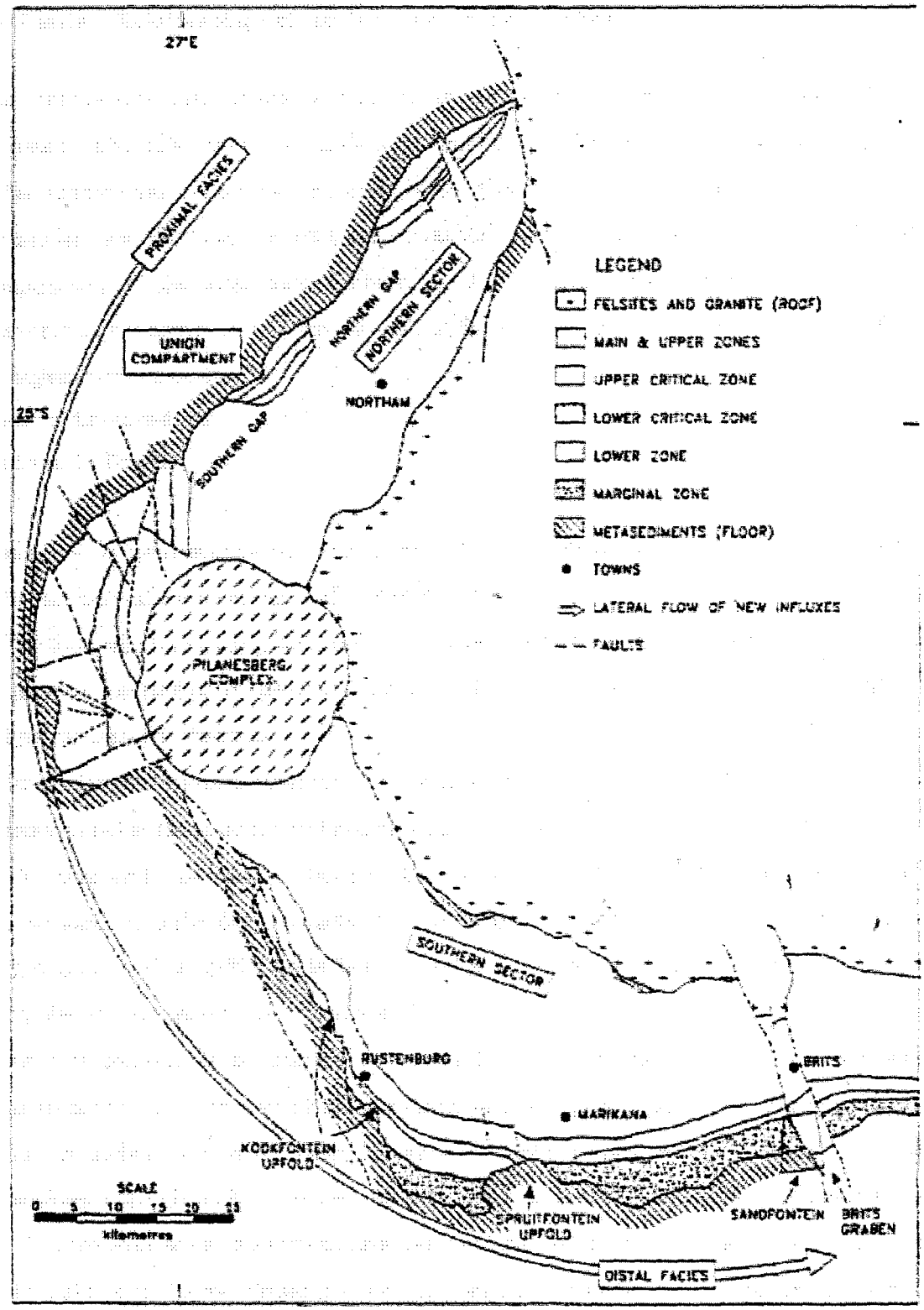

Fig. 9. Simplified regional geological map of the western Bushveld Complex depicting the proximal and distal facies of Eales *et al,* (1988) (modified after Scoon and Teigler, 1994, p1098).

3.5. Contact Relationships of the Massive Chromitite Seams

The composition of the disseminated chromite within the silicate cumulus material differs from the massive chromitite layers, depending on whether it occurs within the hanging wall, footwall, or the intervening silicate host cumulate units. The nature of the contact between the massive chromitites and the host cumulate units, whether gradational or sharp, does not influence the composition of the disseminated chromite. The disseminated chromite has the following characteristics in comparison to the chromite of the massive chromitite seams (McDonald, 1967):

- a higher total iron content,
- a lower Cr content, and
- a lower Cr:Fe ratio.

The following features result from the nature of the contacts of the LG and MG chromitite seams with the footwall and hanging wall cumulates (McDonald, 1967):

- The footwall and hanging wall rocks with sharp contacts with the chromitite layers have little or no disseminated chromite near the contact, but stringers of chromite may occur above and below the massive chromite.
- At gradational contacts with the massive chromitites, abnormally high values of chromite are present in either the footwall or hanging wall, or both.
- The compositional variation between the massive and disseminated chromite occurs within a few centimetres of the sharp contacts, but over several centimetres with the gradational contacts.
- Irregular and cusp-like grain boundaries of the cumulate phases adjacent to the massive chromite are common at sharp contacts.
- At sharp contacts the disseminated chromite is finer-grained, minor silicate recrystallization has occurred, the Cr_2O_3 content of the individual grains or grains that are incorporated by silicate grains is higher than in the large anhedral chromite masses, and the proportion of silicate inclusions in the chromite grains is relatively high compared to the massive chromitite seam.
- The chromitite seams with gradational footwall and hanging wall contacts are characterized by euhedral and subhedral chromite grains, and anhedral masses of chromite are common. In the vicinity of the massive chromitite seams, layering of a few millimetres to tens of millimetres of alternating chromite and silicates occurs.

4. Nomenclature

4.1. Chromite

Chromite is the dominant natural mineral of the element chromium (Cr) and is theoretically represented as $(Mg, Fe)O(Cr, Al, Fe)_2O_3$. It is an oxide mineral, a member of the spinel mineral group, and is represented in general form as $R"O\ R"'_2O_3$, where R" indicates a divalent metal and R"' represents a trivalent metal. The crystal lattice accommodates a variety of elements, such as Mg, Fe, Al, Ti, V, Mn, Ni, Co and Zn. The percentage of these elements that will be accommodated in the Cr-spinel lattice depends on their concentration in the parental melt and their ionic size, electronegativity and valency. All these elements have similar electronegativities to Cr, which has an electronegativity of ~ 1.6 (Battey, 1972). Chromitite is the term used for a rock chiefly composed of chromite.

Cr-spinels occur in two forms, magnesiochromite ($MgOCr_2O_3$) and ferrochromite ($FeOCr_2O_3$). Chromite has a density of 3.8 - 4.9 and a hardness of approximately 8 (Stowe, 1987). The theoretical Cr_2O_3 content in Cr-spinel is 68%. In the Bushveld Complex, however, the Cr-spinel lattice contains variable proportions of magnesium, and iron and aluminium which may substitute for Cr in varying amounts. The amount of substitution of Cr by Al and Fe depends mainly on the chemical environment of the host silicate cumulus minerals, as the chemical evolution of the host rocks influences the composition of the chromitite seams (reviewed in chapters 6 and 7). This substitution results in the lower Cr_2O_3 grades and Cr:Fe ratio found in the various seams. The Cr:Fe ratio determines the ferro-chromium grade that can be smelted from an ore. The Bushveld Complex chromite ore has a Cr:Fe ratio range of 1.1 - 2.5.

In general, the Bushveld Complex chromite is chemical grade ore. Chemical grade ores have low Cr:Fe ratios and are friable. Two physical types of chromite ore occur in the Bushveld Complex, these being "friable" and "hard lumpy" ore. The friable ore is predisposed to crumbling when handled and/or weathering and is not suitable for furnace feed. Lumpy ore is suitable for furnace feed.

4.2. Anorthosites, Norites, Pyroxenites and Harzburgites

Anorthosite is defined according to the IUGS classification system as a plagioclase-rich rock which contains more than 90 % plagioclase (Middlemost, 1985; Ehlers and Blatt, 1982). Norite is a coarse-grained plutonic rock essentially comprised of basic plagioclase and orthopyroxene. By definition, clinopyroxene occurs in relative proportions <5 %. Pyroxenite is an ultramafic plutonic rock chiefly composed of pyroxene with accessory plagioclase, hornblende, biotite, olivine and other phases. In general, pyroxenites contain >50 % cumulus orthopyroxene. Harzburgite is a peridotite composed chiefly of olivine and orthopyroxene (Bates and Jackson, 1987). Table II is an indication of the average compositions of anorthosite, norites and pyroxenites (Best, 1982; Eales *et al.*, 1994).

wt%	*Anorthosite*	*Norite*	*Pyroxenite*
SiO_2	50.28	50.44	55.12
TiO_2	0.64	1.00	0.14
Al_2O_3	25.86	16.28	2.74
Fe_2O_3	0.96	2.21	0.90
FeO	2.07	7.39	9.07
MnO	0.05	0.14	0.22
MgO	2.12	8.73	28.09
CaO	12.48	9.41	2.31
Na_2O	3.15	2.26	0.38
K_2O	0.65	0.70	0.05
H_2O+	1.17	0.84	-
H_2O-	0.14	0.13	-
P_2O_5	0.09	0.15	0.05
CO_2	0.14	0.18	-
Total	*99.80*	*99.86*	*99.99*

Table II. Average composition of the silicate cumulate lithologies found in the Rustenburg Layered Suite (after Best, 1982; pyroxenite data by Eales *et al.*, 1994).

5. Mineralogy and Petrography of the Critical Zone of the Rustenburg Layered Suite, Rustenburg Section

5.1. Petrography

5.1.1. Anorthosites

The anorthosites of the CZ are, on average, composed of 90 % plagioclase, the remaining 10 % comprising orthopyroxene and clinopyroxene. The cumulus plagioclase grains vary between stubby to prismatic grains and are characterized by combined twinning according to the Carlsbad and albite laws. The grain boundaries are often highly irregular with mutual interpenetrating grain boundaries between plagioclase grains. Triple junctions are rare. Intercumulus orthopyroxene and clinopyroxene constitutes the remaining volume of the rock. Orthopyroxene may poikilitically enclose plagioclase. The intercumulus clinopyroxene and orthopyroxene cause the mottled appearance of the rock. Zoning of orthopyroxene grains is infrequent and exsolution lamellae of clinopyroxene are common (fig. 10). Bladed chlorite (fig. 11) and sericite form a minor accessory phase in the anorthosites, resulting from alteration of the primary ferromagnesian minerals.

Where anorthosites constitute the hanging wall to a chromitite seam, stringer and disseminated chromite grains are frequent in the anorthosite, often displaying a preferred orientation which corresponds to the preferred orientation of the plagioclase and orthopyroxene grains.

5.1.2. Leuconorites, Melanorites and Norites

The grain sizes of the cumulus plagioclase are smaller in the norite layers than in the anorthositic layers. On average, orthopyroxene constitutes approximately 25 % of the modal proportion of the investigated samples, plagioclase 60% and clinopyroxene 5 % (this value appears anomalously low). Sericitization is common in the norite layers, constituting up to 10 % modal volume. The orthopyroxene grains are anhedral and subhedral (fig. 12), and vary from poikilitically enclosing plagioclase to cumulate phases and rarely intercumulate phases. The majority of the plagioclase inclusions within the oikocrysts of orthopyroxene are partially resorbed. The inclusions of plagioclase within the orthopyroxene grains are typically well-rounded.

35

Fig. 10. Exsolution lamellae of clinopyroxene in orthopyroxene in the anorthosites of the CZ (width of field 1 mm = 1 cm).

Fig. 11. Blasted texture of chlorite in the anorthosites of the CZ - chlorite alteration of the ferromagnesian minerals (width of field 1 mm = 1 cm).

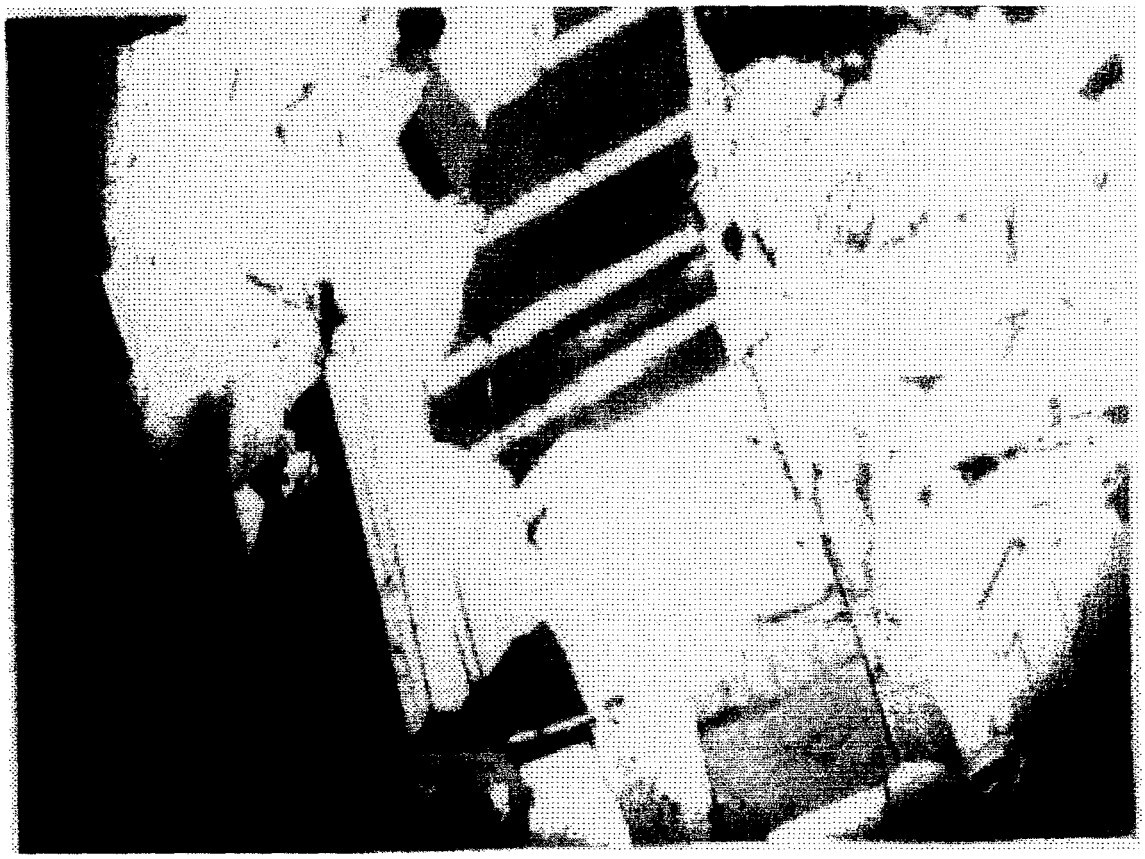

Fig. 12. Anhedral and subhedral orthopyroxene, plagioclase and clinopyroxene grains of the norites of the CZ (width of field 1 mm = 1 cm).

Strain effects, in the form of bending of the plagioclase twin planes and bending of the exsolution lamellae in the orthopyroxene grains, occur in both the orthopyroxene and plagioclase grains. Triple junctions are rare in the norites, leuconorites and melanorites. Clinopyroxene is typically intercumulus and usually surrounds the orthopyroxene grains. Opaque (chromite) grains comprise approximately 3 % of the modal proportion of this rock type.

5.1.3. Pyroxenites

In the mesocumulate pyroxenites, the orthopyroxene grains are anhedral and subhedral and contain abundant inclusions of clinopyroxene and plagioclase. Clinopyroxene and plagioclase are both intercumulus phases and the plagioclase poikilitically encloses both orthopyroxene and clinopyroxene grains. Pyroxenites containing more than 10 % plagioclase are termed feldspathic

pyroxenites. Sericitic alteration is a common characteristic of the pyroxenites.

In the hanging wall pyroxenite layer above the LG6 chromitite seam, alteration halos surround some orthopyroxene grains. Adcumulate pyroxenites are rare, and the majority of the pyroxenites are meso- to ortho-cumulates and plagioclase is the main intercumulus mineral.

On average, the pyroxenites contain:

75 - 85 %	orthopyroxene
3 - 25 %	clinopyroxene
5 - 15 %	plagioclase
1 - 5 %	biotite (anhedral and subhedral)
1 - 5 %	accessory minerals and alteration products

The orthopyroxene and plagioclase grains of the pegmatoidal pyroxenites average 10 mm in width and the orthopyroxenes poikilitically enclose the plagioclase grains and vice versa. The biotite content of the pyroxenites is lower in the author's samples than in the pegmatoidal pyroxenites, corresponding to the lack of intercumulus material in the pegmatoidal pyroxenites.

The resorbed plagioclase inclusions within the cumulus orthopyroxene indicate that plagioclase grains were partly corroded by injection of replenishing primitive magma. The injection of replenishing primitive magma is hypothesized to shift the composition of the resident liquid from the plagioclase- orthopyroxene cotectic back into the primary field of orthopyroxene or olivine alone (Eales *et al.*, 1993b, p 129). In fact, grains displaying this texture should not be classified as poikilitic, as the grains do not display the lath shapes associated with poikilitic textures (Eales *et al.*, 1993b).

5.1.4. Chromitites

The hanging wall rocks of the chromitite seams tend to contain a larger volumetric proportion of chromite than the footwall lithologies. Typically, the chromite in the hanging wall units occurs as stringers that crystallized or were deposited parallel to the massive chromitite seams.

Within the chromitite succession, the chromite grains are euhedral and subhedral (fig. 13). Individual grains tend to be mostly subhedral, whereas the euhedral grains are annealed (fig. 14).

Triple points and the near-perfect cubic form of the euhedral grains typically occur in the annealed areas (fig. 15) and, in most instances, the euhedral grains have a larger surface area than the subhedral grains (fig. 16). No petrographic trait distinguishes the individual LG and MG chromitite seams. Nonetheless, the MG4 chromitite seam tends to be finer-grained than the remaining seams, with fewer triple points and annealed grains.

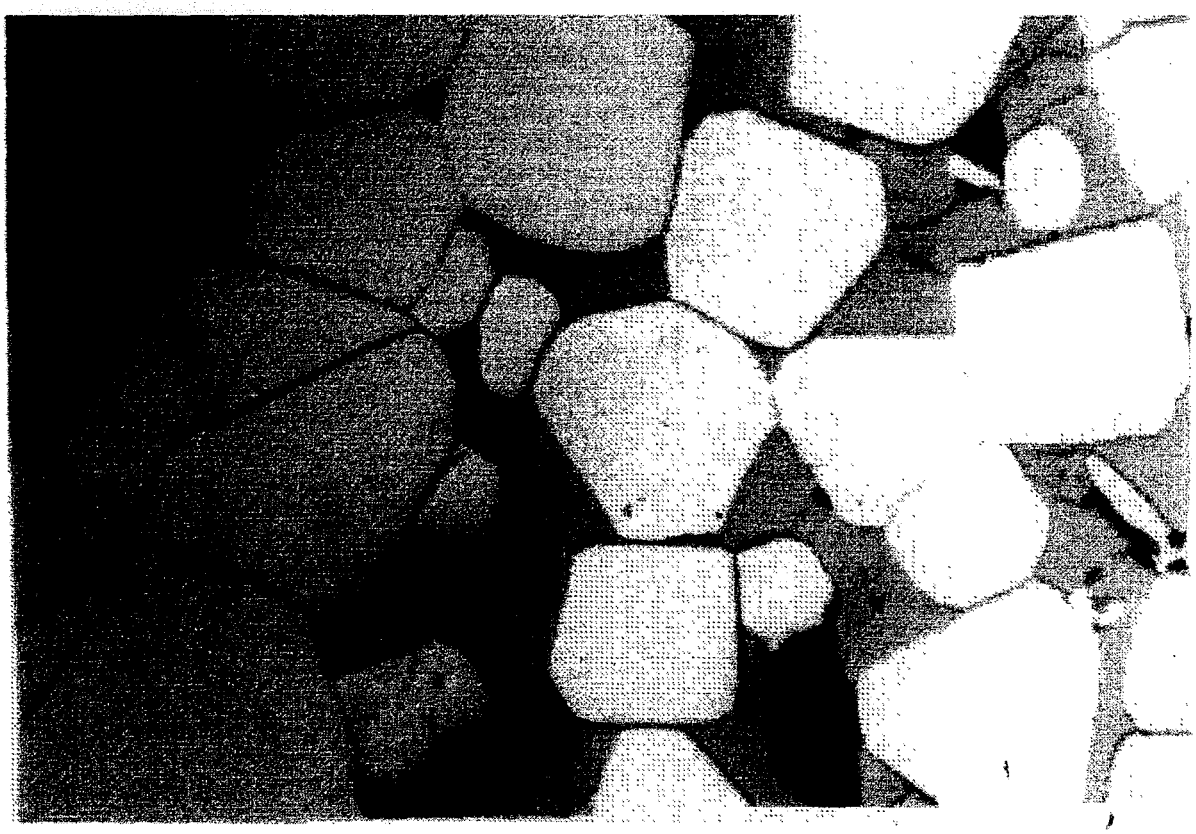

Fig. 13. Euhedral and subhedral chromite grains from the massive chromitite seams of the CZ (LG6) (width of field 1 mm = 1 cm).

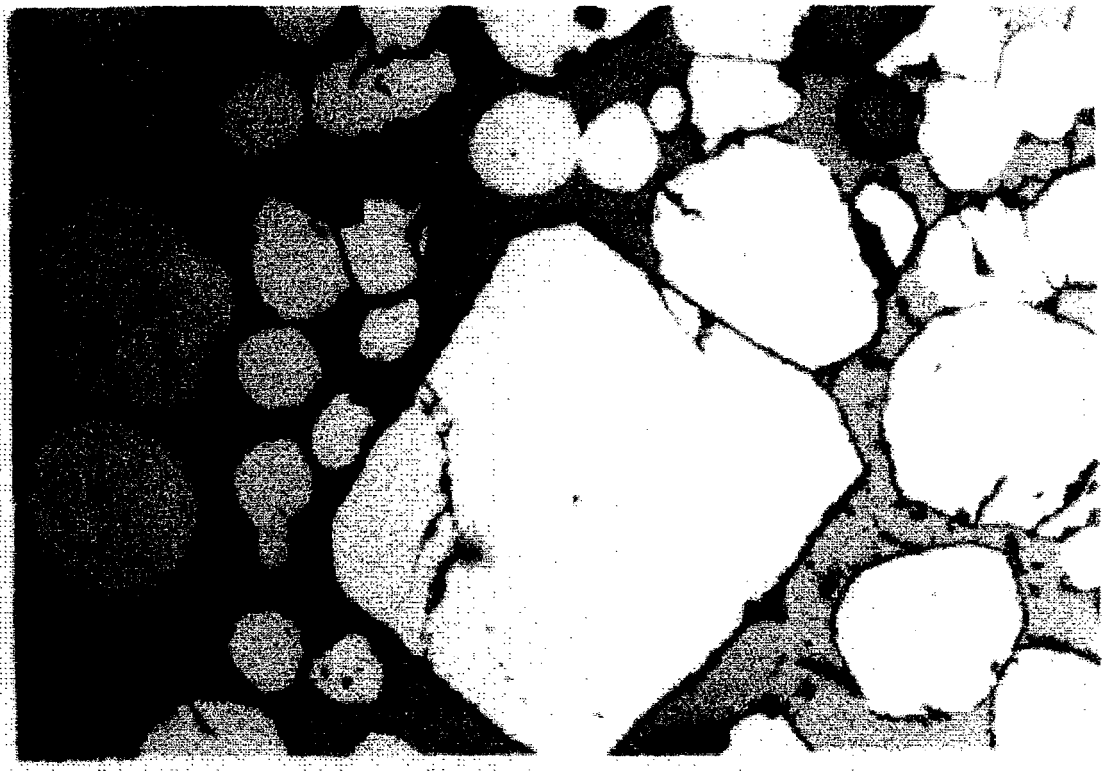

Fig. 14. The individual/separate subhedral chromite grains from the massive chromitite seams (MG1) (width of field 1 mm = 1 cm).

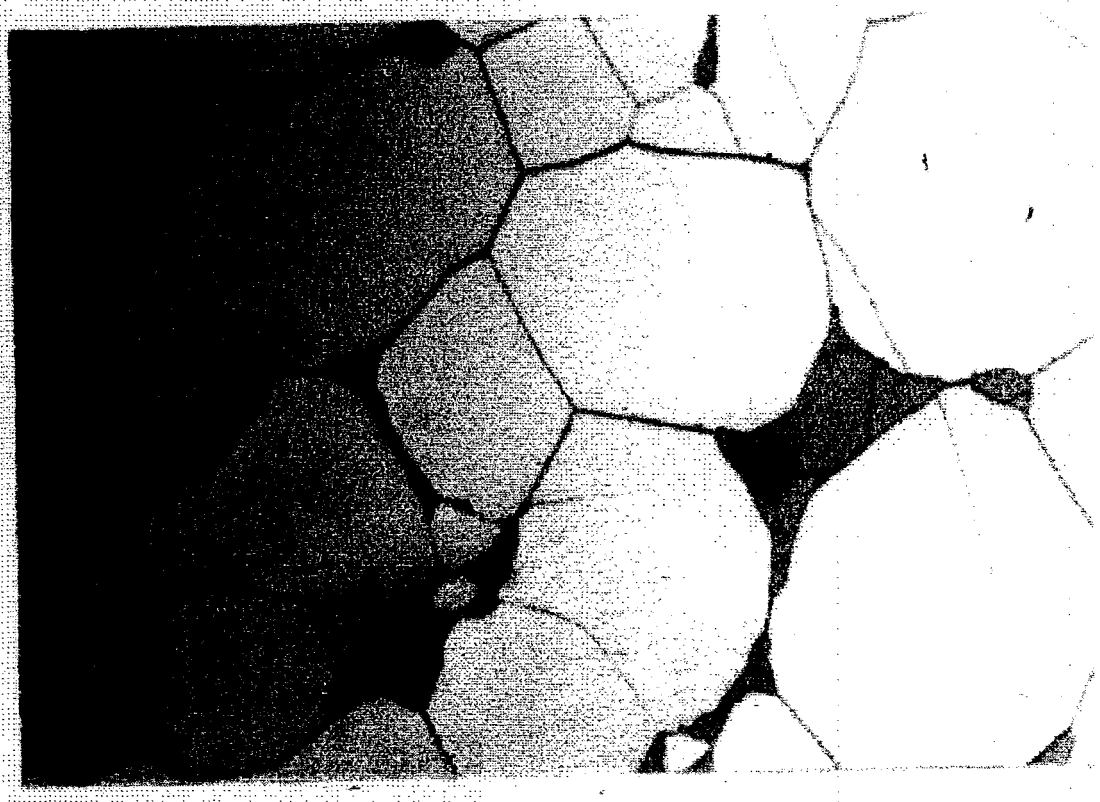

Fig. 15. Triple points of annealed chromite grains (LG6a) (width of field 1 mm = 1 cm).

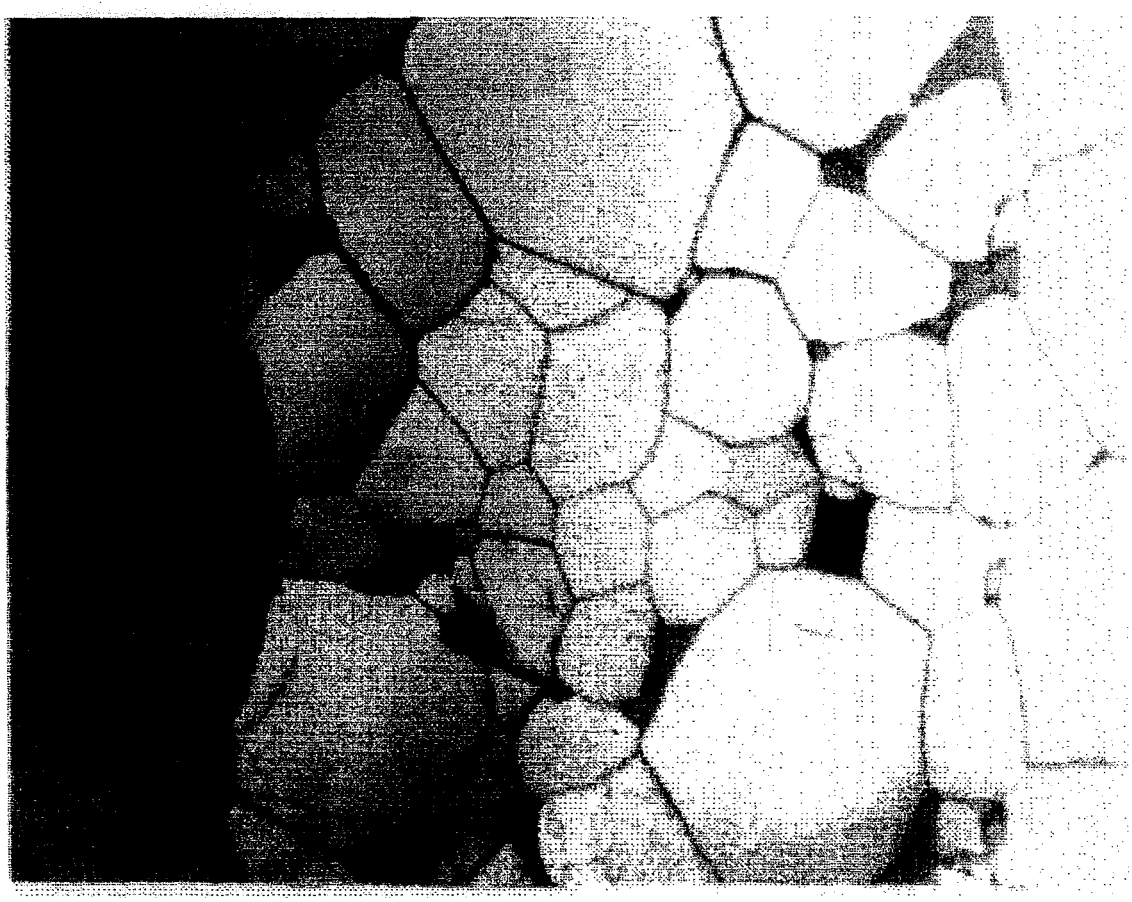

Fig. 16. Progressive annealing of the chromite grains to produce large grains. Carried to extremes, annealing would eliminate the smaller grains (width of field 1 mm = 1 cm).

5.2. Textural Description

In general, the mesocumulates and orthocumulates are the most common textural habit of the cumulate succession, with true adcumulates only rarely developed. In the former two mineral habits, the cumulus minerals tend to be subhedral and the intercumulus phases anhedral. The oikocrysts are generally subhedral and the poikilocrysts are well-rounded. The clinopyroxene grains in the CZ occur as both intercumulus material and as inclusions and from this it is seen that kinetic factors have played a controlling part in the crystallization of the minerals. A poikilitic texture is conventionally interpreted to indicate the crystallization sequence of the minerals and indicates that chemical reactions have occurred between the cumulus minerals and intercumulus liquid. Evidence for this are the large oikocrysts enclosing embayed remnant crystals. The same applies for remnant inclusions of clinopyroxene. Intercumulus overgrowth onto cumulus phases

is indicative of the order of crystallization, but where this phenomenon is observed it is typically intercumulus plagioclase overgrowing cumulus plagioclase (adcumulate growth) (Hughes, 1982).

Triple junctions are common in the chromitite layers, but rare in the silicate cumulates and from this it can be seen that true adcumulates have not developed to any extent in the silicate cumulate succession of the CZ. Triple junction and straight-line boundaries, when observed, are indicative of a subsolidus re-equilibration of the cumulate succession (Hughes, 1982). An igneous lamination, or preferred orientation of the minerals, indicates that crystal settling may have been the dominant process following fractionation. The preferred orientation may also result from compaction or it may be the product of magmatic currents during deposition of the cumulus phases (Hughes, 1982). This is further supported by the chromite stringers conforming to the preferred orientation of the cumulate minerals (Hughes, 1982).

The orthopyroxene grains characteristically display a fine-grained exsolution texture parallel to {100}. Slow cooling is postulated to result in the formation of these optically irresolvable augite lamellae (Hughes, 1982). Clinopyroxene often displays twinning and parallel exsolution lamellae of orthopyroxene. Bending of the exsolution lamellae is indicative of strain either exerted by the expansion of the forming crystal or an overall fabric being applied to the cumulate succession by the weight of the overlying cumulates. Alteration halos (reaction rims) enclosing the orthopyroxene grains may be explained by either (a) an increase in P_{H2O} in the residual pore fluid resulting in the lowering of the liquidus/solidus, with the result that the rims of the orthopyroxene grains were recrystallized, or (b) the influx of less primitive intercumulus fluid creating a chemical gradient resulting in the newly formed orthopyroxene crystals fractionating certain of the ferromagnesian constituents and crystallizing a new rim of orthopyroxene. Sericitic alteration is common in the cumulate succession and is the product of alteration of the primary rock-forming minerals, such as feldspars and mafic minerals. Where magnesium minerals are present in accessory amounts, chlorite will form.

6. Whole-rock Geochemistry - the Compositional Variations of a Portion of the CZ Cumulate Succession and the Effect of Plagioclase Crystallization

The stratigraphic interval under review in this chapter is the silicate succession from the LG6 pyroxenite footwall to the lower part of the uCZ in the Rustenburg section (fig. 17). The interval hosts the succession of chromitite seams from the LG6 to MG4a layers. Thirty samples were taken from a 45 m length of the 190 m CC2 drill core at a sampling spacing of approximately 1.50 m (Appendix C). The compositional trends of the host silicate cumulates aid in the interpretation of the compositional trends of the chromitite seams, as the compositions of the chromitites reflect the chemical evolution of their host environment (Teigler and Eales, 1993).

The compositional variations of the CZ cumulates and their constituent minerals have been shown to be related to the crystallization of cumulus plagioclase (Bence and Papike, 1972; Drake and Weill, 1975; Grove and Bence, 1977; Cawthorn and McCarthy, 1985; Eales *et al.*, 1993a). Whole-rock analyses reflect the cumulus mineralogy and superimposed fractionation effects.

The following trends characterize the CZ cumulate succession:

❒ The highest Al_2O_3 (fig. 18a) values are associated with the more evolved cumulate rocks, namely norites and anorthosites. Eales *et al,* (1993a) noted that the Al content of the orthopyroxene increases through the lCZ pyroxenites, with peak values recorded at the MG2 - MG3 chromitite level, and then declines above this level due to the appearance of cumulus plagioclase. Cumulus plagioclase crystallization causes a decrease in the Al content of pyroxenes. The Al variation of orthopyroxene is not reflected significantly in Al of the whole-rock, since the latter is governed by the plagioclase mode, as the Al content is governed to a large extent by intercumulus plagioclase and may reach several wt % in orthocumulates (Maier, pers. comm.)

❒ The highest TiO_2 values for the silicate lithologies (fig. 18b) are associated with the pyroxenites. Due to the relative incompatibility of Ti in plagioclase, it is assumed that at the lCZ - uCZ boundary the proportion of TiO_2 of orthopyroxene increases, although this is not reflected in the whole-rock composition. The Ti content of the chromitites is elevated in comparison to the host silicate cumulates due to the higher compatibility of Ti in Cr-spinels than in orthopyroxene and plagioclase (Maier, pers. comm.).

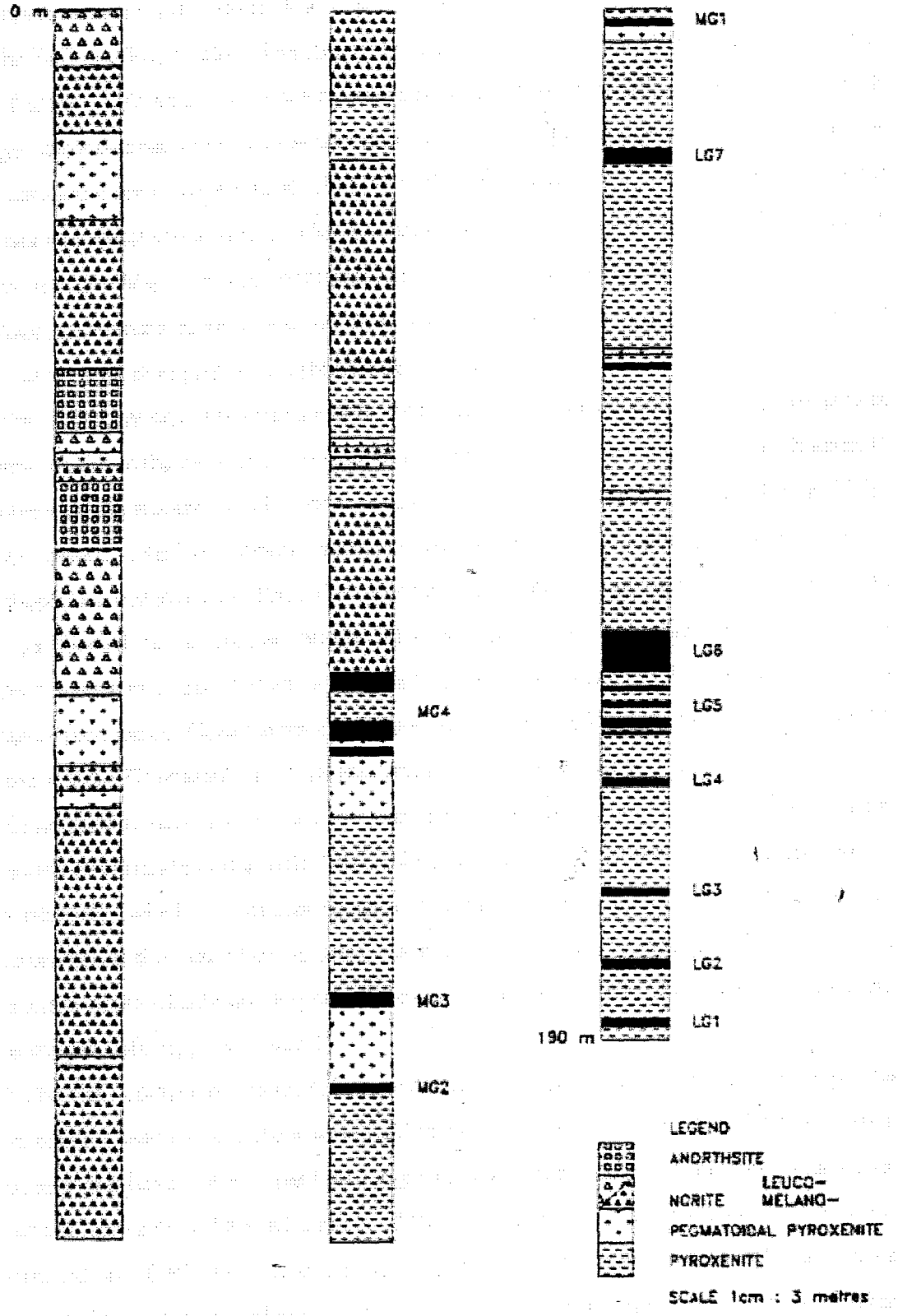

Fig. 17. The cumulate succession from the LG6 pyroxenite footwall to the lower part of the uCZ in the Rustenburg section, CC2 drill core.

❒ The FeO and MgO values decrease from olivine-rich units through to plagioclase-rich units. The highest MgO values are usually recorded in the most primitive (olivine-rich) cumulates, progressively decreasing in the orthopyroxene cumulates and lowest in the plagioclase-rich units. The chromitite seams have a relatively high FeO content (fig. 18c), due to the preference for Fe to enter into spinel-group lattices. The chromitites have a rather static MgO trend, corresponding to the fact that Mg is a major constituent of the magnesiochromite crystal lattice.

❒ Anorthosites commonly have lower SiO_2 than pyroxenites and norites because orthopyroxene has higher SiO_2 than plagioclase (Maier, pers. comm.)

❒ The Cr_2O_3 contents of the silicate host rocks decrease toward the top of the succession under review, that is, in the more evolved leucocratic rocks. The pyroxenites display the highest Cr_2O_3 contents of the silicate cumulus material and the anorthosites the lowest (fig. 18d and 19). The Cr_2O_3 content of the host cumulate rocks is in part a function of the partitioning coefficient of Cr in plagioclase and pyroxene. Plagioclase does not accommodate significant Cr, while Cr tends to be partitioned to a greater extent into orthopyroxene and clinopyroxene. In general, orthopyroxene contains ~ 0.4 wt % Cr_2O_3 and the clinopyroxene ~ 0.3 - 0.8 wt % Cr_2O_3. Cr has a higher partition coefficient in pyroxenes than plagioclase and due to fractionation of pyroxenes in the lCZ the Cr content of the magma will thus become depleted in Cr, resulting in a decrease in Cr up section. Additionally, the total Cr content of the host cumulates is governed by the modal amount of chromite in the rock. Pyroxenites generally contain more chromite than norites and anorthosites, which contributes to their relatively higher Cr contents. Chromite tends to accumulate at the base of cyclic units, but this is not always the case, and therefore, the modal chromite of the silicate lithologies will depend on the proportion of chromite fractionated from the magma (Maier, pers. comm.)

❒ The CaO content of the cumulate succession is regulated by crystallization of plagioclase. Pyroxenites tend to have the lowest CaO values (fig. 18e) due in part to their low plagioclase content and hence, plot in the lower right corner of the diagram. With increasing plagioclase content up section the CaO content of the stratigraphic column displays an overall increase. Although low CaO values characterise the pyroxenites, the CaO content of these rocks can be attributed to minor Ca within the orthopyroxene lattice, the CaO content of clinopyroxene and the modal proportion of intercumulus plagioclase in the pyroxenites.

❒ Pyroxenites have the lowest Na_2O content of the host silicate rocks (fig. 18f). Eales *et al,* (1993a) report that in plagioclase-poor units pyroxene is enriched in Na. With crystallization of cumulus plagioclase the Na_2O content of the pyroxenites decrease. The higher Na_2O values associated with the more evolved rocks up section are attributed to the modal increase in cumulus plagioclase. Massive chromitite contains very low Na_2O values, corresponding to the spinel crystal lattice structure which has a higher site preference energy for Mg and Fe. The Na_2O component of the massive chromitite seams generally reflects modal plagioclase content of the rock.

❒ The V distribution pattern is dependent on the modal percentage of orthopyroxene and plagioclase in the system. Pyroxenites tend to display high V values (fig. 18g) as a response to the presence of accessory chromite and clinopyroxene and the high partition coefficients of V for pyroxene and chromite (Teigler, 1990). In other words, the V trend of the host silicate cumulate succession is inversely related to the proportion of plagioclase and directly proportional to the pyroxene and chromite content of the rock.

❒ Ni may be used as an indicator of fractionation, as it is strongly partitioned by olivine and to a lesser extent by orthopyroxene and chromite, but rarely by plagioclase. However, since Ni also has a very high partition coefficient into sulphide melt, sulphide segregation may deplete the Ni content of the magma. Lee and Fesq (1986) attribute the slightly higher Ni concentrations in the uCZ to possible sulphide control. In the absence of sulphides, the Ni content through a cyclic unit is inversely related to the modal increase in plagioclase (Schürmann, 1991).

❒ The Sr content (fig. 18h) of the host silicate rocks is almost totally dependent on the modal proportion of plagioclase as Sr tends to be strongly partitioned into plagioclase in comparison to orthopyroxene and clinopyroxene. Sr behaves as a residual element in the melt until plagioclase crystallizes, thereafter the concentration of Sr steadily decreases in the magma.

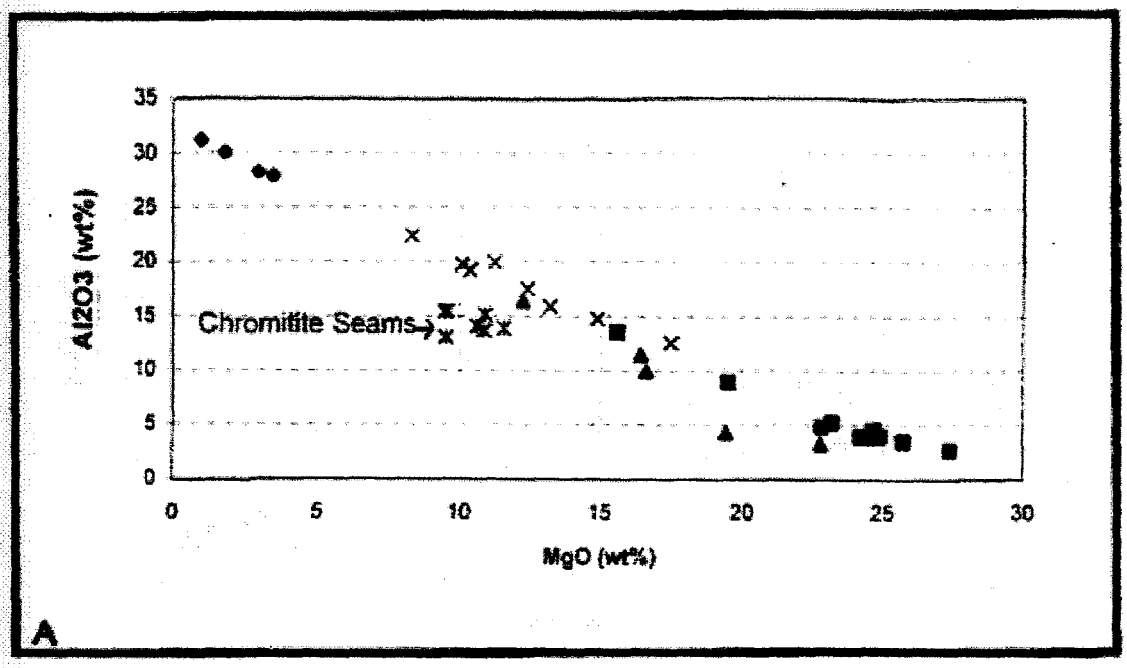

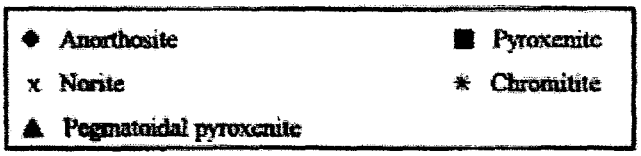

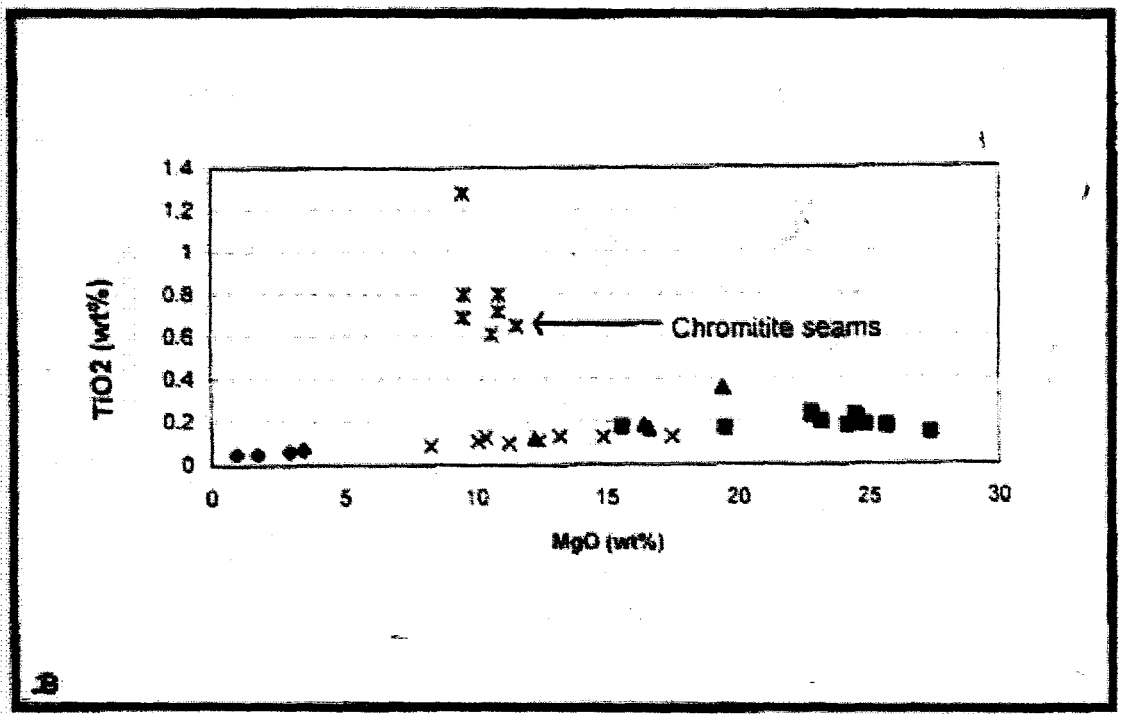

Fig. 18 a & b. Inter-element relationships with MgO for a portion of the cumulate succession, Rustenburg section.

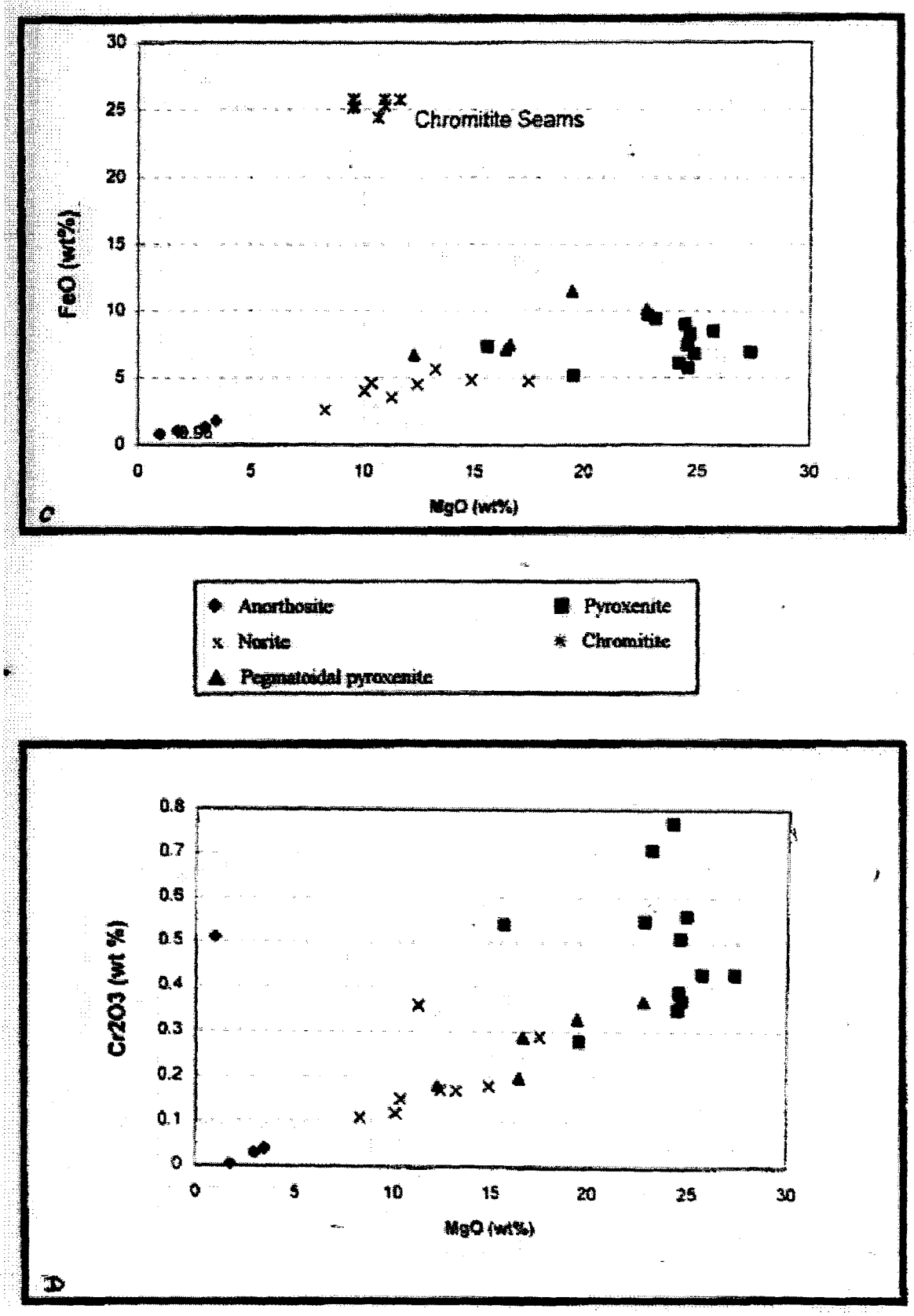

Fig. 18 c & d. Inter-element relationships with MgO for a portion of the cumulate succession, Rustenburg section. Fig 18 d excludes the chromitite data.

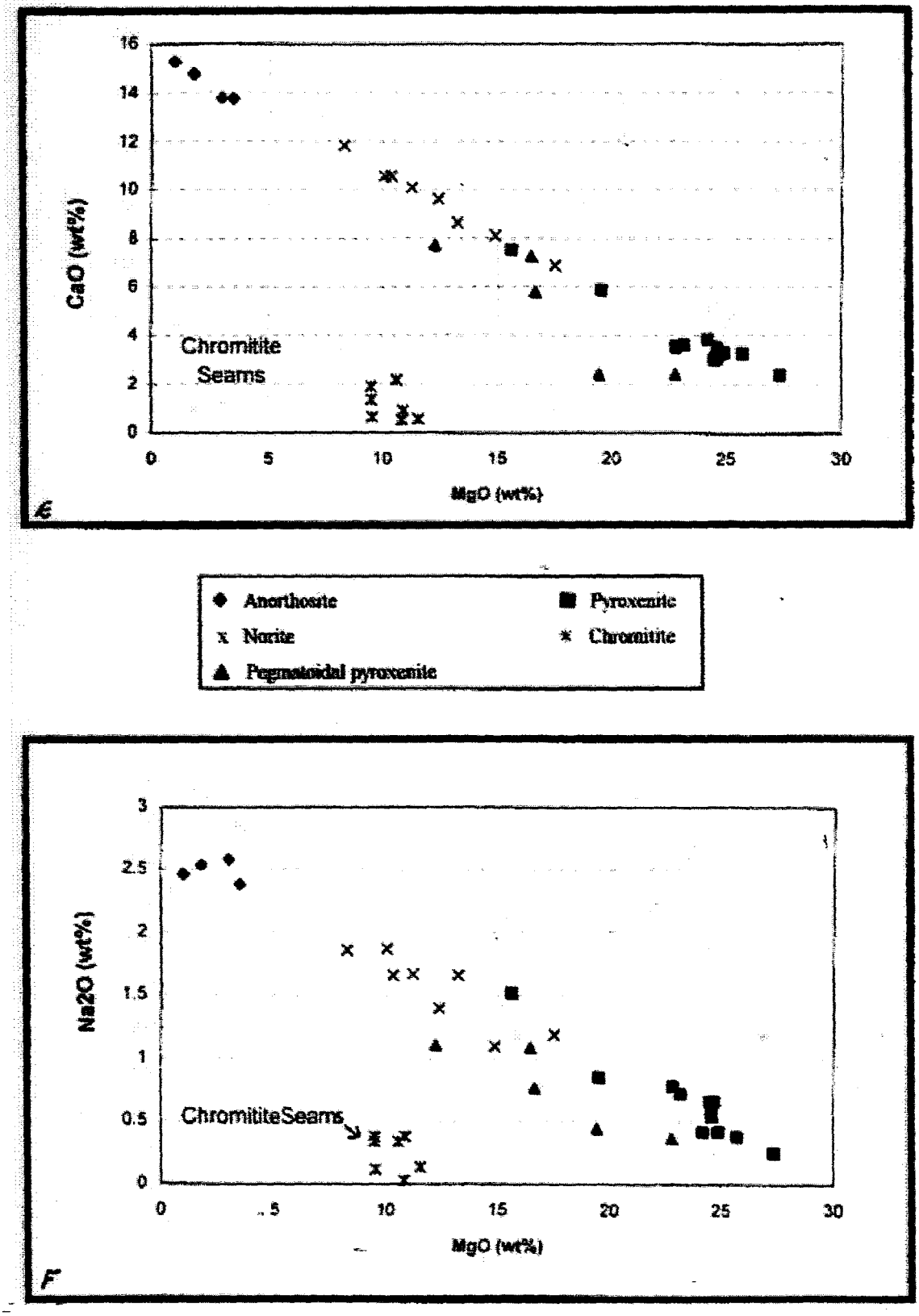

Fig. 18 e & f. Inter-element relationships with MgO for a portion of the cumulate succession, Rustenburg section.

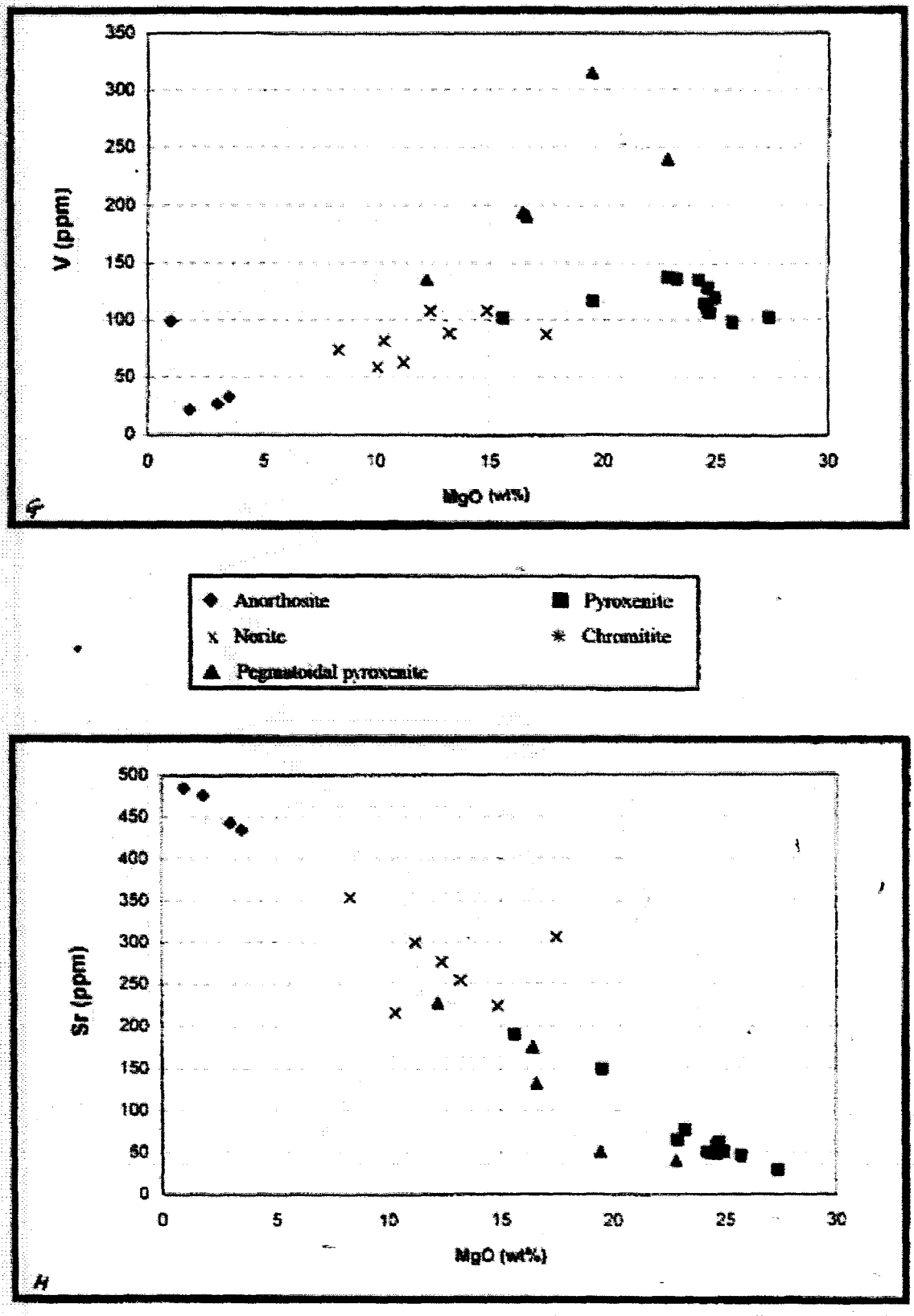

Fig. 18 g & h. Inter-element relationships with MgO for a portion of the cumulate succession, Rustenburg section.

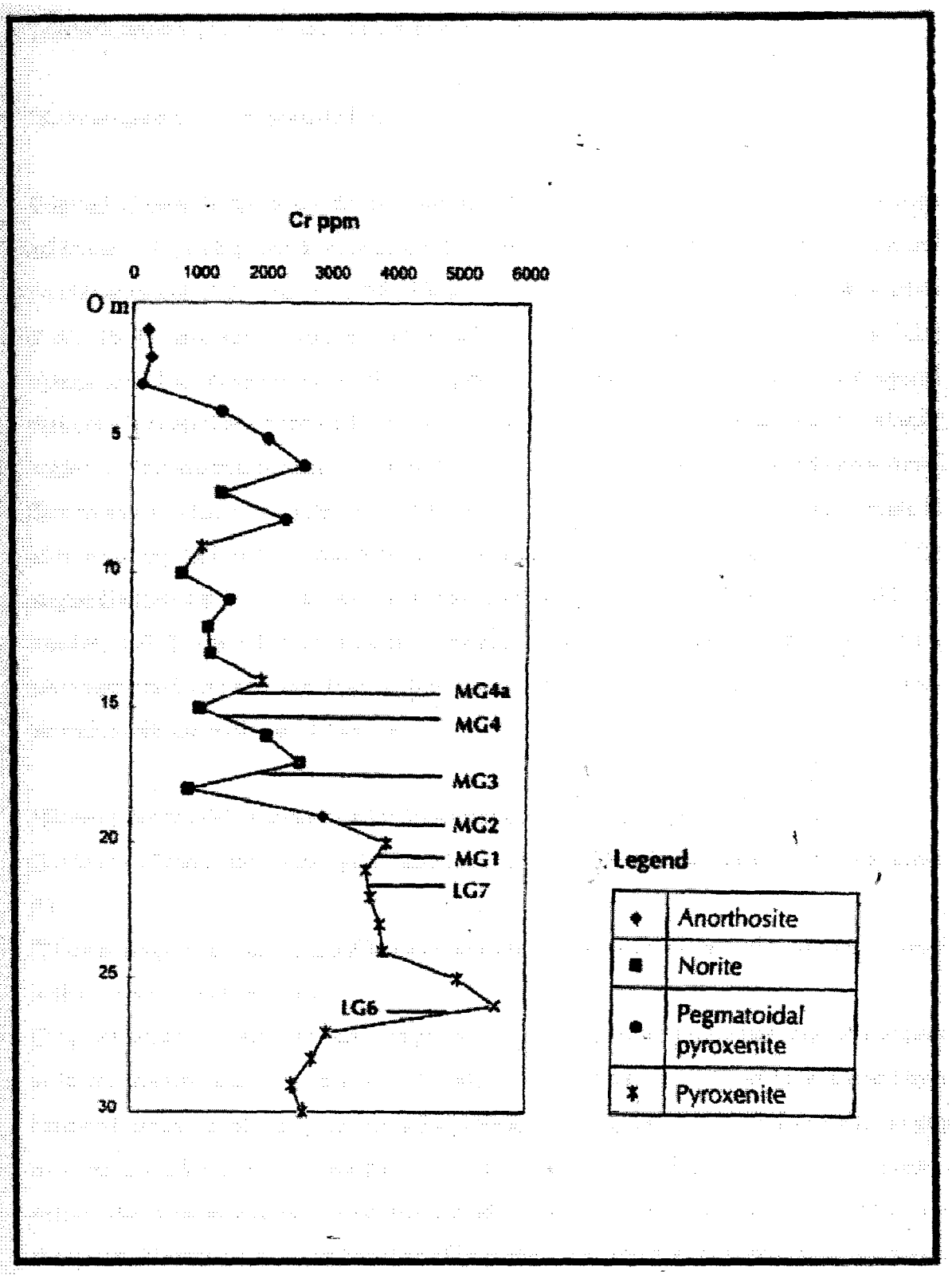

Fig. 19. Variations in Cr_2O_3 content of a portion of the CZ cumulate succession, Rustenburg section, as indicated by whole-rock analysis.

7. Geochemistry of the LG and MG Chromitite Seams

7.1. Petrogenesis of Chromitite Layers

A myriad of research studies and theories (Irvine, 1967; De Waal, 1975; Cameron, 1980; Sharpe and Irvine, 1983; Hulbert and Von Gruenewaldt, 1985; Campbell and Turner, 1986; Hatton and Von Gruenewaldt, 1987; Hatton, 1988; Hatton *et al.*, 1989; Scoon and Teigler, 1994; Mathez *et al.*, 1994) have sought mechanisms by which the massive chromitite layers of the RLS crystallized. The consensus is that the precipitation of copious volumes of chromite in layered intrusions is controlled by the Cr_2O_3 content of the magma, magma rejuvenation and mixing of resident and replenishing magmas, onset of plagioclase crystallization (magma chamber overturn) (Scoon and Teigler, 1994; refer to fig. 21), cotectic crystallization of chromite and silicate in addition to crystallization of chromite alone (Sharpe and Irvine, 1983), oxidation state of the magma (Hulbert and Von Gruenewaldt, 1985), oxygen fugacity (fO_2) and temperature (Hill and Roeder, 1974). The effect of pressure is generally considered negligible. Interaction of the aforementioned controls can lead to the formation of either chromite-poor silicate rocks, chromitite-silicate rocks, or chromitite.

Hill and Roeder (1974) summarise the following controls on chromite crystallization:

- Addition of chromium to the system stabilizes the Cr-spinel at higher temperatures and lower fO_2.
- Lower temperatures and higher fO_2 result in a progressive increase in modal volume of spinel within the spinel stability field.
- Spinel ceases to crystallize when plagioclase and clinopyroxene precipitate, only to reappear at lower temperatures. The cessation of spinel crystallization is postulated to be caused by a reaction between spinel, clinopyroxene and liquid and a lowering in the fO_2. At higher fO_2 no gap in spinel crystallization is evident due to increased ferric iron stabilizing the spinel to a greater extent. The increase in ferric iron content would combat the decreasing amount of chromium in the system. Variation in the oxidation state of iron affects the liquidus temperatures of the phases crystallizing.
- At high fO_2 large volumes of spinel crystallize over a small temperature gradient, due to the

high ferric iron content.

❒ At lower temperatures trace amounts of chromium enter into phases such as clinopyroxene more readily.

Oxygen fugacity (fO_2) is an important control in magmatic systems. In conjunction with TiO_2, fO_2 has an important effect on the Cr:Fe ratio of chromitite layers, in that the two components determine whether chromite is an early crystallizing phase and therefore has a high Cr:Fe ratio, or whether it crystallizes late and hence has low Cr:Fe values (Stowe, 1987).

Using experimental data, Sharpe and Irvine (1983) demonstrate that two parental magmas (U- and A-type), each with chromite on their respective liquidi at elevated fO_2, together with a silicate mineral, will produce cumulates with accessory chromite. Mixing of the two magma types could result in a depression of the respective silicate liquidi in a eutectic-like fashion, with the result that chromite is the sole liquidus phase for a large variety of intermediate compositions.

The phase-diagram model of Irvine (1977) (fig. 20) attempts to account for chromite crystallization and the compositional variations of the Bushveld Complex chromitite layers. The phase diagram models the system MgO-Cr_2O_3-SiO_2. The curved cotectic boundary between olivine and chromite is such that two mineral phases can coprecipitate, with the proportion of chromite to olivine progressively decreasing. At the intersection of the cotectic with the orthopyroxene field, two reaction boundaries extend, these being between olivine and orthopyroxene and between orthopyroxene and chromite. The effect of this during fractional crystallization is that as orthopyroxene crystallizes from the magma that has descended the cotectic, olivine and chromite cease to crystallize (Irvine, 1977).

In fig. 20, mixing of an evolved melt B with a primitive liquid of composition A results in a hybrid/mixed magma C, which lies in the primary phase field of chromite. Chromite crystallizes from the mixed magma until such time as the cotectic surface is intersected. With each successive influx of primitive magma the system follows essentially the same pathways. However, with each cyclic unit (section 7.8) the system evolves slightly, with the result that for each successive chromitite seam precipitated the overall chemistry will be slightly different.

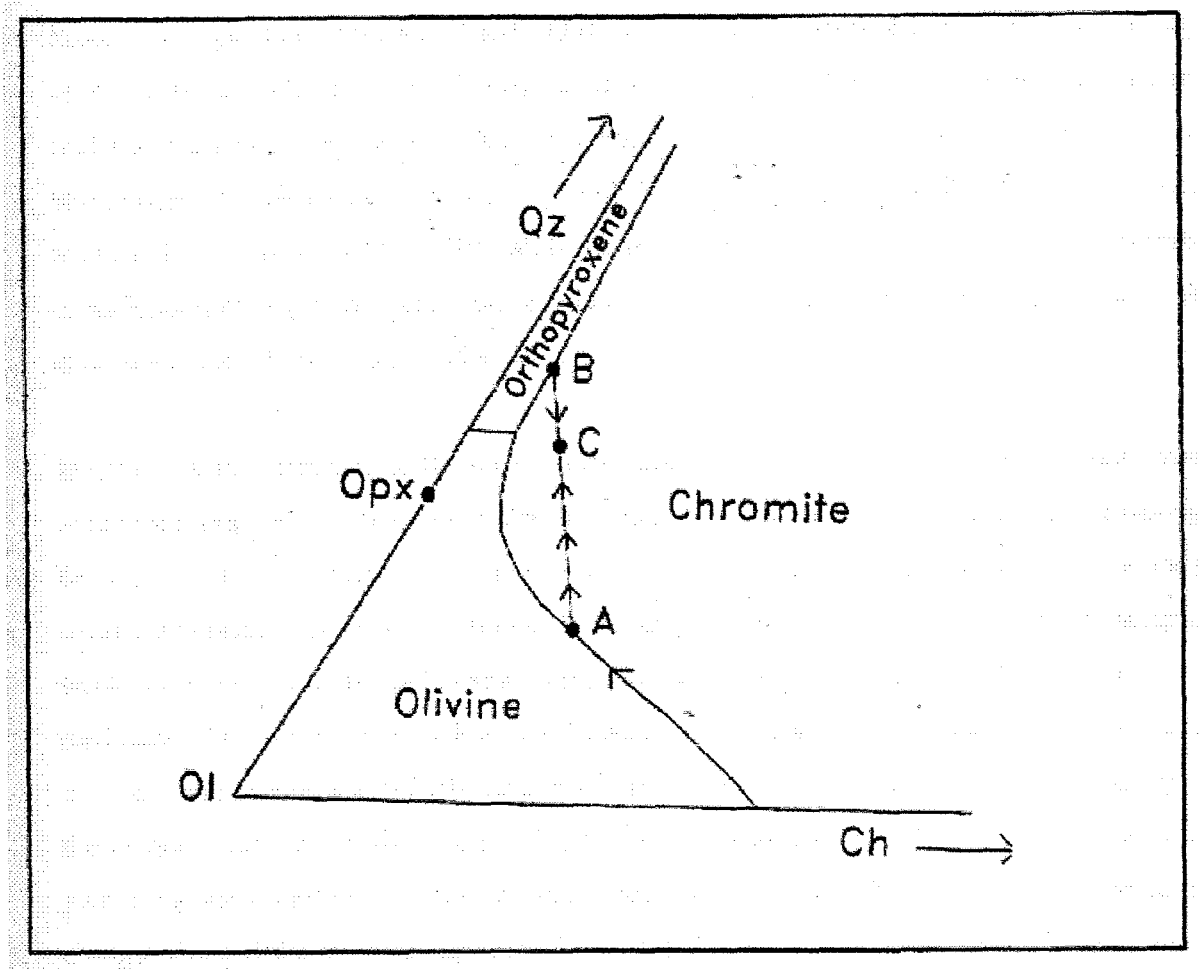

Fig. 20. Phase-diagram model illustrating the formation of the Muskox chromite-rich layers (from Irvine, 1977).

The oxidation state and Cr_2O_3 content of the magma control the volume of chromite that will crystallize. Hulbert and Von Gruenewaldt (1985) propose that the Cr-rich Bushveld magmas contained too low a volume of Cr^{3+} to stabilize chromite during emplacement, but oxidation of the magma accompanied by fractional crystallization would stabilize the chromite in order to precipitate essentially monomineralic chromitite seams.

Scoon and Teigler (1994) propose that influx of replenishing magma of grossly similar composition, magma mixing, differentiation with height, and fractional crystallization led to the formation of the chromitite seams and cumulate succession of the CZ. They attribute the lack of major isotopic inflections in the CZ to the fact that the resident magma was not replenished by a magma of grossly dissimilar lineage.

Scoon and Teigler (1994) propose that the LG1 - LG4 chromitite seams are the product of mixing of lCZ magma with primitive LZ magma, that the LG5 - MG1 seams are the product of replenishing magma mixing with lCZ (pyroxenitic) resident magma, and the MG2 - UG1 chromitites crystallized as a result of replenishing magma mixing with uCZ (noritic) resident magma. The formation of the LG5 - MG1 chromitite seams is attributed, in part, to fractional crystallization of plagioclase which serves to increase the compositional contrast of the parental magma and the differentiated resident fluid.

Influx of magma compositionally similar to the resident magma may occur either as basal flows or fountains (see fig. 21) (Scoon and Teigler, 1994). The majority of workers argue that mixing between replenishing and resident magmas occurs once the resident magma has undergone cooling and plagioclase crystallization and has become denser. The replenishing lighter magma would intrude as a fountain and mixing of the two magmas would be facilitated by this intrusive mechanism (Maier, pers. comm.). Scoon and Teigler (1994) propose that crystallization of olivine, chromite, and pyroxene lowers the density of the resident magma, and together with cooling of the magma would allow the mixing with the replenishing denser, hotter magma. Basal flow permits the lateral mixing of the resident and replenishment magmas, thereby facilitating the facies changes along strike from the supposed feeder site (Union section) to the distal (Brits section) facies. Scoon and Teigler (1994) propose that the magma arrived in the distal facies by basal flow, at the crystal-liquid interface, whereas fountains may have been influential in the proximal facies. In addition, the magma flow will evolve away from the putative feeder site as a result of continual mixing at the basal flow front, resulting in the following:

- The proximal facies (Union section) will be characterized by basal flows rich in chromite, olivine and pyroxene.
- The distal facies will be distinguished by a predominance of cumulus plagioclase, the result of the basal flows being dominated by resident liquid.

Subsequent to the crystallization of copious volumes of plagioclase in the distal facies, Al would be depleted and Cr enriched in the resident magma. Future influxes of primitive magma would mix with this Cr-enriched and Al-depleted resident magma, giving rise to the low Al content and elevated Cr_2O_3 content of the MG seams in the Brits area (Scoon and Teigler, 1994).

The basal flow and, consequently the evolution path of the magma would be influenced by the compartmentalization of the western Bushveld Complex by tectonics, such as the Spruitfontein and Kookfontein Upfolds. The Spruitfontein Upfold formed prior to or during the early stages of magma chamber development, thereby influencing the magma supply to the distal facies, but only up to the MG1 chromitite level. The Upfold inhibited the lateral basal flow to the distal sectors, resulting in the composition of the CZ differing on either side of the Upfold. Subsequent influxes of primitive magma responsible for the compositional variations in the lCZ and uCZ rocks, would not have been able to replenish the resident magma east of the Spruitfontein Upfold, resulting in variations in composition and thickness of the chromitite and silicate successions in the Marikana and Brits sections.

In conclusion, the compositional and morphological differences between the proximal and distal facies are as follows:

- In the distal facies the MG chromitites have higher Cr_2O_3 values.
- The MG1 chromitite has unusually high Al concentrations in the Brits area.
- The LZ is poorly developed in the distal facies.

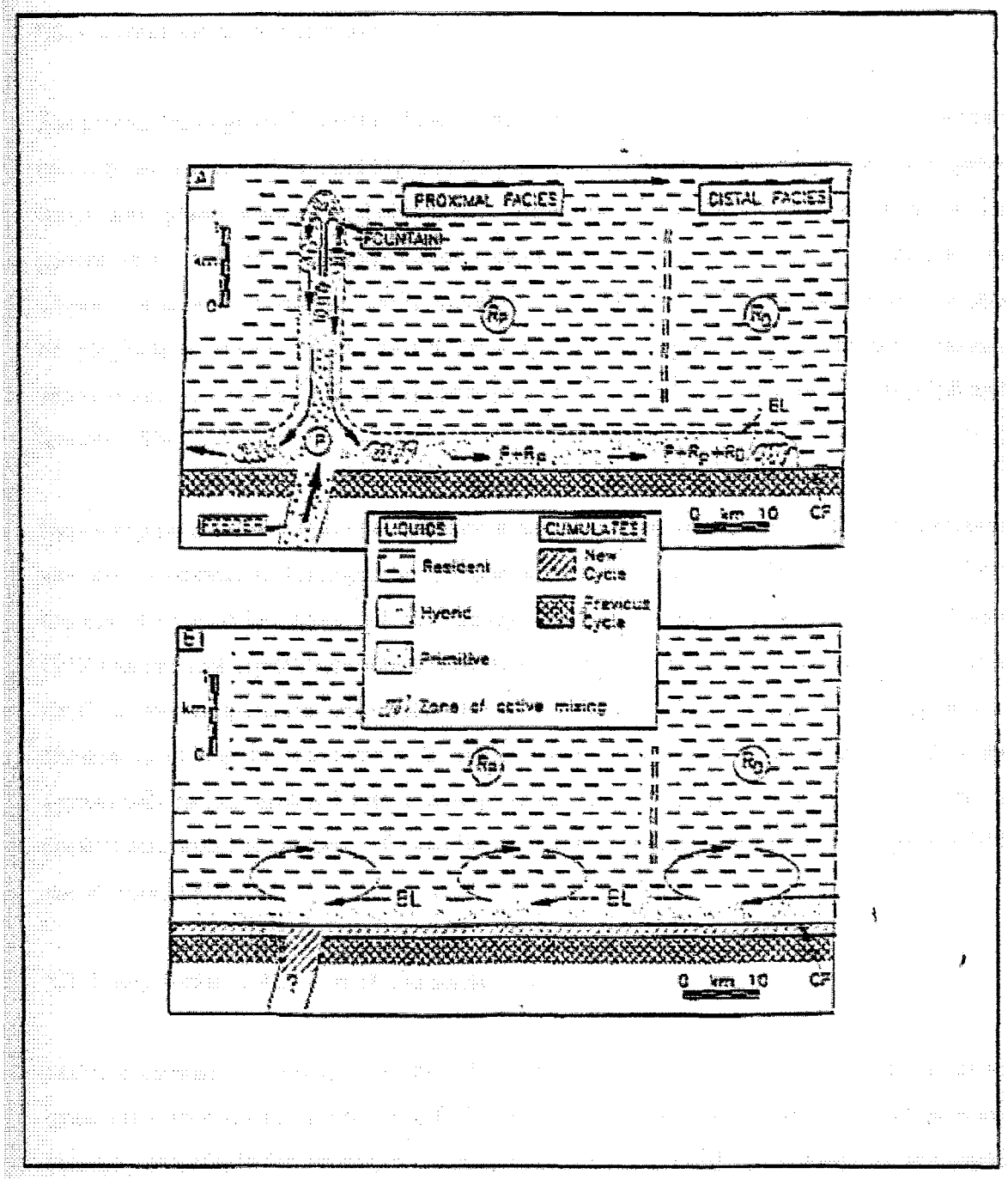

Fig. 21. Replenishment and magma mixing with resident magma. Parental magma (P) enters chamber as fountains into the proximal resident liquid (R_p) or as basal flow into the distal resident magma (R_D) above the crystal pile (CP). The basal flow creates a boundary layer (BL) and resident and replenishing magmas mix to create a hybrid fluid (P + R_p in proximal areas). The hybrid magma experiences increased differentiation towards the distal areas (P + R_p + R_D). Overturn of the chamber occurs and the BL breaks down to allow complete mixing of the basal layer and the resident liquid (from Scoon and Teigler, 1994, 1112).

7.2. Characteristics of the Parental Cr-rich Magma

The greater the degree of partial melting of the mantle, the higher the concentration in the melt of components such as Cr, Fe and Mg, and the greater the depletion in Ca, Na, K and Al. Higher-temperature phases are the initial phases to crystallize out of the melt after emplacement, in the general order: olivine → orthopyroxene → clinopyroxene. A primitive upper mantle melt, in general, contains ~60 % olivine, ~20 % orthopyroxene, ~10 % clinopyroxene, and minor amounts of plagioclase, spinels, mica, zircon, apatite, and hornblende. Orthopyroxene contains approximately 0.4 wt % Cr_2O_3 whilst clinopyroxene contains ~ 0.4 - 0.8 wt % Cr_2O_3 (Hill and Roeder, 1974).

Depending on the mineral phases crystallizing, the Cr content of the melt is affected in varying manners. In the event that clinopyroxene is one of the primary mineral phases to crystallize from the melt, Cr would be partitioned into clinopyroxene and become depleted in the melt. Irvine (1967) reports that crystallization of a copious volume of clinopyroxene containing up to 1.0 % Cr_2O_3 at low temperatures can deplete the Cr_2O_3 content of the melt to such a degree that chromite is no longer a stable phase. If orthopyroxene crystallizes first, the amount of Cr in the system will be less depleted than if clinopyroxene crystallized first, thereby resulting in the possible enrichment of the melt in Cr and hence crystallization of massive chromitite seams (Hill and Roeder, 1974).

7.3. Compositional Features of Chromite

Massive chromitite is physically more stable and less likely to be hydrothermally altered or re-equilibrated with adjoining silicates at falling temperatures than the majority of the silicates and accessory chromite in the magma, and is thus a useful tool in revealing variations in the parental magma composition. Chromite is an early crystallizing phase and is highly responsive to the conditions existing in the magma chamber and is a useful indicator of the degree of differentiation (Thayer, 1970).

The element Cr has the highest site preference energy in the spinel structure and will preferentially

enter into the spinel prior to iron or aluminium. De Waal (1975) noted that in order to account for the tetravalent cations in the chromium spinels, which are not simple $M^{2+}M_2^{3+}O_4$-type spinels, the Bushveld Complex Cr-spinels must contain a small proportion of ulvöspinel-type ($M_2^{2+}M^{4+}O_4$) solid solution. Progressing up stratigraphy from the pyroxene-rich cumulate succession to the plagioclase-rich succession, the $M_2^{2+}M^{4+}O_4$ content increases from around 3.5 per cent to 4.0 per cent (De Waal, 1975).

The effect of major elements within Cr-spinels generally result in the following trends:

- Cr and Al are strongly negatively correlated.
- The main exchange in the trivalent cation site is between Cr and Al, with Fe^{3+} increasing as Mg decreases (De Waal, 1975). Al will substitute for Cr in small amounts. However, plagioclase competes for Al. Therefore, at the onset of plagioclase crystallization a decrease in Al content of the chromite might be expected (Maier, 1998, pers. comm.).
- With decreasing magnesium, Cr decreases and Al and Fe^{3+} show an increase.

The following trends in the variations in the amount of oxides present in the Cr-spinels are documented in De Waal's (1975) work:

- V_2O_5, TiO_2, and Fe_2O_3 show a good correlation and, together with FeO, Al_2O_3, NiO and ZnO, generally increase towards the top of the sequence, due to the ability of the iron and titanium to stabilize the Cr-spinel at lower temperatures and in the absence of chromium.
- The MnO content of the Cr-spinel remains roughly constant. Comparison with De Waal's work (1975) and the compositional trends of the silicate cumulates (chapter 6) and the chromitite layers (7.4) indicates that V_2O_5, TiO_2, and NiO contents of the silicate cumulates increase to the top of the CZ. The Al_2O_3 content of the silicate cumulates decreases due to the crystallization of cumulus plagioclase, whereas the Al_2O_3 content of the chromitite layers increases from the LG6 to MG4 layers. The FeO content of the silicate cumulates decreases to the top of the CZ but increases in the chromitite layers through the same interval.

7.4. Strike Variations of Cr_2O_3 Content and Cr:Fe Ratio for the LG6 to MG4 Chromitite Seams

Fifty three chromitite samples were analysed for major elements by XRF spectrometry. Strike comparison of the geochemistry of the LG and MG chromitite seams, based on whole-rock chemical data, was undertaken in an effort to document strike variations and to propose generalized scenarios for the origin of the chromitite in the CZ for the sectors extending from Ruighoek to Marikana-Brits (see appendix I for sampling localities). The reader is referred to section 4.3 for across-seam compositional variations. Host rock composition will influence the chemistry of the chromite and chromitite (chapter 6). However, sampling of the host rocks was beyond the scope of this study.

Due to the paucity of outcrop in the western Bushveld Complex, 1 - 2 kg samples were taken from available sites such as quarries, pits and underground mining operations. Borehole core from various areas was also sampled. No grid was employed in order to sample the seams, rather samples were gathered where possible and at the discretion of the mining companies involved. Samples were taken from the middle of the seams in order to avoid silicate contamination from the cumulate host rocks.

At the majority of the sampling points (Appendix I), only the LG6, and MG1 to MG4a chromitite seams are exposed by the mining operations. It was, however, possible to sample the entire chromitite stratigraphy from the LG1 to the MG4a chromitite seam in the Ruighoek section (section 7.5). The LG chromitite seams are absent or poorly developed in the Marikana and Brits sections and where thin chromitite seams do occur below the MG chromitite seams in these sections, correlation with the LG seams further west is tenuous (Davey, 1992). The reader is referred back to section 3.1.1 on the lithostratigraphy of the LG seams across the western Bushveld Complex. The paucity of exposed or developed LG1 - LG5 chromitite seams restricted this study to the geochemical examination of the LG6 to MG4a chromitites. The findings and theories suggested below validate the proximal-distal facies model of Eales *et al*, (1988), where it is proposed that the magma flowed away from the supposed proximal (Union section) site towards the distal facies.

7.4.1. Cr_2O_3 Content

In figs. 22 a - d, the Cr_2O_3 content and Cr:Fe ratio trends for the LG6, MG1, MG2 and MG3 chromitites are plotted. Due to the paucity of exposed MG4 chromitite across the western Bushveld Complex, the Cr_2O_3 content and Cr:Fe ratio of this seam were not investigated.

The Cr_2O_3 content of the chromitite seams, with the exception of the LG6 and LG6a chromitite seams, increases eastwards from the more proximal Ruighoek section to the Marikana/Brits section, representing the distal facies. The chromitite seams in the Boshoek section, however, display anomalously low Cr_2O_3 concentrations in comparison to the remaining sectors.

In contrast to the MG chromitites, the Cr_2O_3 content and Cr:Fe ratio of the LG6 and LG6a chromitite seams display a smooth trend from Ruighoek to Rustenburg, with values decreasing eastwards toward Brits. The compositional variability of all the chromitites away from the proximal site is gradational.

The increase in Cr_2O_3 content of the MG seams from the Ruighoek section eastwards may be attributed to chromite crystallizing early in the Marikana/Brits area, induced by both physical and chemical factors, such as floor irregularities and/or upfolds, rapid heat dissipation, and the early crystallization of plagioclase in the more distal facies. Eales *et al,* (1988) attribute the increased thickness of the MG and UG chromitites away from the proximal facies area to advanced compositional contrast between supernatant and replenishing magmas in the distal facies. This contrast enhances the nucleation of chromite from the parental magmas during mixing. This statement can also be invoked to explain the elevated grades of the MG chromitites towards the distal facies. Early crystallisation of plagioclase in the distal facies would result in an Al-depleted and a Cr-enriched magma, which would mix with the replenishing magma and this may have led to the deposition of chromitite seams with elevated Cr_2O_3 contents (Scoon and Teigler, 1994).

7.4.2. Cr:Fe Ratio

The Cr:Fe ratio of the chromitite seams mimics the Cr_2O_3 trends. In figs. 22 b - d, the Cr:Fe ratio

trends for the MG1, MG2 and MG3 display an increase towards the Marikana/Brits area. The Cr_2O_3 and Cr:Fe ratio of the LG6 and LG6a seams, however, decrease eastwards away from the Ruighoek section.

The increase in the Cr:Fe ratio of the MG1, MG2 and MG3 chromitites from proximal to distal facies is related to the early crystallization of plagioclase in the distal facies which would result in an enrichment of Cr and a depletion of Al of the magma and hence elevated Cr_2O_3 grades of the MG chromitite seams. The proximal to distal decrease in the Cr:Fe ratio of the LG6 and LG6a chromitite seams is not well understood or defined. The LG6 and LG6a chromitites appear, in contrast, to become more evolved towards Brits. This may be the result of limited plagioclase crystallisation in the more distal facies of the western Bushveld Complex during formation of the LG chromitite seams, hence there was no Cr-enrichment of the magma to produce elevated Cr:Fe ratios (Maier, pers. comm.).

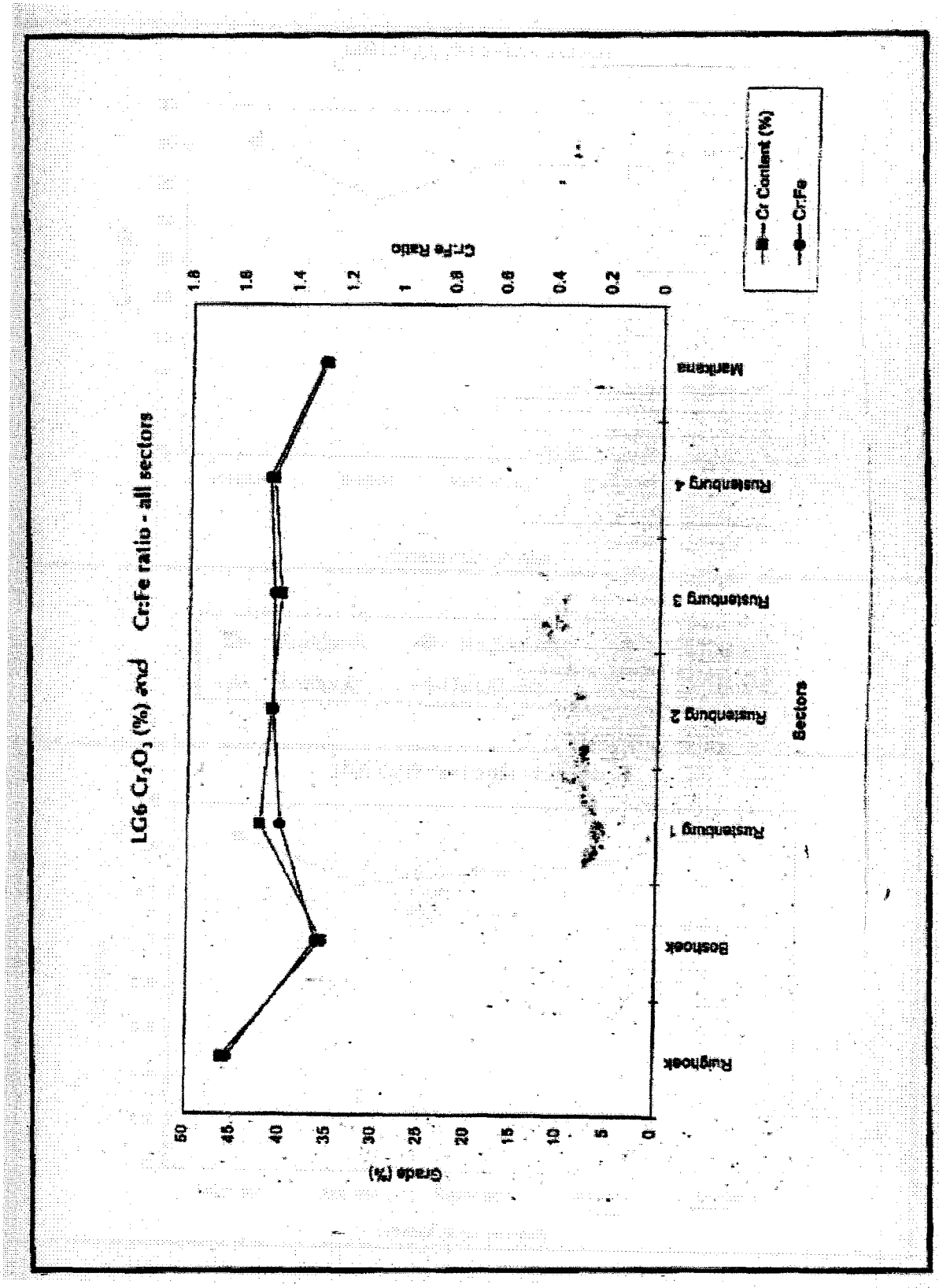

Fig. 22a. LG6 Cr_2O_3 content and Cr:Fe ratio strike variations.

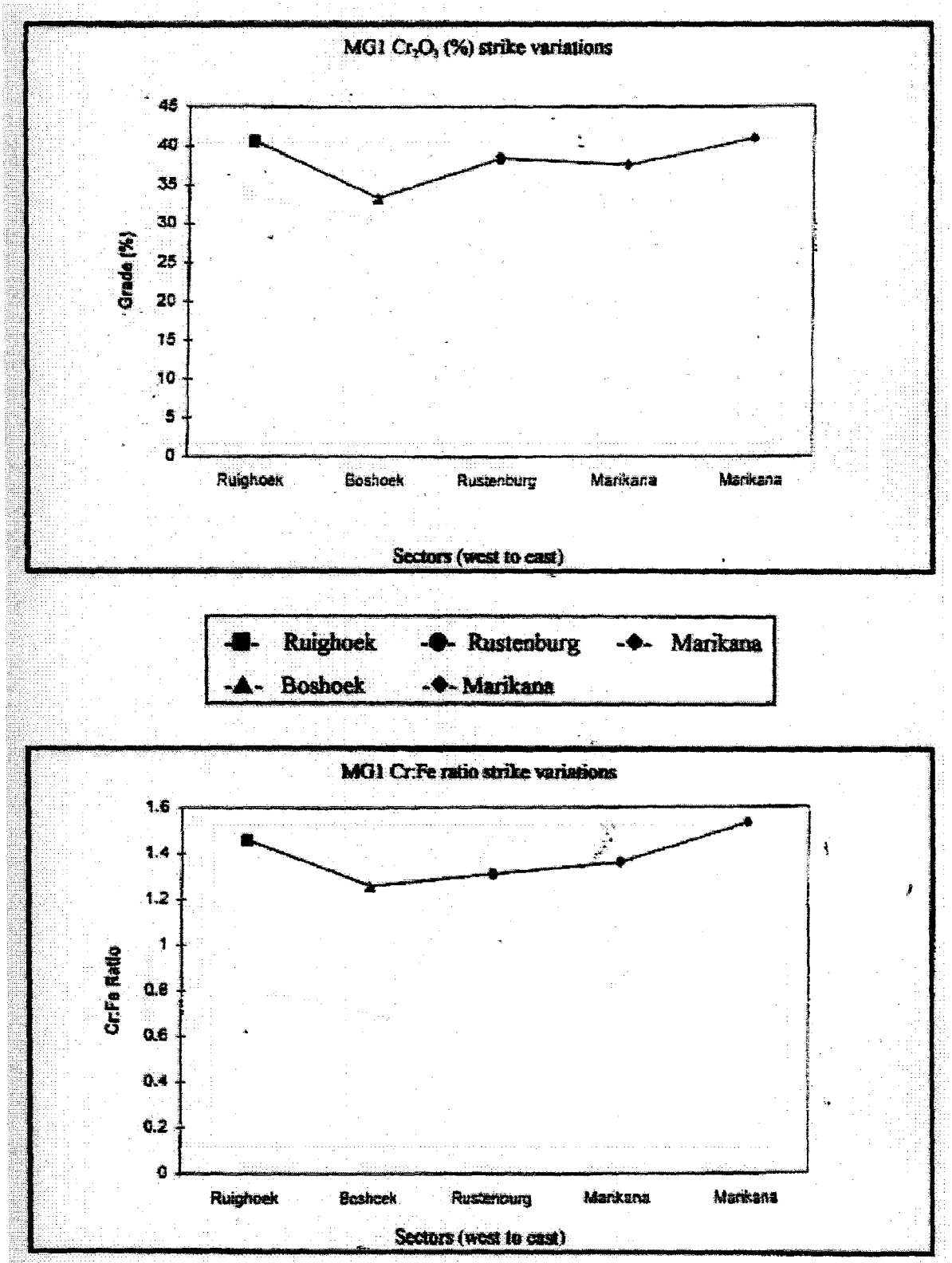

Fig. 22b. MG1 Cr_2O_3 content and Cr:Fe ratio strike variations.

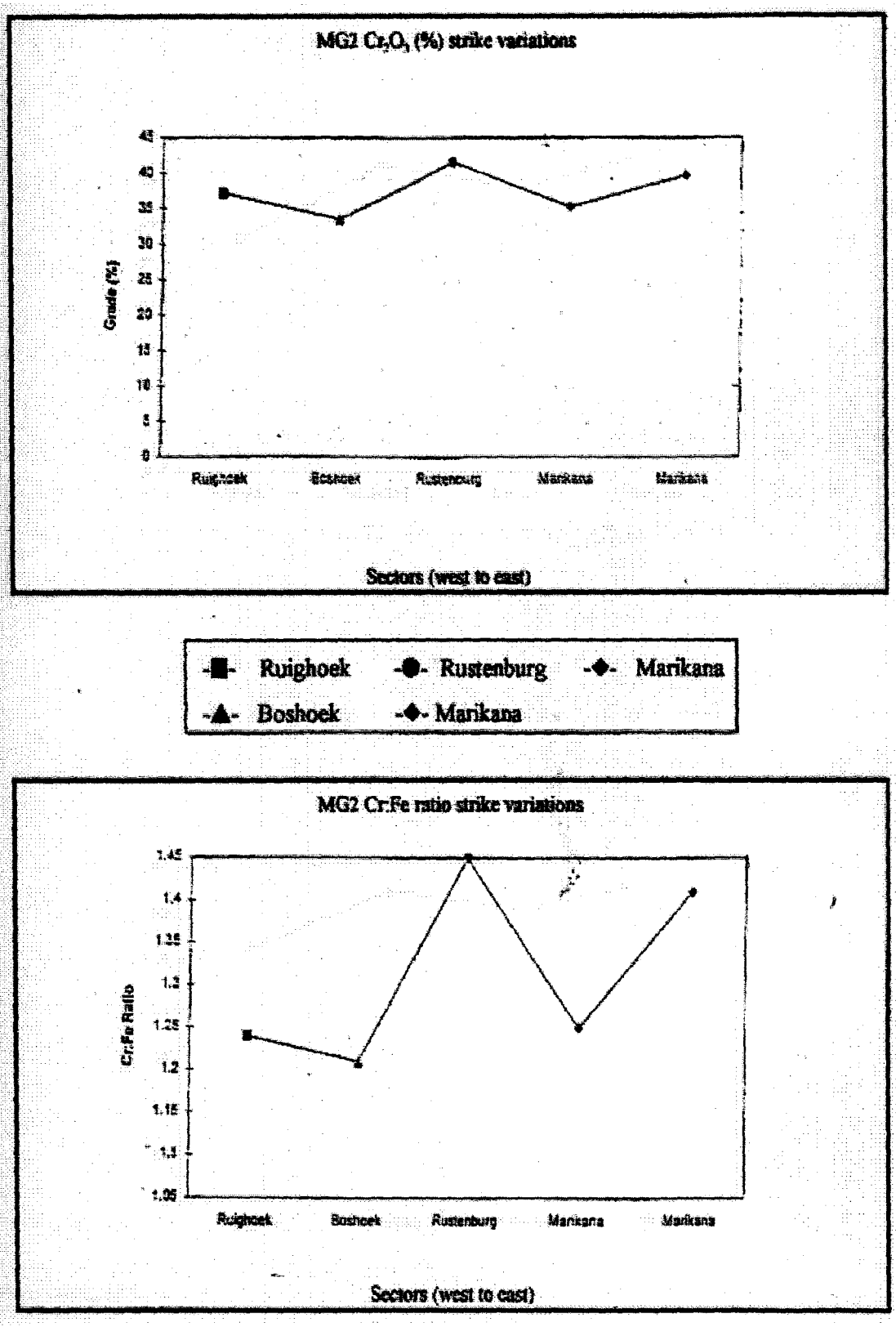

Fig. 22c. MG2 Cr_2O_3 content and Cr:Fe ratio strike variations.

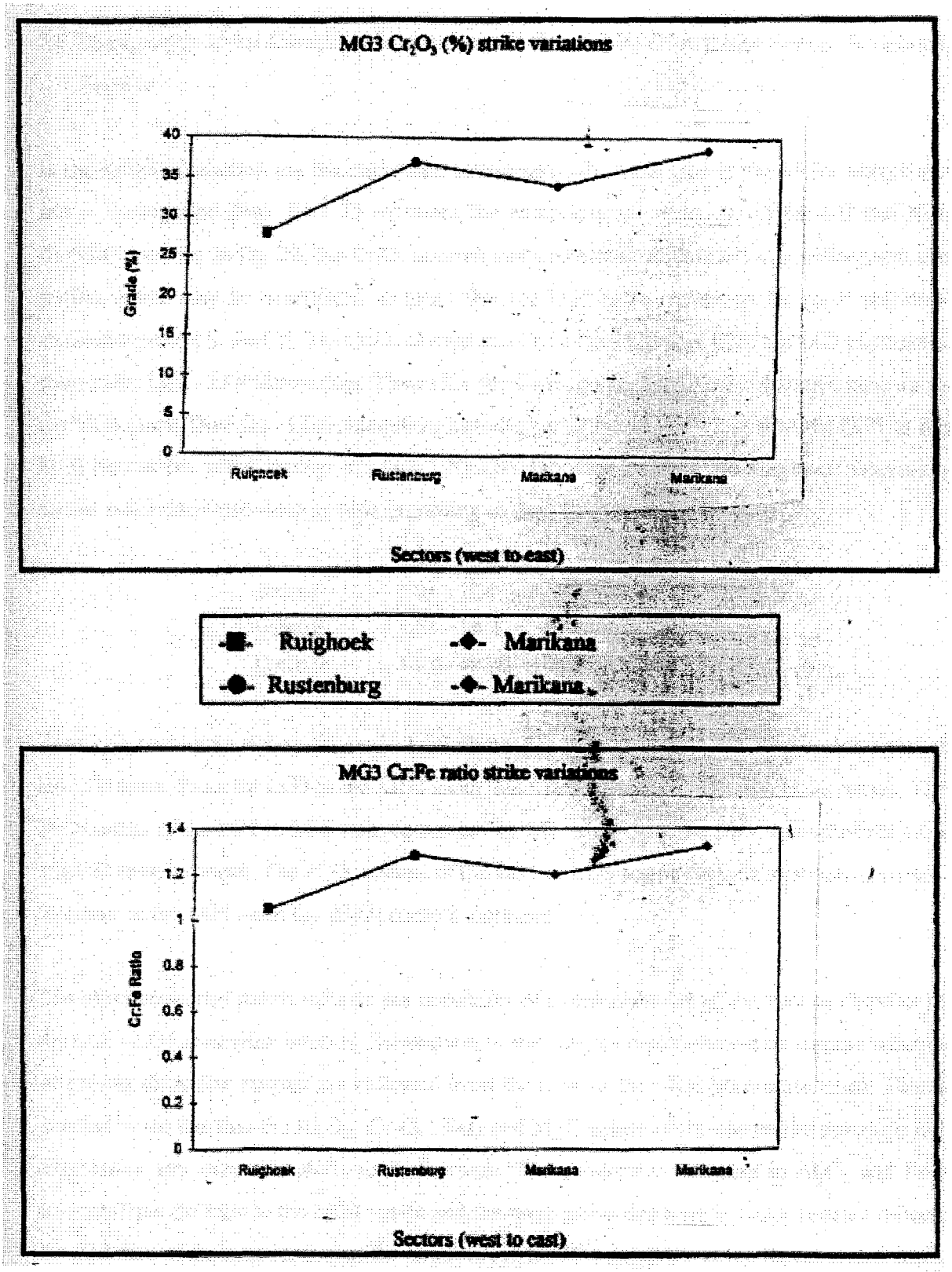

Fig. 22d. MG3 Cr_2O_3 content and Cr:Fe ratio strike variations.

7.5. Petrography of the Complete Succession of LG and MG Chromitite Seams, Ruighoek Section

In the Ruighoek section the full chromitite stratigraphy, from the LG1 to the MG4a chromitite seams, is exposed. Figs. 23 - 25 represent the compositional variations of the LG and MG chromitite seams. In fig. 23, the Cr_2O_3 content and Cr:Fe ratio of the LG1 chromitite seam are similar which may be interpreted to mean that the LG1 seam represents the most primitive chromitite present in the CZ. The Cr_2O_3 content and Cr:Fe ratio increase from the LG1 chromitite seam to the LG3 - LG4 chromitites. Thereafter the Cr_2O_3 content and Cr:Fe ratio decrease up to the MG3 seam. The LG1 - LG4 chromitites have higher Cr:Fe ratios (~ 2.0) than the LG5 to the MG3 chromitites, which average less than 1.70. The chromitite seams of the Ruighoek succession can be subdivided into three groups according to their Cr:Fe ratio:

Group I	LG1 - LG4	Cr:Fe <2.00
Group II	LG5 - MG1	Cr:Fe >1.70
Group III	MG2 - MG4a	Cr:Fe > 1.25.

The Cr_2O_3 content from the LG1 to the LG3 chromitite seam increases, reaching a peak value at the LG3 seam. From the LG3 to the MG3 seam, the Cr_2O_3 content progressively decreases. The FeO content of the LG1 to LG4 seam decreases (fig. 24), after which the FeO content of the LG5 to MG2 seam increases. The Al_2O_3 content of the LG1 to LG3 seams remains relatively constant, however at the LG4 seam the Al_2O_3 content increases.

The aforementioned points indicate the possibility of a replenishment of the magma chamber at the LG3 - LG4 chromitite interval. Subsequent to this magma replenishment no magma influxes of grossly dissimilar magma are indicated from the LG4 to the MG3 chromitite seam. This is justified by the fact that the Al_2O_3, Cr_2O_3, FeO and MgO values of the chromitite seams do not experience any excessive shifts to their trends. The progressive increase in Al_2O_3 and FeO contents from the LG4 to the MG3 seams and the progressive decrease in Cr_2O_3 content reflects the evolution of the magma, in that the Cr_2O_3 content of the magma is being depleted and Al_2O_3 and FeO are representing greater proportions of the chromitite seams.

A further indication of a magma replenishment at the LG3 - LG4 chromitite interval is indicated by the MgO trend in fig. 24. The CZ chromitite seams are predominantly composed of magnesiochromite (see section 7. 6) and hence, the MgO trend for the seams would remain relatively constant. Minor changes in the whole-rock MgO value for the chromitite seams may represent the presence of intercumulus minerals. However, at the LG3 - LG4 chromitite interval a slight increase in the MgO content of the LG4 seam occurs. This increase in MgO may be attributed to influx of replenishing magma.

The Al_2O_3 content at the LG4 seam increases abruptly and thereafter at a more-or-less steady rate (fig. 24). In association with cumulus plagioclase, chromite is depleted in Al. Yet in the western Bushveld Complex, as documented by Teigler *et al,* (1992) from the SF-7 drill hole, the Al content of the chromitites of the uCZ (plagioclase-rich environment) does not decrease but in fact remains more or less constant after an initial increase approximately 125 m below the first appearance of cumulus plagioclase. Early precipitation of chromite alone, which resulted in massive chromitite, is invoked by Teigler *et al,* (1992) to account for the steady levels of Al in the chromitites of the uCZ, that is, chromite crystallization precedes plagioclase crystallization.

The CaO and SiO_2 concentrations in bulk samples of chromitite (fig. 25) increase from the LG6 to the MG1 chromitite intervals and dramatically increase at the MG3 chromitite seam to 1.96 % CaO and 18.55 % SiO_2, returning to lower concentrations (CaO - 0.97 %; SiO_2 - 7.05 %) in the MG4 chromitite. A slight peak in the CaO and SiO_2 concentrations occurs at the LG3 - LG5 chromitite interval but not to the same degree as in the MG3 chromitite seam. This peak at the LG3 - LG4 interval may be attributed to influx of replenishing magma. The progressive increase in CaO from the LG6 to the MG3 interval is related to the onset of plagioclase crystallisation. The dramatic increase in CaO at the MG3 level is attributed to the host rocks being comprised of cumulus plagioclase and the modal content of intercumulus plagioclase in the MG3 chromitite seam will be greater than at any other chromitite seam as the MG2 - MG3 interval represents the boundary between the lCZ and the uCZ, that is crystallisation of copious volumes of cumulus plagioclase.

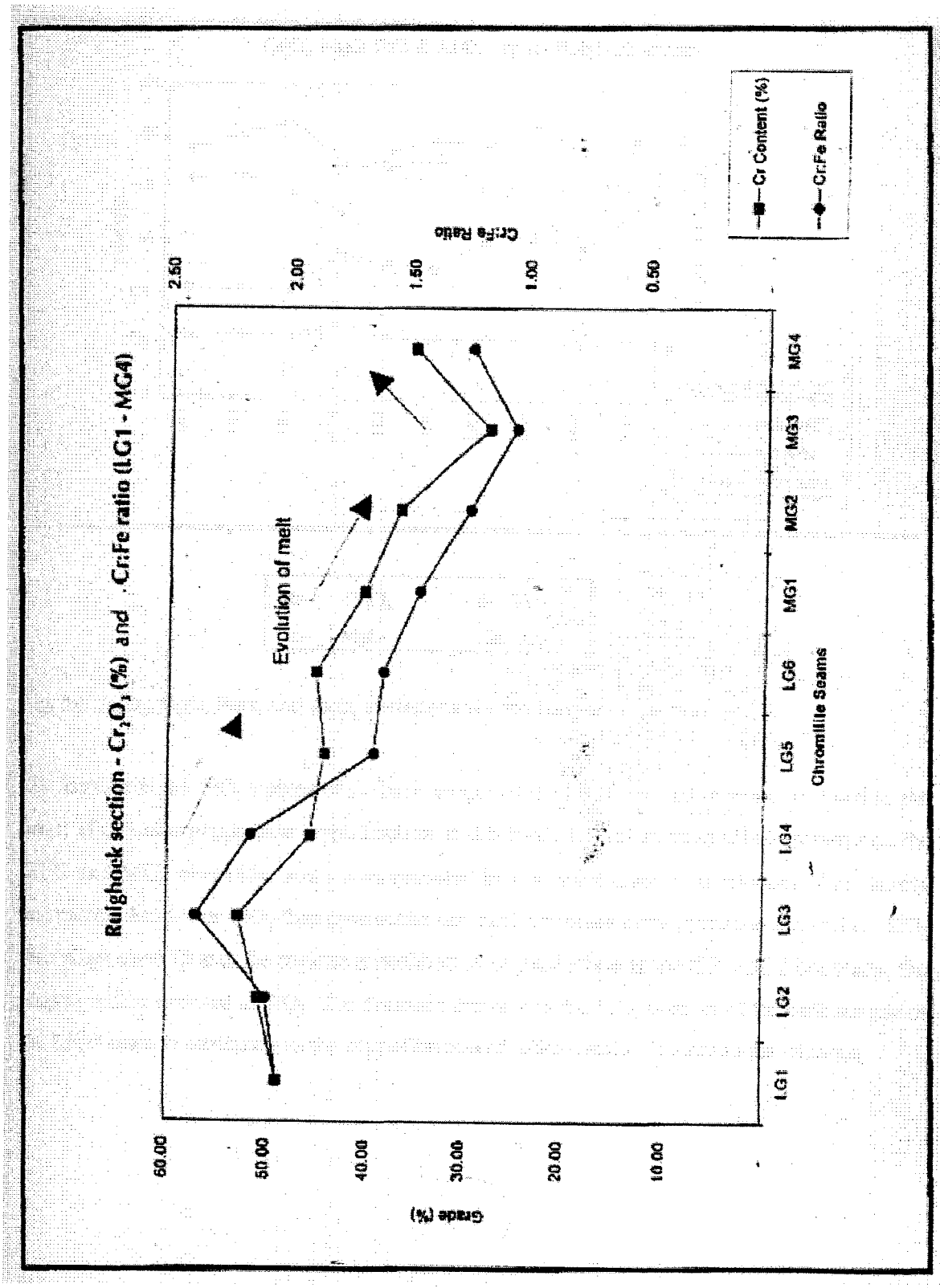

Fig. 23. Cr_2O_3 content and Cr:Fe ratio, Ruighoek section.

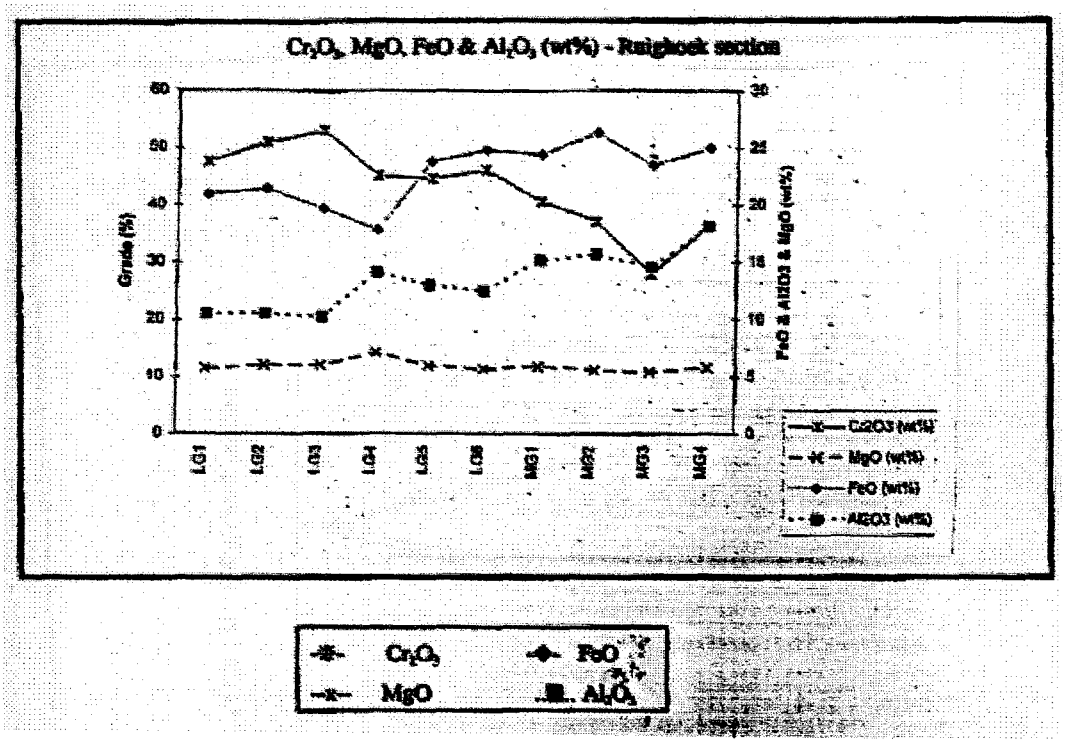

Fig. 24. Cr_2O_3, MgO, FeO, and Al_2O_3 variations for the Ruighoek section.

The increase in the SiO_2 content of the bulk sample of the MG3 chromitite seam is related to the onset of cumulus plagioclase crystallisation at this level. The intervening lithology between the MG2 and MG3 chromitite seam is represented by a massive layer of anorthosite. Anorthosite commonly has lower SiO_2 than pyroxenite and norite because orthopyroxene has higher SiO_2 than plagioclase. Due to the copious crystallization of plagioclase at the lCZ - uCZ boundary, the magma will be enriched in SiO_2. The dramatic increase in the SiO_2 content of the bulk sample of the MG3 seam is attributed to the crystallization of silica-bearing intercumulus minerals.

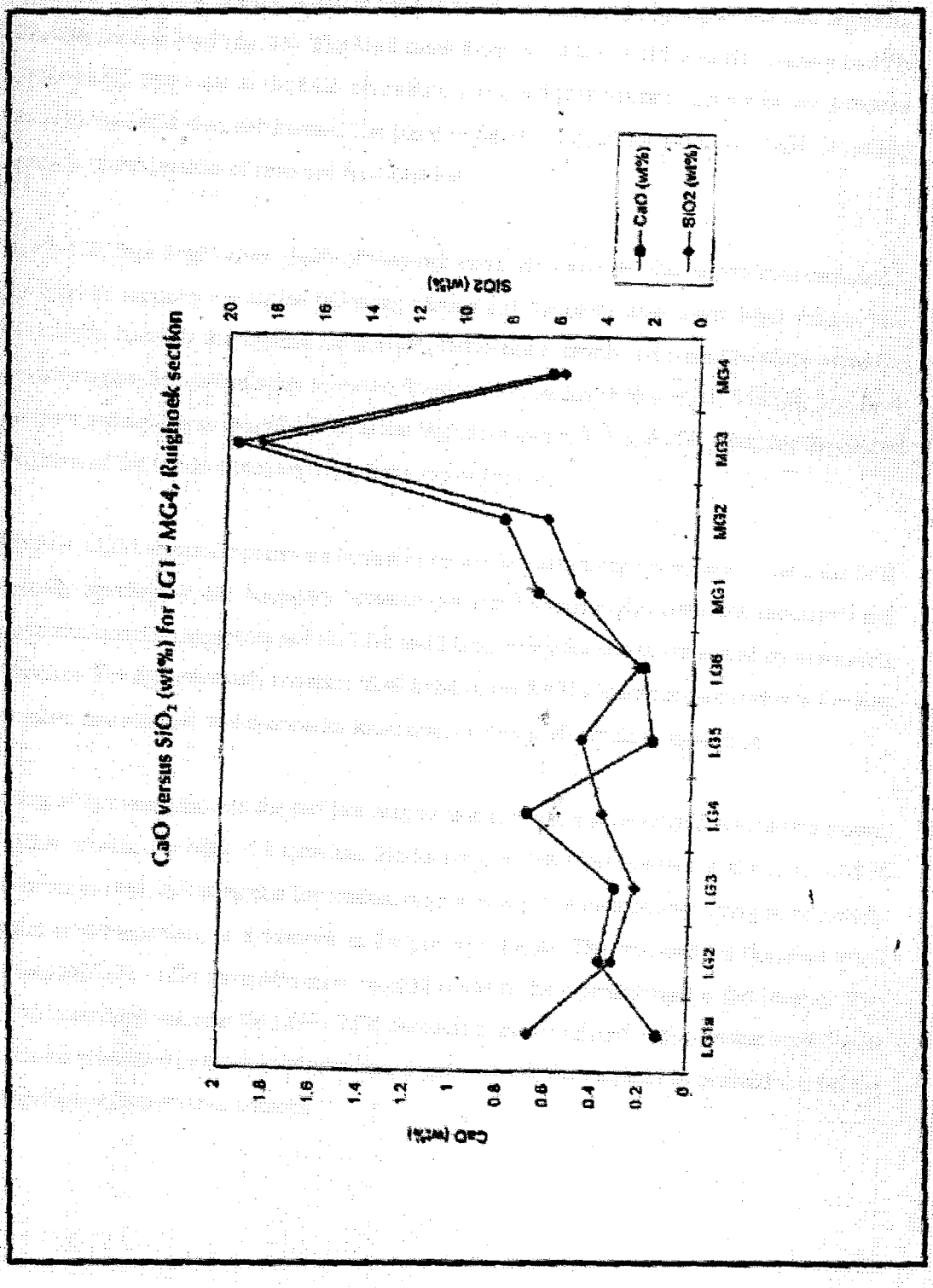

Fig. 25. CaO and SiO_2 variations, Ruighoek section.

The LG1 to MG4 chromitite seams in the Ruighoek section can be grouped into two segments according to their Mg# (fig. 26). The Mg# trend from the LG1 to LG4 chromitite seams steadily increases but decreases at the LG5 chromitite seam, and then assumes a more or less constant trend to the MG4 chromitite seam. The trend outlined in fig. 26 for the LG1 - LG4 chromitite seams is representative of reversed fractionation.

In the CZ, high Mg# values typify olivine-rich cumulate intervals, that is primitive cumulates. Pyroxenites typically crystallize following olivine and therefore have lower Mg# values. The pyroxenite intervals are typified by normal fractionation trends, whereas the more primitive olivine-bearing intervals display reversed fractionation trends (Eales *et al.*, 1993a). The host cumulate rocks show an overall decline in the Mg# through the lCZ and uCZ verifying the overall evolution of the resident magma toward the top of the CZ.

The LG1 - LG4 chromitite seams are hosted by pyroxenite-harzburgite cumulates, whilst the LG5 typically develops at the boundary between pyroxenite-harzburgite cumulate sequences and pyroxenite cumulate sequences and the LG6 and LG6a chromitite seams are hosted by pyroxenite cumulates. The approximately constant Mg# trend to the MG4 chromitite seam reflects the host cumulate environment which contains increasing amounts of cumulus plagioclase.

Mixing of fresh magma with the resident magma will produce a reversal of fractionation trends, in other words, the Mg# will increase. No increase in the Mg# is noted in the LG5 - MG4 chromitite interval, indicating that the resident magma was not replenished by a magma of grossly dissimilar composition, as evidenced in the previous pages. The reversed fractionation trend between the LG1 - LG4 chromitite seams is good evidence for replenishment in this interval. The shift to lower Mg# values at the LG5 - LG6 chromitite level is related to the decline in olivine as a cumulus phase and increase in plagioclase, in other words the magma has evolved toward the plagioclase-orthopyroxene cotectic.

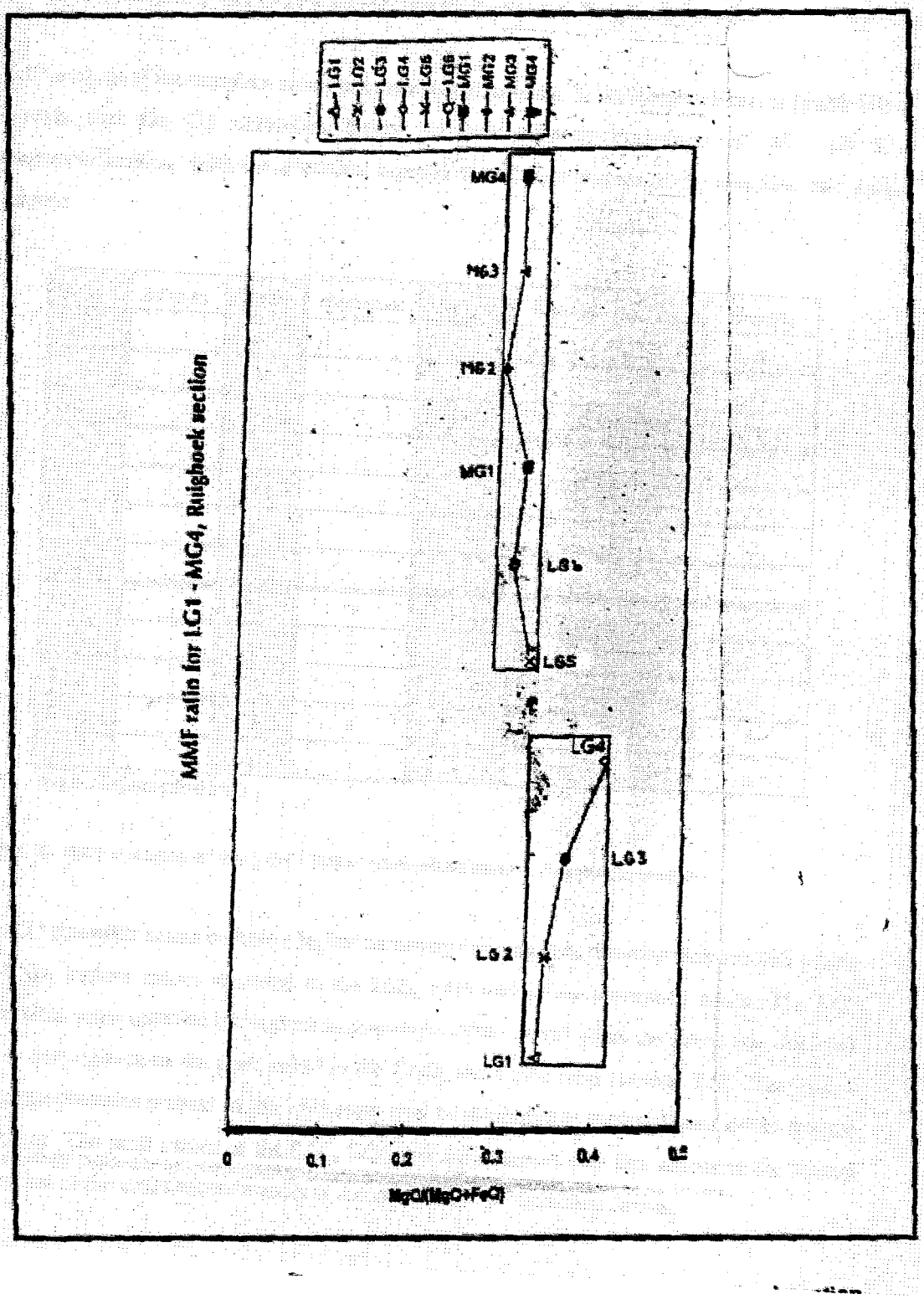

Fig. 26. Mg# (whole-rock) trend for the LG1 to MG4a chromitite seams, Ruighoek section.

7.6. XRD Analysis of the LG1 - MG4 Chromitite Seams, Ruighoek Section

XRD analysis of the complete succession of chromitite seams in the Ruighoek sector (Table III) reveals that the CZ chromitite layers are predominantly composed of 79 - 98 % magnesiochromite, with the alteration mineral assemblage dominated by smectite, talc and chlorite.

Seam	Dolomite	MC	Plagioclase	Quartz	Chlorite	Talc	Smectite
LG1		87				5	8
LG2		84					16
LG3		98					2
LG4	6	87					7
LG5	1	83				3	12
LG6		97					3
LG6a		92				2	6
MG1		81	3		2	9	5
MG2		80	2		4	8	6
MG3		88	3		2	2	5
MG4		79	6		5	6	4
MG4a		80	1	2	7	6	6

(MC - Magnesiochromite)

Table III. XRD analysis of the LG1 - MG4a chromitite layers, Ruighoek section.

The LG chromitite seams contain a higher percentage of magnesiochromite than the MG seams, with the highest values recorded in the LG3, LG6 and LG6a chromitite seams. The LG3 chromitite seam contains the highest magnesiochromite content of all the seams and this peak value corresponds to the peak noted in the Cr_2O_3 and Cr:Fe ratio (section 7.5). The peak in magnesiochromite content of the LG3 seam may be attributed to replenishment of the magma chamber. The peak values of the LG3, LG6 and LG6a seams may also represent the limited alteration of the constituent minerals in comparison to the remaining seams.

The LG chromitite seams have altered to a greater degree than the MG chromitite seams, yet chlorite, an alteration product of the ferromagnesian mineral phases, only occurs in the MG seams. Crystallization of cumulus plagioclase commences at the MG2 - MG3 level. Plagioclase may be replaced by chlorite and, hence, chlorite would therefore be absent or occur in very low concentration in the lCZ, as plagioclase is typically a minor mineral in these rocks.

7.7. Quantitative Electron-Microprobe Analysis of the LG1 - MG4a Chromitite Seams, Ruighoek Section

7.7.1. Analytical Procedure

Chromites from the LG1 - MG4 chromitites from the Ruighoek section were analysed for Al_2O_3, SiO_2, Cr_2O_3, TiO_2, FeO, Fe_2O_3, CaO, K_2O, MgO on a JEOL 733 Superprobe. The accelerating voltage was 10 - 15 kV, with a beam current of 40 nÅ and, a beam size of 3 - 4 micrometers. The chromite standard used was the Jarosewich, Smithsonian USNM 117075 from Tiebaghi Mine, New Caledonia (see Appendix G for the standard values). In the 12 thin sections both core and rim of between 10 and 15 chromitite grains per thin section were analysed. In addition, 11 thin sections were analysed to confirm the lateral (from Ruighoek to Marikana) compositional variations of the LG6 to MG4 chromitite seams.

7.7.2. Core-Rim Analysis

The core-rim analyses of chromite grains for the LG1 - MG4 chromitite seams in the Ruighoek section were conducted to determine the presence of any geochemical gradients. Within a single grain, the chemical gradients may be caused by nucleation and crystal growth, reaction with liquid, varying proportions of trapped liquids and changing intercumulus liquid composition (Roeder and Campbell, 1985), and subsolidus equilibration with the silicate phases (Eales and Reynold, 1983). An absence of chemical gradients characterizes the chromite grains analysed (Appendix E). In addition, within an individual chromitite seam, large variations occur in the composition of the analysed chromite grains. The chromite grains of an individual chromitite seam are characterized by a lack of zoning. The lack of zoning possibly depicts the degree to which the chromite grains have re-equilibrated with adjoining chromite grains and/or the interstitial material, in the postcumulus stage (Schürmann, pers. comm.).

7.7.3. Core Analysis

The Cr_2O_3, Al_2O_3, FeO and TiO_2 contents from the cores of the chromite grains analysed for the LG1 to MG4a chromitite seams is recorded in order to support the findings in section 7.5 (see Table IV below). These values reflect the average compositions of the chromite grains and not the whole-rock composition of the chromitite layers. The findings in this section are in agreement with section 7.5, that is the whole-rock composition of the chromitite seams.

	Cr_2O_3	Al_2O_3	FeO	TiO_2
LG1	51.35	13.01	23.49	0.44
LG2	51.84	12.70	23.33	0.39
LG3	54.09	12.24	21.31	0.39
LG4	53.35	13.45	20.69	0.41
LG5	47.42	15.04	25.62	0.56
LG6	47.45	14.51	26.33	0.58
LG6a	47.69	14.44	26.39	0.60
MG1	45.18	15.99	26.72	0.81
MG2	44.77	16.01	20.91	0.96
MG3	45.77	13.88	30.72	1.15
MG4	42.86	18.21	21.26	0.80
MG4a	43.13	17.11	21.45	0.82

Table IV. Average values for chromite grains for the electron-microprobe analysis of the LG1 - MG4a chromitite seams of the Ruighoek section. (See Appendix J for the standard deviation values).

❒ The MG chromites have higher Al_2O_3 content than the LG chromites. The Al_2O_3 content of the chromite grains increases from the MG1 to the MG4 chromitite seam. However, at the MG3 chromitite seam the Al_2O_3 content of the chromite decreases. This deflection to lower values at the MG3 chromitite level is attributed to the crystallization of copious volumes of plagioclase. Al_2O_3 has been fractionated to a greater extent by the anorthosite layer between the MG2 and MG3 chromitite seams, resulting in a depletion of Al_2O_3 available during the crystallization of the MG3 chromitite seam. The increased Al_2O_3 content within the chromites of the MG chromitite

seams in comparison to the LG seams is attributed to an increase in the amount of Al_2O_3 in the magma due to the progressive onset of plagioclase crystallization. The LG1 - LG4 chromites seams have the lowest Al_2O_3 content, with higher values recorded for the LG5 - LG6a chromites seams. The deflection to slightly higher Al_2O_3 content at the LG5 - LG6a chromitite level is related to the progressive depletion of Cr in the magma due to crystallization of massive chromitite seams. Crystallization of Cr_2O_3 would result in an Cr-depleted and an Al-enriched magma. The main exchange in the trivalent cation site of Cr-spinel is between Cr and Al (De Waal, 1975). In the LZ and lCZ, Al was more concentrated in the magma due to a lack of plagioclase crystallization (Maier, pers. comm.).

❒ The TiO_2 content of the chromite grains steadily increases from the LG1 to MG2 chromitite seams, with a deflection to higher values at the MG3 chromite, after which the TiO_2 decreases in the MG4 and MG4a chromites. The steady increase in TiO_2 is related to the fractionation of olivine, orthopyroxene and plagioclase from the magma, in that Ti is relatively incompatible in plagioclase and orthopyroxene and olivine and will increase in proportion in the parental melt. Ti has a high partition coefficient in Cr-spinels and as the amount of TiO_2 in the magma increases, the TiO_2 content of the chromites will show a corresponding increase. The deflection to higher values at the MG3 chromite may be explained by the appearance of cumulus plagioclase below that layer, considering that, of the major minerals in the CZ, plagioclase can accommodate the least amount of TiO_2 (Maier, pers. comm.)

❒ The Cr_2O_3 content of the chromites decreases, albeit a minor fluctuation at LG3-LG4, from the LG1 to the MG4a chromitite seam reflecting that Cr is progressively replaced by Al and Fe. The deflection to a higher FeO content at the MG3 chromitite seam corresponds to the decrease in the Al_2O_3 content of the chromite. The MG2 - MG3 chromitite interval marks the first appearance of cumulus plagioclase and the magma will therefore be initially depleted in Al and enriched in Cr and Fe. Less Al is available to enter into the Cr-spinel lattice and, therefore, a larger proportion of FeO can be accommodated in the Cr-spinel lattice. In general, the main exchange in the trivalent cation site in the Cr-spinel lattice is between Cr and Al. In the event that Al is depleted in the parental magma, Fe will preferentially occupy the trivalent cation site. The LG5 - MG4a chromites have higher FeO content than the LG1 - LG4 chromites, reflecting the reversal in fractionation trend (see section 7.5). The lower FeO content values in the LG3, LG4, MG2, MG4 and MG4a correspond to an increase in the Al_2O_3 content of the chromites.

7.7.4. Proximal - Distal Compositional Variations

The average core composition of chromites from 11 polished thin sections (Table V), representing the LG6 and MG1-MG3 chromitite seams from the proximal (Ruighoek) facies to the distal (Marikana/Brits) facies were analysed to determine the compositional variations of the chromite grains of the massive seams along strike. Due to the paucity of exposed or developed LG1 - LG5 and the MG4 and MG4a chromitite seams and in keeping with the seams sampled for section 7.4, only the LG6 and MG1 - MG3 chromitite seams were submitted for electron-microprobe analysis (Appendix F).

In section 7.4.1, the whole-rock analysis of the chromitite seams revealed that the Cr_2O_3 content of the MG chromitite seams increases from the Ruighoek section to the Marikana/Brits section and the Cr_2O_3 content of the LG6 chromitite seam decreases from Ruighoek section eastwards. To support these findings, three sets of samples representing the Ruighoek, Rustenburg and Marikana/Brits sections were submitted for electron-microprobe analysis. The results are tabulated in Table VI below. The Cr_2O_3 content of the chromite grains analysed reveals that the Cr_2O_3 content of the chromite grains from the LG6 to the MG3 chromitite seams does not increase from the proximal to the distal facies. The rather constant Cr_2O_3 content for the three sections is attributed to:

❒ The sampling spacing - only three sampling localities were submitted for analysis and, hence, may not be representative of the trend for the Cr_2O_3 content to increase across the western Bushveld Complex. To achieve a more representative indication of the Cr_2O_3 variations of the chromite across the western Bushveld Complex, a closer sampling spacing is necessary.

❒ Local variations such as floor irregularities, reaction and mixing of the magma with rip-up clasts, and variations in the phases crystallizing will all produce variations in the composition of the chromite and chromitite seams.

❒ The composition of the chromite grains varies across an individual seam. The samples submitted for electron-microprobe analysis may not be representative of the compositional variations of the entire chromitite seam. The variations in the composition of the chromitite seams as indicated by the XRF analysis of bulk samples incorporates the interstitial material as well as silicate contamination and modal amount of Cr_2O_3 in the intercumulus phases, hence producing regional trends that are not indicated by analysis of individual chromite grains.

Definitive trends are, however, observed for the Al_2O_3 , FeO and TiO_2 contents of the chromite grains of the massive seams analysed. The following points summarize the variations of these components along strike, from the near proximal to the distal facies of the western Bushveld Complex:

❒ The higher Al_2O_3 content of the MG1 - MG3 chromite grains in the Rustenburg section in comparison to the Ruighoek section may be attributed to either the chromite having reacted with the interstitial liquid or reacted with the fractionated magmatic liquids responsible for the footwall and hanging wall cumulus silicate phases. The higher Al_2O_3 content of the chromites of the MG1 - MG3 chromitite seams, in comparison to the remaining seams, may be attributed to an increase in the amount of Al_2O_3 in the magma due to the progressive onset of plagioclase crystallization below the lCZ - uCZ boundary away from the proximal facies (see section 3.3).

❒ The Al_2O_3 content of the LG6 and MG1 - MG3 chromitite seams increases from Ruighoek to Rustenburg but decreases from Rustenburg to the Marikana/Brits section. The increase from the Ruighoek to Rustenburg sections is attributed to an increase in the amount of Al_2O_3 in the magma due to the progressive onset of plagioclase crystallization below the lCZ - uCZ boundary away from the proximal facies, and/or local variations in the host cumulus silicate phases (see Appendix L for the stratigraphic log of the Rustenburg sampling locality). The decrease in the Al_2O_3 content from Rustenburg to the Marikana/Brits section may be attributed to a depletion in the magma of Al_2O_3 due to the crystallization of copious volumes of plagioclase. In other words, further influxes of primitive magma would mix with this Al-depleted resident magma, therefore resulting in chromitite seams with low Al_2O_3 content. The decrease in Al_2O_3 content from the Rustenburg to the Marikana/Brits section may also be attributed to local variations in the host cumulus silicate phases.

❒ The TiO_2 content of the chromite grains of the massive seams increases from the Ruighoek and Rustenburg section after which it decreases toward the Marikana/Brits sections. The increase in TiO_2 content in the Rustenburg section is attributed to the local variations in the host cumulus silicate phases. This increase in TiO_2 content may also be related to the increase in Al_2O_3 in the magma in the Rustenburg section (see above point), as Ti is relatively incompatible in the plagioclase and orthopyroxene crystal lattices and therefore will preferentially enter the Cr-spinel lattice due to the relative compatibility of Ti in the Cr-spinel structure. The distal facies of the western Bushveld Complex is characterized by a progressive onset of plagioclase crystallization

below the lCZ - uCZ boundary. Due to the fact that Ti is relatively incompatible in plagioclase but has a high partition coefficient in Cr-spinels, it would be expected that in the distal facies, higher TiO_2 contents of the chromite would occur, but this is not observed. The decrease in TiO_2 content of the chromite grains of the MG3 chromitite seam from Ruighoek to Marikana is not well understood but may be related to the progressive evolution of the magma toward the distal facies and local variations in the host cumulus silicate phases.

❒ The overall decrease in the FeO content from the Ruighoek section to the Rustenburg section is again attributed to the composition of the magma evolving toward the distal facies and to the localized variation in the host cumulus stratigraphy in the Rustenburg section.

❒ Although the Spruitfontein upfold is spatially related to the compositional highs noted in the Rustenburg section, the upfold is deemed to be of limited extent (fig. 5) and, therefore, the effect of the structural high is postulated to have had negligible effect on the composition of the LG6 to MG4a chromitite seams.

	Cr_2O_3			FeO		
	Ruighoek	Rustenburg	Marikana/Brits	Ruighoek	Rustenburg	Marikana/Brits
LG6	47.45	46.70	47.48	26.33	22.55	26.08
MG1	45.18	46.00	46.06	26.72	22.93	26.88
MG2	44.77	45.23	43.80	20.91	24.21	29.22
MG3	45.77	45.39	47.68	30.72	23.11	26.49

	TiO_2			Al_2O_3		
	Ruighoek	Rustenburg	Marikana/Brits	Ruighoek	Rustenburg	Marikana/Brits
LG6	0.58	0.80	0.74	14.51	17.11	14.82
MG1	0.81	1.25	0.76	15.99	18.32	15.60
MG2	0.96	1.30	0.95	16.01	18.00	16.06
MG3	1.15	1.08	0.74	13.88	19.20	14.83

Table V. Average Cr_2O_3, FeO, TiO_2 and Al_2O_3 wt. % of chromite from the Ruighoek - Rustenburg - Marikana/Brits sections.

7.8. Cyclic Units in the Critical Zone

The RLS can be subdivided into a number of cyclic units. Cyclic units are defined by parameters which display a consistent relationship, or a chemical evolution, with the most primitive values at the base, progressively evolving until the base of the succeeding unit is encountered (Eales *et al.*, 1990).

A typical cyclic unit commences with the crystallization of ultramafic rocks which grade into mafic rocks, through to leucocratic rocks. Cyclic units in the RLS have the following typical sequence, from primitive lithologies at the base to evolved lithologies at the top, that is, basal chromitite-dunite-harzburgite grades into pyroxenite, which grades into melanorite, norite and leuconorite and, finally, anorthosite at the top of the cyclic unit (Eales *et al.*, 1990). Based on this, Scoon and Teigler (1994) subdivided the lCZ into nine cyclic units and the uCZ into eight cyclic units (fig. 27).

In an ideal cyclic unit, chromitite defines the base. However, this is not a steadfast rule as the base of some cyclic units is defined by pyroxenite alone and an absence of chromitite, or alternating pyroxenite-chromitite layers. Eales (1987) defines a cyclic unit as discrete mappable units which represent separate episodes of magma influx, but the episodes themselves may embrace one or more pulses (Eales, 1987, p 162). The alternating chromitites and pyroxenites at the base of many cyclic units are therefore attributed to crystallization being initiated between the magma pulses. Chromite crystallizes as a result of the mixing of Cr-saturated magma with resident, residual magma, thereby allowing thin pyroxenite layers to precipitate before the hybrid magma has moved into the primary phase field of chromite (Eales, 1987).

The proportions of lithologies within a unit are variable but usually dominated by one or more rock type. Cyclic units of the RLS are typified by this lithological bimodality, with ultramafic and leucocratic rocks dominating the succession and mesotype lithologies constituting a lesser proportion (Eales *et al.*, 1990).

Frequent departures from the crystallization order of lithologies at the base of cyclic units

characterizes the CZ. For example, at Union section, the MG3 chromitite seam is overlain by norite (30 m thickness) which is succeeded by 15 m of pyroxenite. Norite and chromitiferous anorthosite (3 m interval) constitute the hanging wall of the pyroxenite, which lies immediately below the MG4 chromitite seam. On the basis that chromitite typically defines the base of a cyclic unit and is succeeded by pyroxenites, the question arose as to which lithological interval represents the base of the UG1FW unit. Two intervals were proposed, these being the MG4 chromitite seam or the pyroxenite interval approximately 15 m below the MG4 seam. Geochemical evidence suggests that the base of the UG1FW unit be taken as the base of the MG4 chromitite seam and therefore the interval between the MG3 and MG4 seams represents the MG3 unit (Eales *et al.*, 1990). Convincing evidence for the MG4 seam being the base of the UG1FW unit is:

- The steady decline in Al_2O_3 and the increase in the whole-rock Mg# up to the base of the MG4 seam.
- Relatively uniform levels of Ni/V between the MG3 and MG4 chromitite seams. The uniform levels are interpreted to represent coherent geochemical properties in response to continuous operation of a uniform process (Eales *et al.*, 1990, p 268).
- The MG4 chromitite seam is characterised by shifts in whole-rock Mg# values and Ni/V and Cr/Co ratios, as well as, varying Cr levels of the orthopyroxene.
- Differing regression lines for the lithologies above and below the MG4 chromitite due to regression of the whole-rock Sr against V (Eales *et al.*, 1990).

With relevance to this study, the compositional variations of the chromitite layers reflect the chemical evolution of the silicate host rocks, as seen in section 7.4 and 7.5. Therefore, the compositional variations of the chromitite layers may be interpreted by means of the small-scale compositional cyclicity of the CZ cumulate succession (Teigler and Eales, 1993).

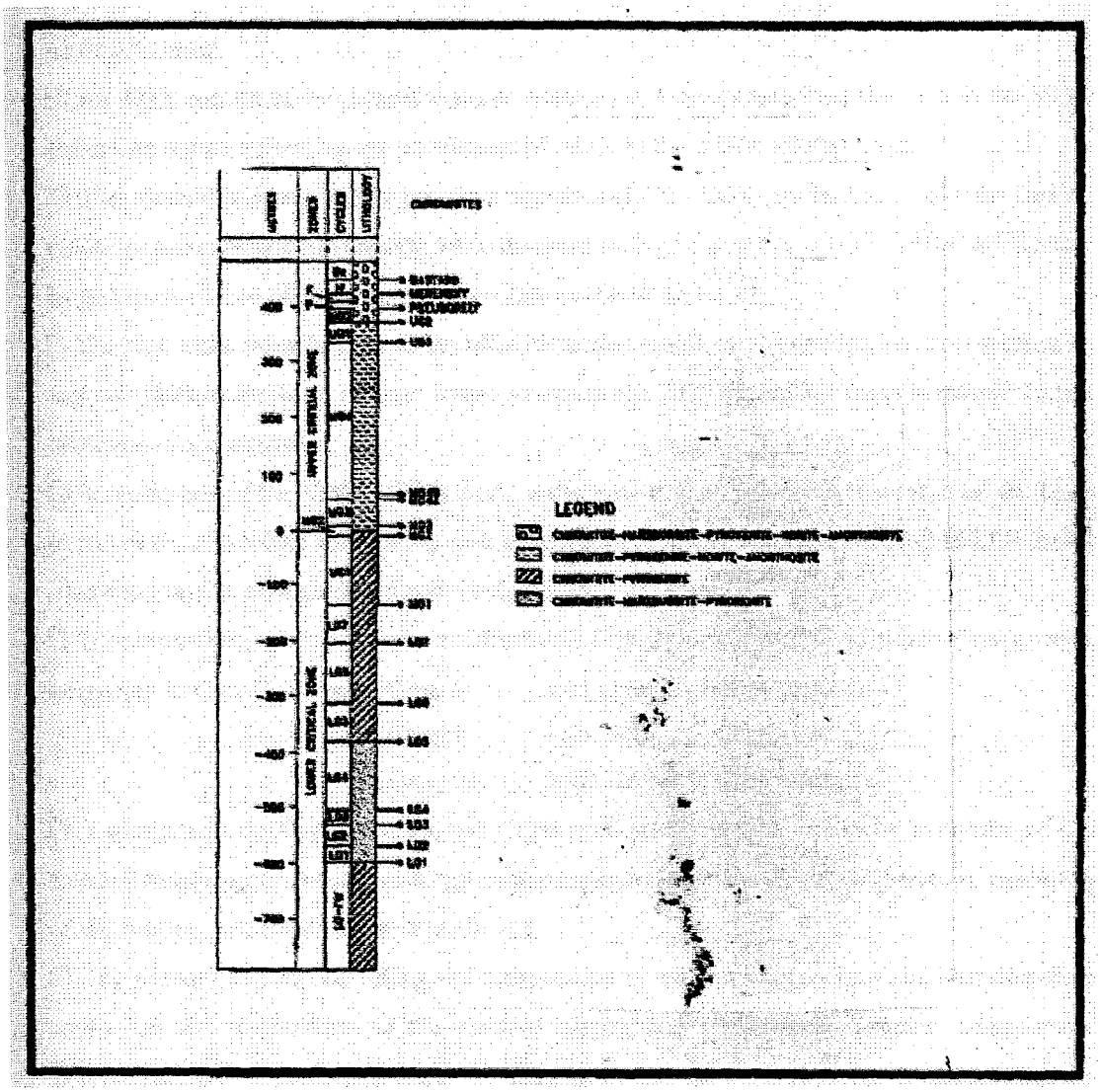

Fig. 27. Cyclic units of the ICZ and uCZ, western Bushveld Complex, with the main subdivisions of the CZ represented (modified after Scoon and Teigler, 1994, p 1096).

7.9. Conclusions and Observations

The chromite grains and the massive chromitite seams of the western Bushveld Complex are characterized by the following:

- ❒ The whole-rock Cr_2O_3 content of the MG chromitite seams increases from the proximal facies to the distal facies, as does the thickness.
- ❒ Cr is progressively replaced by Al and Fe from the lowest (LG1) to topmost (MG4a)

chromitite seam.

❒ The Al_2O_3 content of the chromitite seams increases at a steady rate from the LG6 to the MG4 chromitite seams, reflecting the enrichment of Al_2O_3 in the differentiating magma.

❒ The chromitite seams with a primitive signature (LG1 - LG4) are hosted by olivine- and/or pyroxene-rich cumulate successions, while the more evolved chromitites (LG5 - MG4) are hosted by pyroxene-rich to plagioclase-rich cumulate successions.

❒ The Mg# ratios from the LG1 to the MG4 chromitite seams can be divided into two segments, and the shift in the Mg# ratio to lower values at the LG6 chromitite seam is related to the evolution of the magma.

❒ In verification of De Waal's (1975) work, a decrease in the Cr:Fe ratio is noted from the base to top of the chromitite succession, with a departure to higher values at the LG2 to LG4 level. This departure is attributed to magma influx at the LG3 level.

❒ The chromitite seams of the western Bushveld Complex can be subdivided into three groups according to their Cr:Fe ratio:

Group I	LG1 - LG4	Cr:Fe <2.00
Group II	LG5 - MG1	Cr:Fe >1.70
Group III	MG2 - MG4a	Cr:Fe >1.25.

❒ Variations in the Cr_2O_3 content and Cr:Fe ratio are controlled in part by evolution of the resident magma upon mixing with replenishing magma, a decline in the temperature, oxidation of the magma, and the minerals crystallizing.

❒ The primary factors controlling the composition of the chromitite seams and host cumulate rocks are the composition of the resident magma and replenishing magmas, components crystallized and crystallizing from the magma at the time of chromite precipitation, the temperature gradients at the time of crystallization, and fO_2.

❒ Compositional variations of the chromitites and host cumulus phases may be further attributed to varying degrees of assimilation and post-cumulus re-equilibration with residual liquids (Teigler, 1990).

❒ The increase in Cr_2O_3 content from the proximal to the distal facies may be attributed to enhanced plagioclase crystallisation in the distal facies, thereby enriching the magma in Cr_2O_3, as well as advanced compositional contrast between the resident and the replenishing magmas in the distal facies, thereby enhancing the nucleation of chromite from the parental magmas during mixing.

❒ The host cumulate environment and co-precipitating phases directly control the composition

of the chromitite seams, resulting in slight but distinctive variations from the LG1 to MG4a chromitite seams. The whole-rock composition of the massive chromitite layers can not be decoupled from the chemical evolution of the silicate cumulus phases. The progressive compositional evolution of the chromitites from the LG1 up to the MG4 seams is attributed to evolution of the resident magma away from olivine-rich phase field toward the orthopyroxene-plagioclase cotectic.

❒ The progressive evolution a single magma type from the proximal to the distal facies of the western Bushveld Complex is proposed to have affected the composition of the chromitite seams and host cumulus silicate phases. Hence, the compositional trends of the chromitite seams is deemed not to support the theory of the existence of two compositionally different magmas responsible for the CZ.

❒ The cyclic layering of the CZ is the result of reversals in the fractionation trends, due to repeated emplacement and mixing of primitive magma with resident magma, and progression along the orthopyroxene-plagioclase cotectic and orthopyroxene-chromite cotectic.

❒ The individual chromite grains of the massive chromitite layers (LG1 - MG4a) do not show any systematic zoning or chemical gradients between the core and rim of the grains. Intra-sample variability is too great to recognize any regional strike compositional trends. The compositional variability of the individual chromitite seams is related to the chemical evolution of the parental magma.

8. Synopsis of the Western Bushveld Complex LG and MG Chromitite Seams

The following are the key features of the western Bushveld Complex LG and MG chromitite layers:

- The Cr_2O_3 content of the MG chromitite seams increases from the Ruighoek (near proximal) section to the distal facies (Brits section) of the western Bushveld Complex. The Cr_2O_3 content and Cr:Fe ratio of the LG6 and LG6a chromitite layers, however, decreases away from the putative feeder zone (proximal facies). The compositional variations of the LG1 - LG5 chromitite seams were not investigated due to a paucity of exposed LG1 - LG5 chromitite layers, and in parts of the western Bushveld Complex, the LG chromitite seams are poorly developed or absent.
- The Cr:Fe ratio mimics the Cr_2O_3 trends for each chromitite seam across the western Bushveld Complex. However, the general Cr:Fe trend from the LG1 to the MG4 chromitite seams is one of decreasing values, with deviation to higher values at the LG2 - LG4 chromitite seams.
- The primary factor controlling the compositional trends of the chromitite seams above and below the lCZ and uCZ boundary is the appearance of cumulus plagioclase.
- The variations in single element trends of the chromitite seams reflect the cumulus mineralogy of the host rocks.
- The compositional variations from the LG1 to the MG4a chromitite seams reflect the chemical evolution of the parental magma and the co-precipitating interstitial mineral phases.
- The compositional and morphological variations of the LG6 to MG4 chromitite layers from the proximal to distal facies are attributed to advanced compositional contrast between the replenishing primitive magma and the resident magma due to the chemical evolution of the magma along strike from the proximal facies/putative feeder site to the distal facies.
- Basal flow along strike may have an effect on the variations in chemical composition of the chromitite seams, with local tectonics, such as upfolded floor rocks, controlling the compositional variations to an extent.
- The compositional trends of the chromitite seams and silicate host rocks do not support the existence of two compositionally different magmas in the CZ, rather the cyclic layering and compositional variations of the CZ chromitite and silicate succession are the result of repeated injections of primitive magma of essentially similar composition to the resident magma.
- The chromitite seams can be grouped into two segments according to their Mg#. The reverse

fractionation trend between the LG1 - LG4 chromitite seams reflects the replenishment of the chamber and the reversal in the fractionation trend (decrease in Mg#) at the LG5- LG6 level did not result from the addition of grossly dissimilar magma. Rather, it is the product of the evolution of the parental magma towards the plagioclase-orthopyroxene cotectic.

- Although the presence of chemical gradients in chromite grains have been established by Eales & Reynold (1983) and Roeder & Campbell (1985), no systematic zoning or chemical gradients were recognized from the core-rim analyses of individual chromite grains from the LG1 to MG4a chromitite seams in this study.
- No definitive geochemical "fingerprint" characterizes the individual chromitite seams. The composition of the chromitite seams reflects, in part, the chemical evolution of the host cumulus phases. It is therefore possible to differentiate the LG1 - MG2 seams and the MG3 - MG4a seams from one another. The only conclusive and relatively constant criteria to identify the individual chromitite seams, other than by their stratigraphic position, is by the Cr_2O_3 content and the Cr:Fe ratio. The Cr_2O_3 content and Cr:Fe ratio of a chromitite seam may be indicative of a group of chromitite seams - for example, the LG1 - LG6a chromitite seams are characterized by a Cr_2O_3 content in the range of 47 - 54 Cr_2O_3 % and the MG1 - MG4a have values in the range of 42 - 45 Cr_2O_3 %, with Cr:Fe ratios of ~ 2.0 and ~ 1.70 respectively. Along strike, however, the Cr_2O_3 content and the Cr:Fe ratios for the chromitite seams vary from the proximal to distal facies. Therefore, it is only possible to use the Cr_2O_3 content and Cr:Fe ratio of a chromitite sample to roughly identify whether the seam is located in the lCZ or uCZ within a specific sector. The Al_2O_3 and TiO_2 contents of the seams will indicate whether the chromitite sample came from the lCZ or the uCZ, but cannot identify which chromitite seam was sampled. This is due in part to the within-seam compositional variability of the chromitite seams.

In conclusion, the purpose of this study has been to review the compositional variations of the LG and MG chromitite layers of the western Bushveld Complex, in an effort to provide a comprehensive database and a greater understanding of the CZ chromitite layers, thereby assisting in the exploration and economical exploitation of these vast chromite reserves.

9. References

Bates, R.L. and Jackson, J.A. (1987). *Glossary of Geology*. Am. Geol. Inst., USA, 788 pp.

Battey, M. H. (1981). *Mineralogy for students*, 2nd Ed. Longman, New York, 355 pp.

Best, M.G. (1982). *Igneous and Metamorphic Petrology*. WH Freeman & Co., New York, 630 pp.

Cheney, E.S. and Twist, D. (1991). The conformable emplacement of the Bushveld mafic rocks along a regional unconformity in the Transvaal succession of South Africa. *Precambr. Research*, **52**, 115 - 132.

Coertze, F.J. (1958). Intrusive relationships and ore-deposits in the western part of the Bushveld Igneous Complex. *Trans. Geol. Soc. S. Afr.*, **61**, 387 - 392.

- (1962). The Rustenburg fault as a controlling factor of ore-deposition southwest of Pilanesberg. *Trans. Geol. Soc. S. Afr.*, **65**, 253 - 262.

- (1970). The geology of the western part of the Bushveld Igneous Complex, 5 - 22. *In* Visser, D.J.L. and Von Gruenewaldt, G. Eds., *Symposium of the Bushveld Igneous Complex and Other Layered intrusions, Geol. Soc. S. Afr.*, **Spec. Publn. 1,** 763 pp.

Cousins, C.A. and Feringa, G. (1964). The chromite deposits of the western belt of the Bushveld Complex, 183 - 202. *In* Haughton, S.H. Ed., *The geology of some ore deposits in Southern Africa,* **Vol. 2**, Geological Society of South Africa, 739 pp.

Davey, E.R. (1992). Lateral variations within the upper Critical Zone of the Bushveld Complex on the farm Rooikoppies 297 JQ, Marikana, South Africa. *S. Afr. J. Geol.*, **95**, 141 - 149.

De Waal, S.A. (1975). The mineralogy, chemistry, and certain aspects of reactivity of chromitite from the Bushveld Igneous Complex. *S. Afr. Nat. Inst. Metallurgy,* Rep. **1709**, 80 pp.

Du Plessis, C.P. and Walraven, F. (1990). The tectonic setting of the Bushveld complex in Southern Africa, Part 1. Structural deformation and distribution. *Tectonophysics*, **179**, 305 - 319.

Eales, H.V. and Reynolds, I.M. (1983). Factors influencing the composition of chromite and magnetite in some Southern African rocks. *Geol. Soc. S. Afr.*, **Spec. Publn.** 7, 5 - 20.

Eales, H.V. (1987). Upper Critical Zone Chromitite Layers at R.P.M. Union Section Mine, Western Bushveld Complex, 144 - 168. *In* Stowe, C.W. Ed., *Evolution of chromium ore fields*. Van Nostrand Reinhold Company Inc., Stroudsburg, Pennsylvania, 340 pp.

- ., Field, M., De Klerk, W.J. and Scoon, R.N. (1988). Regional trends of chemical variation and thermal erosion in the Upper Critical zone, Western Bushveld Complex. *Mineralog. Mag.*, **52**, 63 - 79.

- ., De Klerk, W.J. and Teigler, B. (1990). Evidence for magma mixing processes within the Critical and Lower Zones of the northwestern Bushveld Complex, South Africa. *Chem. Geol.*, **88**, 261 - 278.

- ., Teigler, B. and Maier, W.D. (1993a). Cryptic variations of minor elements Al, Cr, Ti and Mn in Lower and Critical Zone orthopyroxenes of the Western Bushveld Complex. *Mineralog. Mag.*, **57**, 257 - 264.

- ., Botha, W.J., Hattingh, P.J., De Klerk, W.J., Maier, W.D. and Odgers, A.T.R. (1993b). The mafic rocks of the Bushveld Complex: a review of emplacement and crystallization history, and mineralization, in light of recent data. *J. Afr. Earth Sciences*, **16**, 121 - 142.

Ehlers, E.G. and Blatt, H. (1982). Petrology. Igneous, Sedimentary and Metamorphic. W.H. Freeman and Company, San Francisco, 100 - 145.

Hatton, C.J. (1988). Densities and liquidus temperatures of Bushveld parental magmas as constraints on the formation of the Merensky Reef, 87 - 93. *In* Prendergast, M.D. and Jones, M. J. Eds., *Magmatic sulphides - the Zimbabwe Volume*. IMM, London.

Hatton, C.J. and Von Gruenewaldt, G. (1985). The geological setting and petrogenesis of the Bushveld chromitite layers. *Inst. Geol. Res. Bushveld Complex*. Univ. Pretoria, Report **57**, 48 pp.

- and - (1987). The geological setting and petrogenesis of the Bushveld chromitite layers, 109 - 143. *In* Stowe, C.W. Ed., *Evolution of chromium ore fields*. Van Nostrand Reinhold Company Inc., Stroudsburg, Pennsylvania, 340 pp.

Hill, R. and Roeder, P. (1974). The crystallization of spinel from basaltic liquid as a function of oxygen fugacity. *J. Geol.*, **82**, 709 - 729.

Hughes, C.J. (1982). *Igneous Petrology, Developments in Petrology 7*. Elsevier Scientific Publishing Co., New York, 551 pp.

Hulbert, L.J. and Von Gruenewaldt, G. (1985). Textural and compositional features of chromite in the Lower and Critical Zones of the Bushveld Complex south of Potgietersrus. *Econ. Geol.*, **80**, 872 - 895.

Irvine, T.N. (1967). Chromium spinel as a petrogenetic indicator. 2. Petrologic implications: *Can. J. Earth Sci.*, **4**, 71 - 103.

- (1975). Crystallization sequences in the Muskox intrusion and other layered intrusions - II. Origin of chromitite layers and similar deposits of other magmatic ores. Geochimica et Cosmochimica Acta, **39**, 991 - 1020.

- (1977). Origin of chromitite layers in the Muskox Intrusion and other stratiform intrusions: A new interpretation. *Geol*ogy, **5**, 273 - 277.

- ., Keith, D.W. and Todd, S.G. (1983). The J-M platinum-palladium reef of the Stillwater Complex, Montana, Vol. II, Origin by double diffusive convective magma mixing and implications for the Bushveld Complex, *Econ. Geol.*, **78**, 1287 - 1334.

Lee, C.A. and Fesq, H.W. (1986). Au, Ir, Ni and Co in some chromitites of the eastern Bushveld Complex South Africa. *Chem. Geol.*, **62**, 227 - 237.

Maier, W.D. and Eales, H.V. (1997). Correlation within the UG2-Merensky Reef interval of the Western Bushveld Complex, based on geochemical, mineralogical and petrological data. *Geol. Soc. S. Afr.*, **Bull. 120**, 56 pp.

McDonald, J.A. (1967). Evolution of part of the Lower Critical Zone, farm Ruighoek, western Bushveld. *J. Petrol.*, **8**, 165 - 209.

McLaren, C.H. and De Villiers, J.P.R. (1982). The Platinum-Group Chemistry and Mineralogy of the UG-2 Chromitite Layer of the Bushveld Complex. *Econ. Geol.*, **77**, 1348 - 1366.

Middlemost, E.K.A. (1985). Magmas and Magmatic rocks. An introduction to igneous petrology. Longman Group Limited, 168 - 175.

M.Sc. Module course notes (1998). *Ore forming processes and magmatic ore deposits.*

Roeder, P.L. and Campbell, I. H. (1985). The Effect of Postcumulus Reactions on Composition of Chrome-spinels from the Jimberlana Intrusion. J. Petrol., **26**, 763 - 786.

South African Committee for Stratigraphy (SACS), (1980). Stratigraphy of South Africa. Part 1. *(Comp. L.E. Kent). Lithostratigraphy of South Africa, South West Africa / Namibia, and the Republic of Bophuthatswana, Transkei, and Venda,* Geological Society of South Africa, **Handbook 8,** Pretoria, 690 pp.

SADC Excursion Guide, (1995). *Geological overview of the Bushveld Complex* (unpubl.), In-house document, Council for Geoscience, 9 pp.

Schürmann, L.W. (1991). *The geochemistry & petrology of the upper Critical Zone in the Boshoek section, of the Western Bushveld Complex.* M.Sc. thesis (unpubl.), Univ. Pretoria, 120 pp.

Scoon, R.N. and Teigler, B. (1994). Platinum-Group Element Mineralization in the Critical Zone of the Western Bushveld Complex: I. Sulfide Poor-Chromitites below the UG-2. *Econ. Geol.*, **89**, 1094 - 1121.

Sharpe, M.R., Bahat, D. and Von Gruenewaldt, G. (1981). The concentric elliptical structure of feeder sites to the Bushveld Complex and possible economic implications. *Trans. Geol. Soc. S. Afr.*, **84**, 239 - 244.

- and Irvine, T.N. (1983). *Melting relations of two Bushveld chilled margin rocks and implications for the origin of chromite*. Yearbook Carnegie Inst., Washington, 82, 295 - 300.

- and Snyman, J.A. (1980). A model for the emplacement of the eastern compartment of the Bushveld Complex. *Tectonophysics*, **65**, 85 - 110.

Stowe, C.W. (1987). The mineral chromite, 1 - 22. *In* Stowe, C.W. Ed., *Evolution of chromium ore fields*. Van Nostrand Reinhold Company, Stroudsburg, Pennsylvania, 340 pp.

Teigler, B. (1990). *Mineralogy, Petrology and Geochemistry of the Lower and Lower Critical Zones, Northwestern Bushveld Complex*. Ph.D. thesis (unpubl.), Rhodes Univ., 247 pp.

- ., Eales, H.V. and Scoon, R.N. (1992). The cumulate succession in the Critical Zone of the Rustenburg Layered Suite at Brits, Western Bushveld Complex. *S. Afr. J. Geol.*, **95**, 17 - 28.

- and Eales, H.V. (1993). Correlation between chromite composition and PGE mineralization in the Critical Zone of the Western Bushveld Complex. *Mineral. Deposita*, **28**, 291 - 302.

Thayer, T.P. (1970). Chromite segregations as petrogenetic indicators. Symposium on the Bushveld Igneous Complex and other Layered Intrusions. *Geol. Soc. S. Afr.*, **Spec. Publn. 1**, 380 - 390.

Vermaak, C.F. and Von Gruenewaldt, G. (1981). *Bushveld Excursion - Guidebook. Third International Platinum Symposium*. Geological Society. South Africa, Geocongress '81. 62 pp.

Von Gruenewadlt, G., Sharpe, M.R. and Hatton, C.J. (1985). The Bushveld Complex: Introduction and review. *Econ. Geol.*, **80**, 803 - 812.

Worst, B.G. (1993). The geology and environment of the mafic portion of the Bushveld Complex, Vol. VI and III. *Geol. Surv. S. Afr.*, **unpubl. report, No. 1993-0235**.

Appendix A. Whole-rock Chemical Data for LG and MG Chromitite Seams (chromite and intercumulus minerals). Ruighoek Section.

Wt %	LG1	LG2	LG3	LG4	LG5	LG6	LG6a	MG1	MG2	MG3	MG4	MG4a
SiO_2	3.60	3.27	2.32	3.77	4.74	2.35	2.14	4.94	6.36	18.55	5.79	7.05
TiO_2	0.41	0.39	0.31	0.54	0.44	0.47	0.49	0.63	0.64	0.76	0.55	0.62
Al_2O_3	11.12	10.54	10.25	14.07	12.95	12.48	14.02	15.14	15.67	14.54	18.09	17.66
FeO	21.17	21.40	19.65	19.64	23.75	24.80	24.96	24.41	26.31	23.49	24.99	25.71
MnO	0.39	0.40	0.40	0.37	0.42	0.41	0.37	0.41	0.41	0.52	0.34	0.41
MgO	11.92	12.05	12.00	14.17	11.93	11.30	10.90	11.78	11.19	10.80	11.49	10.53
CaO	0.10	0.38	0.32	0.70	0.17	0.21	0.39	0.67	0.82	1.96	0.63	0.97
Na_2O	0.00	0.00	0.00	0.00	0.00	0.00	0.03	0.14	0.25	0.37	0.24	0.38
K_2O	0.00	0.00	0.00	0.00	0.00	0.00	0.07	0.00	0.02	0.04	0.03	0.02
P_2O_5	0.00	0.00	0.00	0.00	0.00	0.00	0.02	0.00	0.00	0.01	0.01	0.02
Cr_2O_3	50.56	50.92	52.98	45.08	44.54	46.12	44.85	40.62	37.07	27.94	36.37	35.27
NiO	0.20	0.15	0.08	0.10	0.12	0.13	0.16	0.22	0.10	0.13	0.16	0.14
V_2O_5	0.26	0.27	0.13	0.22	0.37	0.36	0.28	0.27	0.34	0.26	0.36	0.34
Cr:Fe	2.10	2.09	2.37	2.02	1.65	1.64	1.58	1.46	1.24	1.05	1.28	1.21
Total	99.73	99.77	98.44	98.66	99.43	98.63	98.68	99.23	99.18	99.37	99.05	99.12

Ruighoek Section.

Wt %	LG3	LG4	LG5	LG6	LG6a	MG4
SiO_2	7.22	6.43	4.42	1.43	1.58	8.77
TiO_2	0.42	0.36	0.41	0.53	0.47	0.61
Al_2O_3	11.84	15.82	13.84	14.58	13.56	18.01
FeO	20.82	22.66	23.39	25.28	25.4	23.82
MnO	0.55	0.36	0.40	0.40	0.44	0.38
MgO	12.58	11.16	12.17	11.40	11.09	10.94
CaO	0.12	0.17	0.15	0.26	0.32	0.99
Na_2O	0.00	0.00	0.00	0.00	0.06	0.37
K_2O	0.00	0.00	0.00	0.01	0.00	0.04
P_2O_5	0.00	0.00	0.00	0.01	0.00	0.00
Cr_2O_3	45.32	44.12	43.18	44.25	45.76	34.09
NiO	0.17	0.12	0.10	0.07	0.14	0.17
V_2O_5	0.20	0.22	0.28	0.39	0.39	0.38
Cr:Fe	1.92	1.71	1.62	1.54	1.61	1.26
Total	98.74	98.42	98.34	99.33	98.85	98.57

Boshoek Section.

Wt %	LG6	LG6a	MG1	MG2
SiO_2	12.38	31.21	13.78	13.32
TiO_2	0.48	0.41	0.60	0.70
Al_2O_3	14.79	9.31	14.54	15.47
FeO	24.12	17.83	23.23	24.26
MnO	0.40	0.29	0.36	0.39
MgO	10.27	19.22	12.47	9.70
CaO	0.64	1.48	0.67	0.63
Na_2O	0.12	0.42	0.00	0.00
K_2O	0.05	0.18	0.00	0.00
P_2O_5	0.02	0.02	0.00	0.00
Cr_2O_3	35.78	18.58	33.28	33.43
NiO	0.14	0.13	0.14	0.15
V_2O_5	0.30	0.27	0.24	0.37
Cr:Fe	1.31	0.92	1.26	1.21
Total	99.49	99.35	99.31	98.42

Rustenburg Section - Drill core CC2.

Wt %	LG6	LG7	MG1	MG2	MG3	MG4b	MG4c
SiO_2	4.86	9.47	7.41	5.46	8.68	9.20	11.44
TiO_2	0.72	0.69	0.65	0.80	0.80	1.28	0.61
Al_2O_3	13.77	15.43	13.95	15.49	15.18	13.11	14.14
FeO	25.77	25.12	25.75	25.28	25.30	25.79	24.40
MnO	0.26	0.27	0.27	0.25	0.29	0.27	0.25
MgO	10.85	9.51	11.56	9.57	10.89	9.52	10.60
CaO	0.54	1.91	0.57	0.64	0.93	1.38	2.19
Na_2O	0.03	0.38	0.14	0.12	0.38	0.34	0.34
K_2O	0.00	0.00	0.00	0.00	0.00	0.07	0.00
P_2O_5	0.00	0.00	0.01	0.00	0.00	0.00	0.02
Cr_2O_3	42.34	36.98	38.37	41.57	36.97	37.49	35.18
NiO	0.32	0.20	0.27	0.23	0.38	0.21	0.32
V_2O_5	0.30	0.26	0.30	0.39	0.32	0.33	0.25
Cr:Fe	1.45	1.30	1.31	1.45	1.29	1.28	1.27
Total	99.76	100.22	99.25	99.80	100.12	98.99	99.74

Rustenburg Section - Sampling Locality 2.

Wt %	LG6	LG6a	LG6	LG6a	LG6	LG6a
Level	2L	2L	4L	4L	6L	6L
SiO_2	5.13	4.34	20.35	6.35	4.33	4.85
TiO_2	0.51	0.54	0.40	0.61	0.56	0.48
Al_2O_3	13.66	14.20	11.55	15.02	13.74	14.21
FeO	24.52	24.51	20.33	23.62	24.76	24.49
MnO	0.37	0.35	0.37	0.39	0.44	0.33
MgO	12.10	11.44	16.68	11.39	11.75	12.17
CaO	0.82	0.96	1.20	0.70	0.59	0.59
Na_2O	0.42	0.27	0.30	0.12	0.09	0.09
K_2O	0.12	0.23	0.12	0.05	0.00	0.05
P_2O_5	0.02	0.00	0.02	0.00	0.02	0.02
Cr_2O_3	41.27	41.08	27.06	40.21	42.37	41.51
NiO	0.18	0.17	0.26	0.17	0.14	0.18
V_2O_5	0.37	0.34	0.23	0.37	0.30	0.42
Cr:Fe	1.48	1.47	1.17	1.50	1.51	1.49
Total	99.19	98.43	98.87	99.00	99.09	99.39

Rustenburg Section - Sampling Locality 3.

Wt %	LG6
SiO_2	6.06
TiO_2	0.62
Al_2O_3	14.74
FeO	24.03
MnO	0.40
MgO	10.93
CaO	1.00
Na_2O	0.32
K_2O	0.15
P_2O_5	0.01
Cr_2O_3	40.37
NiO	0.12
V_2O_5	0.34
Cr:Fe	1.48
Total	99.10

Rustenburg Section - Sampling Locality 4.

Wt %	LG6	LG6a	LG6	LG6a	LG6	LG6a
Level	7L	7L	9L	9L	13L	13L
SiO_2	4.77	7.53	4.03	21.76	8.89	3.51
TiO_2	0.62	0.53	0.59	0.45	0.49	0.61
Al_2O_3	14.48	13.60	13.44	10.40	13.65	13.63
FeO	24.25	23.86	24.40	20.57	22.64	23.96
MnO	0.34	0.37	0.42	0.31	0.43	0.41
MgO	11.48	12.09	11.87	18.05	13.25	11.88
CaO	0.62	0.72	0.47	1.22	0.63	0.22
Na_2O	0.26	0.29	0.10	0.32	0.22	0.08
K_2O	0.09	0.20	0.13	0.14	0.07	0.10
P_2O_5	0.02	0.03	0.02	0.02	0.01	0.01
Cr_2O_3	41.23	39.86	42.56	26.11	37.68	43.52
NiO	0.11	0.15	0.09	0.12	0.11	0.13
V_2O_5	0.28	0.28	0.31	0.27	0.23	0.33
Cr:Fe	1.50	1.47	1.53	1.12	1.46	1.60
Total	98.55	99.51	98.43	99.74	98.39	98.29

Marikana Section - Sampling Locality 1.

Wt %	LG6	MG1
SiO_2	11.33	12.44
TiO_2	0.60	0.42
Al_2O_3	13.27	15.40
FeO	24.33	22.36
MnO	0.44	0.35
MgO	12.40	11.71
CaO	0.62	1.23
Na_2O	0.03	0.27
K_2O	0.03	0.10
P_2O_5	0.00	0.02
Cr_2O_3	35.82	33.56
NiO	0.18	0.16
V_2O_5	0.25	0.39
Cr:Fe	1.30	1.32
Total	99.30	98.41

Marikana Section- Sampling Locality 2.

Wt %	MG1	MG2	MG3
SiO_2	9.22	10.12	10.23
TiO_2	0.62	0.70	0.78
Al_2O_3	13.35	15.72	16.22
FeO	24.24	24.77	25.03
MnO	0.37	0.35	0.36
MgO	11.95	10.31	10.27
CaO	0.60	1.35	1.25
Na_2O	0.19	0.28	0.39
K_2O	0.21	0.04	0.04
P_2O_5	0.03	0.00	0.04
Cr_2O_3	37.55	35.24	34.05
NiO	0.19	0.10	0.21
V_2O_5	0.32	0.39	0.28
Cr:Fe	1.36	1.25	1.20
Total	98.84	99.37	99.15

Marikana Section - Sampling Locality 3.

Wt %	MG1	MG1	MG1	MG2	MG2	MG3
SiO_2	5.27	4.58	2.71	5.16	2.24	9.14
TiO_2	0.58	0.67	0.72	0.72	0.63	0.66
Al_2O_3	13.33	15.95	14.55	16.07	13.71	14.26
FeO	23.48	24.89	24.85	25.72	25.20	25.34
MnO	0.39	0.44	0.45	0.41	0.46	0.44
MgO	12.76	11.52	12.07	10.92	11.71	11.09
CaO	0.53	0.84	0.24	0.79	0.21	0.49
Na_2O	0.16	0.19	0.00	0.16	0.00	0.21
K_2O	0.14	0.04	0.00	0.00	0.00	0.12
P_2O_5	0.00	0.01	0.00	0.00	0.01	0.00
Cr_2O_3	40.94	39.77	43.15	38.49	44.14	36.49
NiO	0.16	0.18	0.13	0.16	0.15	0.21
V_2O_5	0.30	0.36	0.34	0.37	0.34	0.38
Cr:Fe	1.53	1.41	1.53	1.32	1.54	1.27
Total	98.04	99.44	99.21	98.97	98.80	98.83

Appendix B. Average Compositions of Chromite in Sulfide-poor Chromitite Layers below the UG2 - after Scoon and Teigler, 1994.

Wt %	MG4B	MG4a	MG3	MG2	MG1	LG	LG	LG	LG	LG	LG	LG
TiO_2	1.50	0.73	0.71	0.91	0.58	1.33	0.61	0.53	0.95	1.44	1.00	0.99
Al_2O_3	12.63	16.41	15.36	13.67	19.02	10.55	16.58	19.27	15.03	9.68	14.39	10.58
Cr_2O_3	45.22	43.60	44.91	46.67	45.65	47.42	43.23	41.54	41.75	43.31	43.14	49.79
FeO	25.26	20.70	21.05	20.72	22.02	23.06	18.60	18.60	20.62	25.49	21.18	20.82
Fe_2O_3	8.58	9.24	9.03	8.65	3.97	10.95	9.35	9.76	12.76	13.80	11.27	8.87
MnO	0.34	0.29	0.33	0.33	0.30	0.33	0.31	0.30	0.31	0.38	0.32	0.33
NiO	0.14	0.14	0.14	0.13	0.09	0.13	0.14	0.14	0.13	0.09	0.05	0.18
MgO	6.22	9.27	8.91	9.00	8.64	8.22	10.31	10.96	9.38	5.69	8.88	8.67
Total	99.89	100.38	100.44	100.08	100.27	101.99	99.13	101.10	100.93	99.88	100.23	100.23
Cr:Fe	1.21	1.32	1.36	1.44	1.57	1.31	1.41	1.34	1.14	1.01	1.21	1.52

Appendix C. Rustenburg Section - Cumulate Succession.

Sample	1	2	3	4	5	6	7	8
Lithology	Anor	Anor	Anor	PPegm	PPegm	PPegm	Norite	PPegm
Depth	3.82	6.55	8.96	11.50	13.04	16.25	16.89	18.07
SiO_2	49.96	49.61	48.87	51.13	52.90	52.46	51.43	52.16
TiO_2	0.06	0.07	0.05	0.12	0.17	0.23	0.13	0.36
Al_2O_3	28.25	27.86	30.06	16.46	9.98	3.32	14.80	4.24
FeO	1.30	1.80	1.00	6.74	7.50	10.14	4.82	11.51
Fe_2O_3	0.77	0.57	0.37	0.87	2.51	5.50	3.72	5.11
MnO	0.04	0.05	0.03	0.13	0.16	0.27	0.16	0.26
MgO	2.97	3.47	1.77	12.24	16.62	22.78	14.88	19.43
CaO	13.76	13.75	14.77	7.75	5.83	2.44	8.12	2.45
Na_2O	2.58	2.38	2.53	1.11	0.77	0.37	1.10	0.45
K_2O	0.15	0.12	0.17	0.13	0.17	0.10	0.13	0.44
P_2O_5	0.01	0.01	0.01	0.01	0.01	0.01	0.01	0.04
Cr_2O_3	0.03	0.04	<0.01	0.18	0.29	0.37	0.18	0.33
H_2O+	0.20	0.21	0.12	2.60	2.53	0.75	0.17	0.82
CO_2	<0.01	0.11	0.05	0.02	0.01	0.30	0.10	0.50
S	<0.001	0.00	<0.001	<0.001	<0.001	0.14	<0.001	0.86
Total	100.08	100.04	99.80	99.52	99.44	99.16	99.75	98.96

Rustenburg Section - Cumulate Succession Continued.

Sample	9	10	11	12	13	14	15	16
Lithology	Pyroxenite	Lnorite	PPegm	Norite	Norite	Pyroxenite	Lnorite	Mnorite
Depth	23.03	29.02	31.63	35.02	40.06	44.82	47.06	54.42
SiO_2	51.29	50.42	52.36	50.84	52.13	52.87	50.61	51.89
TiO_2	0.10	0.09	0.19	0.11	0.13	0.17	0.13	0.13
Al_2O_3	18.03	22.41	11.53	17.60	15.94	8.99	19.27	12.66
FeO	4.31	2.60	7.10	4.51	5.63	5.17	4.60	4.77
Fe_2O_3	2.25	1.97	2.39	2.07	1.68	5.30	1.24	3.20
MnO	0.13	0.09	0.17	0.13	0.14	0.20	0.12	0.16
MgO	11.99	8.30	16.44	12.41	13.23	19.51	10.35	17.49
CaO	9.65	11.83	7.27	9.62	8.64	5.88	10.56	6.88
Na_2O	1.58	1.86	1.09	1.40	1.66	0.85	1.66	1.19
K_2O	0.10	0.13	0.20	0.11	0.11	0.08	0.17	0.16
P_2O_5	<0.01	0.01	0.01	0.01	0.01	0.01	0.01	0.01
Cr_2O_3	0.15	0.11	0.20	0.17	0.17	0.28	0.15	0.29
H_2O+	0.11	0.11	0.29	0.48	0.11	0.30	0.52	0.59
CO_2	0.03	0.02	0.10	0.25	0.04	0.09	0.30	0.29
S	0.00	<0.001	0.09	0.05	<0.001	0.00	0.03	0.01
Total	99.71	99.93	99.43	99.74	99.61	99.71	99.71	99.71

Rustenburg Section - Cumulate Succession Continued.

Sample	17	18	19	20	21	22	23	24
Lithology	Mnorite	Mnorite	Pyroxenite	Pyroxenite	Anor	Pyroxenite	Pyroxenite	Pyroxenite
Depth	60.24	65.03	69.64	75.04	80.29	85.63	90.05	95.01
SiO_2	50.74	51.10	53.39	53.83	48.03	54.13	51.51	54.52
TiO_2	0.10	0.11	0.18	0.19	0.05	0.19	0.18	0.24
Al_2O_3	19.94	19.73	3.49	4.01	31.23	4.50	13.66	4.83
FeO	3.55	4.00	8.52	6.79	0.81	5.72	7.36	9.73
Fe_2O_3	1.71	1.57	2.90	4.93	0.34	5.25	0.00	1.24
MnO	0.10	0.11	0.23	0.23	0.09	0.22	0.15	0.22
MgO	11.24	10.06	25.70	24.89	0.96	24.60	15.60	22.82
CaO	10.08	10.57	3.29	3.33	15.28	3.55	7.55	3.55
Na_2O	1.67	1.87	0.38	0.42	2.46	0.60	1.52	0.78
K_2O	0.10	0.14	0.06	0.11	0.11	0.10	0.21	0.33
P_2O_5	<0.01	0.01	0.01	0.01	0.01	0.02	0.02	0.07
Cr_2O_3	0.36	0.12	0.43	0.56	0.51	0.51	0.54	0.55
H_2O+	0.21	0.27	0.29	0.13	0.19	0.19	0.55	0.21
CO_2	0.04	0.10	0.13	0.04	0.02	0.07	0.32	0.05
S	<0.001	0.01	0.01	0.01	<0.001	0.00	0.01	0.01
Total	99.83	99.76	99.02	99.47	100.10	99.65	99.19	99.15

Rustenburg Section - Cumulate Succession Continued.

Sample	25	26	27	28	29	30
Lithology	Pyroxenite	Pyroxenite	Pyroxenite	Pyroxenite	Pyroxenite	Pyroxenite
Depth	100.42	104.82	110.49	114.65	119.90	124.63
SiO_2	53.67	54.54	54.78	55.13	54.86	54.38
TiO_2	0.20	0.18	0.15	0.22	0.23	0.19
Al_2O_3	5.25	3.90	2.68	3.88	3.87	4.55
FeO	9.44	6.10	6.89	7.49	8.98	8.28
Fe_2O_3	1.77	5.29	4.07	3.15	1.92	2.39
MnO	0.22	0.22	0.22	0.21	0.23	0.21
MgO	23.17	24.19	27.35	24.57	24.48	24.68
CaO	3.64	3.87	2.42	3.10	3.04	3.26
Na_2O	0.72	0.42	0.25	0.55	0.66	0.66
K_2O	0.14	0.10	0.08	0.33	0.25	0.11
P_2O_5	0.01	0.01	0.01	0.16	0.03	0.02
Cr_2O_3	0.71	0.77	0.43	0.39	0.35	0.37
H_2O+	0.18	0.30	0.19	0.29	0.28	0.27
CO_2	0.06	0.06	0.02	0.03	0.03	0.03
S	0.01	0.011	0.006	0.020	0.018	0.013
Total	99.20	99.95	99.55	99.52	99.23	99.42

Legend for Rustenburg Cumulate Results.

Pyroxenite	Pyroxenite
PPegm	Pegmatoidal pyroxenite
Anor	Anorthosite
Lnorite	Leuconorite
Mnorite	Melanorite
Depth	Average depth at which sample was taken

Appendix D. Regional Map of the Economically Important Chromitite Seams and Merensky Reef.

Appendix E. Electron Microprobe Data of the Complete Succession of the LG and MG Chromitite Seams, Ruighoek Section.

Code	SiO_2	TiO_2	Al_2O_3	Cr_2O_3	Fe_2O_3	FeO	MnO	MgO	CaO	Na_2O	TOTAL	
LG1	0.00 0.45	13.45	52.61	4.25	18.96	0.00	10.16	0.00	0.00	99.89	RIM	
LG1	0.00	0.49	12.94	51.28	6.28	17.61	0.00	10.92	0.00	0.00	99.52	CORE
LG1	0.12	0.40	12.90	51.43	4.81	18.70	0.00	10.03	0.00	0.00	98.39	RIM
LG1	0.00	0.43	13.06	51.44	6.58	17.40	0.00	11.14	0.00	0.00	100.05	CORE
LG1	0.55	0.42	12.55	51.40	4.21	19.00	0.00	10.16	0.00	0.00	98.29	RIM
LG1	0.00	0.49	14.20	55.48	7.46	19.23	0.00	11.92	0.00	0.00	108.78	CORE
LG1	0.00	0.44	12.92	52.64	4.73	18.41	0.00	10.38	0.00	0.00	99.51	RIM
LG1	0.00	0.48	13.04	51.59	5.75	18.19	0.00	10.57	0.00	0.00	99.62	CORE
LG1	0.00	0.43	13.28	52.07	4.66	18.54	0.00	10.27	0.00	0.00	99.25	RIM
LG1	0.00	0.43	13.01	50.39	7.36	17.31	0.00	11.09	0.00	0.00	99.59	CORE
LG1	0.00	0.45	13.38	51.60	5.23	18.06	0.00	10.62	0.00	0.00	99.33	RIM
LG1	0.00	0.43	13.22	51.72	5.73	18.14	0.00	10.65	0.00	0.00	99.88	CORE
LG1	0.36	0.45	12.95	52.19	3.58	19.61	0.00	9.80	0.00	0.00	98.94	RIM
LG1	0.00	0.40	12.89	51.38	6.72	17.62	0.00	10.94	0.00	0.00	99.95	CORE
LG1	0.05	0.42	13.20	53.01	3.51	19.22	0.00	9.87	0.00	0.00	99.28	RIM
LG1	0.00	0.43	12.99	51.75	6.41	17.71	0.00	10.98	0.00	0.00	100.27	CORE
LG1	0.90	0.35	12.60	51.58	2.93	20.02	0.00	9.73	0.00	0.00	98.11	RIM
LG1	0.0 0	0.43	12.93	51.95	4.53	18.27	0.00	10.22	0.00	0.00	98.33	CORE
LG1	0.00	0.42	13.10	50.88	5.84	17.90	0.00	10.53	0.00	0.00	98.66	RIM
LG1	0.00	0.45	12.98	50.06	6.44	17.45	0.00	10.64	0.08	0.00	98.11	CORE

Code	SiO_2	TiO_2	Al_2O_3	Cr_2O_3	Fe_2O_3	FeO	MnO	MgO	CaO	Na_2O	TOTAL	
LG2	0.00	0.35	12.51	52.44	5.77	17.83	0.00	10.66	0.00	0.00	99.57	RIM
LG2	0.00	0.36	12.54	52.02	6.52	17.46	0.00	10.97	0.00	0.00	99.87	CORE
LG2	0.00	0.37	12.63	52.57	6.12	17.69	0.00	10.93	0.00	0.00	100.31	RIM
LG2	0.00	0.38	12.82	51.81	6.52	17.68	0.00	10.92	0.00	0.00	100.13	CORE
LG2	0.00	0.32	12.43	52.06	5.88	17.49	0.00	10.72	0.00	0.00	98.90	RIM
LG2	0.00	0.35	12.63	50.92	6.30	17.06	0.00	10.87	0.00	0.00	98.13	CORE
LG2	0.00	0.38	12.55	52.29	6.32	17.56	0.00	10.96	0.00	0.00	100.05	RIM
LG2	0.00	0.41	12.79	50.17	6.90	16.98	0.00	10.99	0.00	0.00	98.24	CORE
LG2	0.00	0.45	12.32	52.27	5.42	17.52	0.00	10.73	0.00	0.00	98.70	RIM
LG2	0.00	0.46	12.34	51.49	6.83	17.23	0.00	11.06	0.00	0.00	99.40	CORE
LG2	0.00	0.38	12.44	52.95	5.02	18.01	0.00	10.51	0.00	0.00	99.31	RIM
LG2	0.00	0.38	12.57	51.57	6.69	17.41	0.00	10.95	0.00	0.00	99.57	CORE
LG2	0.00	0.28	12.46	52.34	5.55	17.69	0.00	10.57	0.00	0.00	98.89	RIM
LG2	0.00	0.33	12.79	51.56	6.94	17.20	0.00	11.17	0.00	0.00	99.98	CORE
LG2	0.00	0.32	12.35	53.56	5.20	18.48	0.00	10.31	0.06	0.00	100.28	RIM
LG2	0.00	0.40	12.57	52.35	6.21	17.76	0.00	10.86	0.00	0.00	100.15	CORE
LG2	0.00	0.36	12.25	52.89	5.94	17.94	0.00	10.67	0.00	0.00	100.06	RIM
LG2	0.00	0.40	12.57	52.08	6.70	17.77	0.00	10.91	0.00	0.00	100.43	CORE
LG2	0.00	0.37	12.37	52.22	6.48	17.66	0.00	10.84	0.00	0.00	99.94	RIM
LG2	0.00	0.39	12.24	49.17	7.63	16.54	0.00	10.92	0.00	0.00	96.89	CORE
LG2	0.00	0.40	12.31	53.12	5.29	17.93	0.00	10.64	0.00	0.00	99.69	RIM
LG2	0.00	0.47	12.64	51.94	6.50	17.84	0.00	10.84	0.06	0.00	100.29	CORE
LG2	0.00	0.38	12.40	52.77	5.25	17.70	0.00	10.68	0.00	0.00	99.18	RIM
LG2	0.00	0.40	12.77	51.84	6.05	17.52	0.00	10.90	0.00	0.00	99.48	CORE
LG2	0.05	0.38	12.55	51.88	6.05	17.95	0.00	10.63	0.00	0.00	99.49	RIM
LG2	0.00	0.34	13.02	51.52	5.82	17.71	0.00	10.69	0.00	0.00	99.10	CORE
LG2	0.00	0.45	12.48	52.29	6.07	17.59	0.00	10.92	0.00	0.00	99.81	RIM
LG2	0.00	0.50	12.75	51.79	6.43	17.74	0.00	10.95	0.00	0.00	100.16	CORE
LG2	0.08	0.41	12.64	52.36	5.29	17.86	0.00	10.72	0.00	0.00	99.36	RIM
LG2	0.00	0.42	12.72	51.80	5.79	17.65	0.00	10.75	0.00	0.00	99.13	CORE

Code	SiO_2	TiO_2	Al_2O_3	Cr_2O_3	Fe_2O_3	FeO	MnO	MgO	CaO	Na_2O	TOTAL	
LG3	0.00	0.30	11.43	56.07	4.13	17.28	0.00	11.04	0.00	0.00	100.25	RIM
LG3	0.00	0.37	12.24	53.66	5.19	16.64	0.00	11.42	0.00	0.00	99.52	CORE
LG3	0.00	0.37	12.20	55.36	4.00	17.18	0.00	11.25	0.00	0.00	100.36	RIM
LG3	0.00	0.40	12.26	54.41	5.12	16.89	0.00	11.50	0.00	0.00	100.58	CORE
LG3	0.00	0.39	12.01	54.37	4.69	16.93	0.00	11.25	0.00	0.00	99.64	RIM
LG3	0.00	0.38	12.06	53.76	5.33	16.59	0.00	11.45	0.00	0.00	99.56	CORE
LG3	0.00	0.42	12.25	54.98	4.93	17.12	0.00	11.49	0.00	0.00	101.18	RIM
LG3	0.00	0.41	12.41	54.55	4.93	16.99	0.00	11.50	0.00	0.00	100.79	CORE
LG3	0.00	0.37	12.20	54.40	5.44	16.70	0.00	11.63	0.00	0.00	100.75	RIM
LG3	0.00	0.44	12.19	53.69	5.55	16.71	0.00	11.53	0.00	0.00	100.12	CORE
LG3	0.00	0.42	12.30	54.27	4.50	16.79	0.00	11.40	0.00	0.00	99.68	RIM
LG3	0.00	0.43	12.33	53.61	5.28	16.65	0.00	11.52	0.00	0.00	99.82	CORE
LG3	0.00	0.37	12.03	55.19	4.58	16.76	0.00	11.52	0.00	0.00	100.45	RIM
LG3	0.00	0.37	11.95	54.28	5.11	16.44	0.00	11.56	0.00	0.00	99.71	CORE
LG3	0.00	0.33	11.82	54.81	3.30	17.07	0.00	10.80	0.00	0.00	98.13	RIM
LG3	0.00	0.39	11.75	53.60	5.29	16.19	0.00	11.51	0.00	0.00	98.73	CORE
LG3	0.00	0.37	11.93	55.19	4.10	16.91	0.00	11.28	0.00	0.00	99.78	RIM
LG3	0.00	0.41	12.33	54.46	4.80	16.71	0.00	11.57	0.00	0.00	100.28	CORE
LG3	0.00	0.37	11.51	56.44	3.80	17.22	0.00	11.19	0.00	0.00	100.53	RIM
LG3	0.00	0.41	12.14	54.14	5.11	16.39	0.00	11.67	0.00	0.00	99.86	CORE
LG3	0.00	0.42	12.15	54.44	4.48	17.04	0.00	11.24	0.00	0.00	99.77	RIM
LG3	0.00	0.43	12.26	53.71	5.20	16.57	0.00	11.54	0.00	0.00	99.71	CORE
LG3	0.00	0.37	12.45	53.96	5.07	16.54	0.00	11.61	0.00	0.00	100.00	RIM
LG3	0.00	0.36	12.21	53.08	5.44	16.37	0.00	11.46	0.00	0.00	98.93	CORE
LG3	0.00	0.36	12.45	53.82	5.00	17.19	0.00	11.18	0.00	0.00	100.00	RIM
LG3	0.07	0.34	12.34	54.04	4.67	16.99	0.00	11.30	0.00	0.00	99.75	CORE
LG3	0.00	0.39	12.23	55.17	4.24	17.29	0.00	11.23	0.00	0.00	100.55	RIM
LG3	0.00	0.38	12.26	54.46	5.02	16.88	0.00	11.47	0.00	0.00	100.47	CORE
LG3	0.00	0.30	12.44	55.36	4.20	17.12	0.00	11.32	0.06	0.00	100.80	RIM
LG3	0.00	0.33	12.41	54.46	5.19	16.75	0.00	11.60	0.00	0.00	100.74	CORE

Code	SiO_2	TiO_2	Al_2O_3	Cr_2O_3	Fe_2O_3	FeO	MnO	MgO	CaO	Na_2O	TOTAL	
LG4	0.70	0.39	13.61	51.26	3.95	17.53	0.00	11.47	0.00	0.00	98.92	RIM
LG4	0.00	0.45	13.87	52.97	4.21	17.29	0.00	11.35	0.00	0.00	100.14	CORE
LG4	0.00	0.38	13.54	53.78	3.74	16.75	0.00	11.55	0.00	0.00	99.73	RIM
LG4	0.00	0.35	13.84	53.19	4.48	16.46	0.00	11.83	0.00	0.00	100.15	CORE
LG4	0.00	0.41	13.77	53.64	4.23	17.12	0.00	11.55	0.00	0.00	100.71	RIM
LG4	0.00	0.41	13.93	53.59	4.34	16.92	0.00	11.74	0.00	0.00	100.92	CORE
LG4	0.00	0.43	13.79	53.46	4.33	17.07	0.00	11.58	0.00	0.00	100.66	RIM
LG4	0.00	0.43	13.77	53.06	4.54	16.54	0.00	11.82	0.00	0.00	100.17	CORE
LG4	0.00	0.40	14.04	52.00	4.70	16.30	0.00	11.79	0.00	0.00	99.23	RIM
LG4	0.00	0.45	14.26	52.12	4.83	16.82	0.00	11.70	0.00	0.00	100.17	CORE
LG4	0.00	0.43	13.86	53.57	3.85	16.80	0.00	11.67	0.00	0.00	100.18	RIM
LG4	0.00	0.47	13.67	53.23	3.72	16.77	0.00	11.53	0.00	0.00	99.38	CORE
LG4	0.00	0.46	13.37	53.62	4.72	16.83	0.00	11.72	0.00	0.00	100.72	RIM
LG4	0.00	0.45	13.45	53.44	4.55	16.82	0.00	11.66	0.00	0.00	100.37	CORE
LG4	0.00	0.42	13.25	54.78	3.76	16.87	0.00	11.64	0.05	0.00	100.78	RIM
LG4	0.00	0.39	13.25	54.10	4.25	16.66	0.00	11.65	0.08	0.00	100.38	CORE
LG4	0.00	0.42	13.39	53.93	3.96	16.65	0.00	11.68	0.00	0.00	100.03	RIM
LG4	0.00	0.44	13.26	53.38	4.09	16.41	0.00	11.67	0.00	0.00	99.25	CORE
LG4	0.00	0.42	13.14	54.22	4.29	16.87	0.00	11.62	0.00	0.00	100.56	RIM
LG4	0.00	0.43	13.23	53.67	4.37	16.60	0.00	11.69	0.00	0.00	99.99	CORE
LG4	0.00	0.48	13.69	53.73	2.78	17.23	0.00	11.11	0.10	0.00	99.12	RIM
LG4	0.00	0.41	13.30	54.17	3.17	17.58	0.00	10.98	0.00	0.00	99.61	CORE
LG4	0.00	0.42	13.25	53.65	4.05	16.87	0.00	11.45	0.00	0.00	99.69	RIM
LG4	0.00	0.45	13.14	53.24	4.83	16.65	0.00	11.65	0.00	0.00	99.96	CORE
LG4	0.00	0.42	13.08	53.97	3.71	16.95	0.00	11.34	0.00	0.00	99.47	RIM
LG4	0.00	0.47	14.63	58.11	4.70	18.18	0.00	12.66	0.00	0.00	108.75	CORE
LG4	0.00	0.35	13.48	53.20	4.51	16.79	0.00	11.51	0.00	0.00	99.84	RIM
LG4	0.00	0.32	13.11	52.87	5.00	16.68	0.00	11.43	0.00	0.00	99.41	CORE
LG4	0.00	0.41	12.61	53.78	4.64	16.57	0.00	11.49	0.07	0.00	99.58	RIM
LG4	0.00	0.36	12.25	53.92	4.89	16.35	0.00	11.57	0.00	0.00	99.34	CORE

Code	SiO_2	TiO_2	Al_2O_3	Cr_2O_3	Fe_2O_3	FeO	MnO	MgO	CaO	Na_2O	TOTAL	
LG5	0.00	0.55	15.60	47.92	3.78	21.19	0.00	8.50	0.00	0.00	97.54	RIM
LG5	0.00	0.58	15.37	46.90	7.44	18.47	0.00	10.62	0.00	0.00	99.38	CORE
LG5	0.00	0.55	15.32	48.16	5.53	19.65	0.00	9.76	0.00	0.00	98.96	RIM
LG5	0.00	0.57	15.05	47.20	7.49	18.74	0.00	10.42	0.00	0.00	99.47	CORE
LG5	0.00	0.51	14.94	48.11	4.98	19.34	0.00	9.59	0.00	0.00	97.47	RIM
LG5	0.00	0.58	14.69	47.55	6.37	18.67	0.00	10.14	0.00	0.00	98.00	CORE
LG5	0.00	0.54	15.59	48.93	3.96	20.74	0.00	9.05	0.00	0.00	98.82	RIM
LG5	0.00	0.56	15.10	47.47	7.54	18.66	0.00	10.56	0.00	0.00	99.90	CORE
LG5	0.00	0.60	15.67	48.30	3.60	21.16	0.00	8.65	0.00	0.00	97.98	RIM
LG5	0.00	0.56	15.32	47.42	7.44	18.94	0.00	10.45	0.00	0.00	100.14	CORE
LG5	0.00	0.56	15.25	48.18	4.67	20.16	0.00	9.24	0.00	0.00	98.06	RIM
LG5	0.00	0.58	15.14	47.68	7.69	18.54	0.00	10.76	0.00	0.00	100.39	CORE
LG5	0.00	0.57	15.31	48.92	4.22	20.89	0.00	8.95	0.00	0.00	98.86	RIM
LG5	0.00	0.52	15.21	47.15	7.63	18.72	0.00	10.47	0.00	0.00	99.69	CORE
LG5	0.00	0.61	15.10	48.76	4.36	20.20	0.00	9.25	0.05	0.00	98.34	RIM
LG5	0.00	0.58	14.99	47.12	7.63	18.55	0.00	10.53	0.00	0.00	99.40	CORE
LG5	0.10	0.55	15.45	47.65	3.81	21.40	0.00	8.39	0.00	0.00	97.35	RIM
LG5	0.00	0.57	15.18	47.08	7.79	18.66	0.00	10.56	0.00	0.00	99.84	CORE
LG5	0.08	0.55	15.14	48.12	3.80	20.76	0.00	8.72	0.00	0.00	97.17	RIM
LG5	0.00	0.57	15.15	47.32	7.76	18.55	0.00	10.67	0.00	0.00	100.0	CORE
LG5	0.00	0.51	15.32	47.31	6.44	18.94	0.00	10.12	0.00	0.00	98.65	RIM
LG5	0.00	0.52	15.05	47.17	7.23	18.63	0.00	10.36	0.00	0.00	98.96	CORE
LG5	0.00	0.52	15.07	48.45	4.71	20.61	0.00	8.96	0.00	0.00	98.32	RIM
LG5	0.00	0.55	15.24	47.36	7.76	18.68	0.00	10.62	0.00	0.00	100.21	CORE
LG5	0.00	0.64	15.07	48.09	4.98	19.35	0.00	9.76	0.00	0.00	97.89	RIM
LG5	0.00	0.62	15.06	47.40	7.23	18.73	0.00	10.47	0.00	0.00	99.50	CORE
LG5	0.00	0.59	15.11	48.91	4.12	20.80	0.00	8.91	0.00	0.00	98.44	RIM
LG5	0.00	0.56	14.91	47.89	7.35	18.86	0.00	10.44	0.00	0.00	100.0	CORE
LG5	0.00	0.57	14.87	48.37	5.69	19.59	0.00	9.69	0.06	0.00	98.84	RIM
LG5	0.00	0.61	14.83	47.89	7.68	19.09	0.00	10.41	0.00	0.00	100.5	CORE

Code	SiO_2	TiO_2	Al_2O_3	Cr_2O_3	Fe_2O_3	FeO	MnO	MgO	CaO	Na_2O	TOTAL	
LG6	0.00	0.61	14.31	46.60	7.78	18.98	0.00	9.95	0.00	0.00	98.23	RIM
LG6	0.00	0.60	14.49	45.95	8.58	18.95	0.00	10.06	0.00	0.00	98.63	CORE
LG6	0.00	0.61	13.92	47.72	7.79	19.13	0.00	10.01	0.00	0.00	99.18	RIM
LG6	0.00	0.57	14.37	47.42	8.09	19.22	0.00	10.09	0.00	0.00	99.76	CORE
LG6	0.00	0.54	14.65	47.40	8.01	19.52	0.00	9.98	0.00	0.00	100.10	RIM
LG6	0.00	0.54	14.65	47.85	7.75	19.49	0.00	10.05	0.00	0.00	100.34	CORE
LG6	0.00	0.58	13.73	47.89	7.06	18.57	0.00	10.08	0.00	0.00	97.91	RIM
LG6	0.00	0.59	13.77	46.68	7.66	18.28	0.00	10.10	0.00	0.00	97.08	CORE
LG6	0.00	0.59	14.45	47.46	7.74	19.52	0.00	9.90	0.00	0.00	99.67	RIM
LG6	0.00	0.59	14.58	47.27	7.86	19.45	0.00	9.97	0.00	0.00	99.72	CORE
LG6	0.00	0.64	14.60	47.82	6.60	19.33	0.00	9.92	0.00	0.00	98.91	RIM
LG6	0.00	0.60	14.59	47.39	7.47	18.98	0.00	10.18	0.00	0.00	99.21	CORE
LG6	0.00	0.55	14.24	47.73	7.22	19.37	0.00	9.80	0.00	0.00	98.91	RIM
LG6	0.00	0.63	14.27	47.16	7.64	19.26	0.00	9.91	0.00	0.00	98.86	CORE
LG6	0.00	0.63	14.11	47.64	7.76	19.09	0.00	10.10	0.00	0.00	99.33	RIM
LG6	0.00	0.60	14.35	47.44	8.07	19.14	0.00	10.16	0.00	0.00	99.76	CORE
LG6	0.00	0.60	14.36	47.19	7.87	19.08	0.00	10.08	0.00	0.00	99.18	RIM
LG6	0.00	0.59	14.56	47.09	7.90	19.16	0.00	10.09	0.00	0.00	99.39	CORE
LG6	0.00	0.58	14.75	47.88	6.35	19.80	0.00	9.61	0.00	0.00	98.98	RIM
LG6	0.00	0.63	14.54	47.06	7.48	18.91	0.00	10.15	0.00	0.00	98.77	CORE
LG6	0.00	0.58	14.36	47.63	7.95	18.90	0.00	10.30	0.00	0.00	99.73	RIM
LG6	0.00	0.58	14.51	47.36	7.87	18.99	0.00	10.22	0.00	0.00	99.53	CORE
LG6	0.00	0.52	14.22	47.68	7.75	19.07	0.00	10.05	0.00	0.00	99.29	RIM
LG6	0.06	0.58	14.28	47.28	7.75	19.09	0.00	10.10	0.00	0.00	99.14	CORE
LG6	0.00	0.61	14.63	48.06	7.61	19.42	0.00	10.17	0.00	0.00	100.50	RIM
LG6	0.00	0.61	14.41	47.74	7.79	19.26	0.00	10.14	0.00	0.00	99.95	CORE
LG6	0.00	0.58	14.56	47.59	6.83	19.11	0.00	9.97	0.00	0.00	98.63	RIM
LG6	0.00	0.60	14.53	47.29	7.23	18.96	0.00	10.08	0.00	0.00	98.69	CORE
LG6	0.25	0.57	14.36	48.01	5.71	20.36	0.00	9.30	0.06	0.00	98.61	RIM
LG6	0.00	0.62	14.43	47.56	7.64	19.08	0.00	10.17	0.00	0.00	99.49	CORE

Code	SiO_2	TiO_2	Al_2O_3	Cr_2O_3	Fe_2O_3	FeO	MnO	MgO	CaO	Na_2O	TOTAL	
LG6a	0.00	0.63	14.53	47.84	7.76	19.53	0.00	10.07	0.00	0.00	100.37	RIM
LG6a	0.00	0.60	14.69	47.59	7.99	19.47	0.00	10.13	0.00	0.00	100.47	CORE
LG6a	0.00	0.66	14.53	48.04	7.44	19.45	0.00	10.12	0.00	0.00	100.23	RIM
LG6a	0.00	0.62	14.35	47.64	7.44	19.26	0.00	10.01	0.00	0.00	99.32	CORE
LG6a	0.00	0.59	14.59	47.91	8.04	19.32	0.00	10.26	0.00	0.00	100.72	RIM
LG6a	0.00	0.55	14.47	47.25	8.20	19.10	0.00	10.16	0.00	0.00	99.73	CORE
LG6a	0.00	0.66	14.70	48.22	5.57	20.31	0.00	9.28	0.00	0.00	98.74	RIM
LG6a	0.00	0.66	14.26	47.21	7.38	19.32	0.00	9.85	0.00	0.00	98.68	CORE
LG6a	0.00	0.70	14.62	48.52	5.35	20.01	0.00	9.48	0.00	0.00	98.68	RIM
LG6a	0.00	0.65	14.27	47.69	7.47	19.08	0.00	10.13	0.00	0.00	99.29	CORE
LG6a	0.00	0.51	14.86	47.91	7.81	19.15	0.00	10.29	0.05	0.00	100.58	RIM
LG6a	0.00	0.69	14.54	47.00	7.95	19.21	0.00	10.14	0.00	0.00	99.53	CORE
LG6a	0.00	0.66	14.58	48.15	6.86	19.88	0.00	9.78	0.00	0.00	99.91	RIM
LG6a	0.00	0.71	15.82	51.98	8.70	21.22	0.00	11.05	0.00	0.00	109.48	CORE
LG6a	0.00	0.62	14.52	48.32	6.70	19.78	0.00	9.78	0.00	0.00	99.72	RIM
LG6a	0.00	0.60	14.06	48.11	7.55	19.34	0.00	9.98	0.00	0.00	99.64	CORE
LG6a	0.06	0.63	14.33	47.90	7.76	19.49	0.00	10.11	0.00	0.00	100.29	RIM
LG6a	0.00	0.61	14.41	46.84	7.61	19.44	0.00	9.75	0.00	0.00	98.66	CORE
LG6a	0.00	0.67	14.72	47.81	7.35	19.52	0.00	10.08	0.00	0.00	100.16	RIM
LG6a	0.00	0.65	14.41	47.46	7.00	19.37	0.00	9.84	0.00	0.00	98.73	CORE
LG6a	0.00	0.51	14.34	48.09	7.78	19.31	0.00	10.07	0.00	0.00	100.10	RIM
LG6a	0.00	0.48	14.28	47.86	7.89	19.19	0.00	10.05	0.00	0.00	99.75	CORE
LG6a	0.00	0.64	14.63	48.20	7.21	20.03	0.00	9.80	0.00	0.00	100.51	RIM
LG6a	0.00	0.63	14.50	48.06	7.81	19.69	0.00	10.04	0.00	0.00	100.73	CORE
LG6a	0.00	0.65	14.45	48.19	7.73	19.63	0.00	10.09	0.00	0.00	100.74	RIM
LG6a	0.00	0.66	14.58	47.76	8.00	19.53	0.00	10.16	0.00	0.00	100.69	CORE
LG6a	0.00	0.67	14.29	47.80	7.68	19.24	0.00	10.15	0.00	0.00	99.83	RIM
LG6a	0.00	0.62	14.55	47.99	7.72	19.33	0.00	10.21	0.00	0.00	100.42	CORE
LG6a	0.06	0.65	14.50	48.30	6.30	19.54	0.00	9.91	0.00	0.00	99.25	RIM
LG6a	0.00	0.67	14.14	47.69	7.38	18.98	0.00	10.13	0.00	0.00	98.99	CORE

Code	SiO_2	TiO_2	Al_2O_3	Cr_2O_3	Fe_2O_3	FeO	MnO	MgO	CaO	Na_2O	TOTAL	
MGI	0.00	0.82	16.10	45.13	8.34	19.25	0.00	10.47	0.00	0.00	100.11	RIM
MGI	0.00	0.89	16.09	44.61	8.61	19.24	0.00	10.47	0.00	0.00	99.91	CORE
MGI	0.00	0.80	15.93	45.80	6.22	19.38	0.00	9.95	0.00	0.00	98.08	RIM
MGI	0.00	0.81	15.69	45.53	7.85	19.11	0.00	10.36	0.00	0.00	99.35	CORE
MGI	0.00	0.77	15.83	45.75	7.81	19.33	0.00	10.30	0.00	0.00	99.79	RIM
MGI	0.00	0.81	16.11	44.65	8.09	19.48	0.00	10.14	0.00	0.00	99.28	CORE
MGI	0.00	0.72	16.48	45.28	7.32	18.86	0.00	10.52	0.00	0.00	99.17	RIM
MGI	0.00	0.81	16.24	45.33	8.02	19.24	0.00	10.45	0.06	0.00	100.14	CORE
MGI	0.05	0.81	16.08	45.28	8.00	19.33	0.00	10.43	0.00	0.00	99.98	RIM
MGI	0.00	0.80	15.97	45.35	8.64	19.34	0.00	10.48	0.00	0.00	100.59	CORE
MGI	0.00	0.72	15.99	45.30	8.53	19.29	0.00	10.36	0.05	0.00	100.24	RIM
MGI	0.00	0.72	15.81	45.57	8.37	19.10	0.00	10.46	0.00	0.00	100.03	CORE
MGI	0.00	0.84	15.89	46.38	7.43	19.60	0.00	10.31	0.00	0.00	100.45	RIM
MGI	0.00	0.81	16.14	45.31	7.99	19.29	0.00	10.36	0.07	0.00	99.97	CORE
MGI	0.00	0.73	15.95	44.95	8.42	18.93	0.00	10.47	0.00	0.00	99.45	RIM
MGI	0.00	0.71	15.88	44.95	8.67	19.03	0.00	10.43	0.00	0.00	99.67	CORE
MGI	0.00	0.74	15.93	45.47	8.15	19.17	0.00	10.36	0.07	0.00	99.89	RIM
MGI	0.00	0.79	15.93	45.30	8.44	19.27	0.00	10.43	0.00	0.00	100.17	CORE
MGI	0.00	0.82	15.88	45.62	8.55	19.15	0.00	10.62	0.00	0.00	100.64	RIM
MGI	0.00	1.02	15.76	45.01	7.68	19.48	0.00	10.21	0.00	0.00	99.16	CORE
MGI	0.00	0.82	15.73	45.69	7.19	18.95	0.00	10.35	0.00	0.00	98.73	RIM
MGI	0.00	0.83	15.75	44.78	8.23	18.89	0.00	10.42	0.00	0.00	98.90	CORE
MGI	0.00	0.79	16.04	45.98	7.52	19.65	0.00	10.21	0.00	0.00	100.18	RIM
MGI	0.00	0.69	15.88	46.01	8.07	19.24	0.00	10.42	0.00	0.00	100.31	CORE
MGI	0.00	0.81	16.04	45.72	8.65	19.45	0.00	10.56	0.00	0.00	101.23	RIM
MGI	0.00	0.82	15.96	45.53	8.32	19.29	0.00	10.45	0.06	0.00	100.42	CORE
MGI	0.00	0.79	15.65	46.03	8.04	19.17	0.00	10.47	0.00	0.00	100.15	RIM
MGI	0.00	0.82	15.97	45.31	8.34	19.15	0.00	10.52	0.00	0.00	100.12	CORE
MGI	0.00	0.81	15.50	45.58	8.17	19.34	0.00	10.25	0.00	0.00	99.65	RIM
MGI	0.00	0.85	16.16	44.48	8.63	19.15	0.00	10.48	0.00	0.00	99.75	CORE

Code	SiO_2	TiO_2	Al_2O_3	Cr_2O_3	Fe_2O_3	FeO	MnO	MgO	CaO	Na_2O	TOTAL	
MG2	0.00	0.84	16.01	44.49	7.71	21.13	0.00	9.07	0.00	0.00	99.25	RIM
MG2	0.00	0.97	15.71	44.09	0.00	20.78	0.00	9.24	0.00	0.00	90.79	CORE
MG2	0.00	1.01	16.25	44.20	0.00	20.82	0.00	9.49	0.00	0.00	91.77	RIM
MG2	0.00	0.99	15.84	44.96	7.85	20.94	0.00	9.42	0.00	0.00	100.00	CORE
MG2	0.00	0.90	16.60	43.81	0.00	21.29	0.00	8.89	0.00	0.00	91.49	RIM
MG2	0.00	0.99	16.28	44.27	0.00	20.94	0.00	9.45	0.00	0.00	91.93	CORE
MG2	0.00	0.95	16.00	44.38	8.26	21.07	0.00	9.32	0.00	0.00	99.98	RIM
MG2	0.00	0.96	16.23	43.54	8.49	20.81	0.00	9.40	0.00	0.00	99.43	CORE
MG2	0.00	0.92	16.17	44.09	0.00	20.96	0.00	9.22	0.00	0.00	91.36	RIM
MG2	0.00	0.97	16.16	43.97	0.00	20.73	0.00	9.34	0.00	0.00	91.17	CORE
MG2	0.00	0.91	16.01	44.47	7.46	20.81	0.00	9.25	0.00	0.00	98.91	RIM
MG2	0.00	1.01	16.08	44.75	0.00	20.84	0.00	9.50	0.00	0.00	92.18	CORE
MG2	0.00	0.91	16.17	44.36	8.05	20.64	0.00	9.53	0.00	0.00	99.66	RIM
MG2	0.00	0.98	16.27	44.30	0.00	20.58	0.00	9.61	0.00	0.00	91.74	CORE
MG2	0.00	1.01	15.85	44.52	8.11	20.98	0.00	9.37	0.00	0.00	99.84	RIM
MG2	0.00	0.99	15.85	44.31	0.00	20.61	0.00	9.33	0.00	0.00	91.09	CORE
MG2	0.00	0.95	16.23	44.66	8.39	21.10	0.00	9.50	0.00	0.00	100.83	RIM
MG2	0.00	0.91	15.84	45.33	7.71	20.96	0.00	9.39	0.00	0.00	100.14	CORE
MG2	0.00	0.96	15.81	44.27	0.00	20.62	0.00	9.37	0.00	0.00	91.03	RIM
MG2	0.00	0.95	15.83	44.68	7.78	20.82	0.00	9.35	0.00	0.00	99.41	CORE
MG2	0.00	0.92	15.89	44.77	7.49	20.79	0.00	9.31	0.00	0.00	99.17	RIM
MG2	0.00	0.93	15.92	45.17	7.55	20.96	0.00	9.36	0.00	0.00	99.89	CORE
MG2	0.00	0.91	16.17	45.16	7.80	20.83	0.00	9.57	0.00	0.00	100.44	RIM
MG2	0.00	0.94	15.96	45.16	0.00	21.00	0.00	9.40	0.00	0.00	92.46	CORE
MG2	0.00	0.94	15.86	45.98	0.00	21.15	0.00	9.39	0.00	0.00	93.32	RIM
MG2	0.00	0.94	16.16	45.55	7.61	21.21	0.00	9.44	0.00	0.00	100.91	CORE
MG2	0.00	0.98	15.94	45.18	8.07	21.41	0.00	9.30	0.00	0.00	100.88	RIM
MG2	0.00	0.97	15.86	45.90	7.76	21.25	0.00	9.46	0.00	0.00	101.20	CORE
MG2	0.00	0.99	16.15	45.35	0.00	21.34	0.00	9.39	0.00	0.00	93.22	RIM
MG2	0.00	0.97	16.16	45.70	7.69	21.28	0.00	9.49	0.00	0.00	101.29	CORE

Code	SiO_2	TiO_2	Al_2O_3	Cr_2O_3	Fe_2O_3	FeO	MnO	MgO	CaO	Na_2O	TOTAL	
MG3	0.00	1.23	13.77	45.87	8.18	23.43	0.00	7.77	0.00	0.00	100.25	RIM
MG3	0.00	1.21	13.87	46.07	8.12	23.52	0.00	7.78	0.00	0.00	100.57	CORE
MG3	0.00	1.31	13.75	45.65	8.16	23.54	0.00	7.72	0.00	0.00	100.13	RIM
MG3	0.00	1.14	13.89	46.02	7.81	23.53	0.00	7.62	0.00	0.00	100.01	CORE
MG3	0.00	1.12	14.05	45.72	7.41	22.75	0.00	7.92	0.00	0.00	98.96	RIM
MG3	0.00	1.09	13.66	46.10	7.52	22.88	0.00	7.79	0.00	0.00	99.04	CORE
MG3	0.00	0.91	14.11	46.12	7.81	23.14	0.00	7.72	0.00	0.00	99.80	RIM
MG3	0.00	0.88	14.23	45.70	8.50	22.91	0.00	7.93	0.00	0.00	100.15	CORE
MG3	0.00	1.12	13.40	45.98	8.44	23.21	0.00	7.73	0.00	0.00	99.89	RIM
MG3	0.00	1.10	13.80	45.52	8.06	23.07	0.00	7.73	0.00	0.00	99.29	CORE
MG3	0.00	1.14	14.07	45.90	7.86	23.37	0.00	7.76	0.00	0.00	100.10	RIM
MG3	0.00	1.22	13.78	45.36	8.51	23.12	0.00	7.89	0.00	0.00	99.88	CORE
MG3	0.00	1.14	13.86	46.23	8.21	23.52	0.00	7.77	0.00	0.00	100.72	RIM
MG3	0.00	1.19	13.90	46.06	8.00	23.52	0.00	7.74	0.00	0.00	100.41	CORE
MG3	0.00	1.14	13.53	46.05	7.89	23.09	0.00	7.69	0.08	0.00	99.47	RIM
MG3	0.00	1.24	13.85	45.48	8.45	23.39	0.00	7.80	0.00	0.00	100.22	CORE
MG3	0.00	1.18	13.68	46.26	7.27	23.23	0.00	7.67	0.00	0.00	99.29	RIM
MG3	0.00	1.09	13.87	45.78	8.40	23.15	0.00	7.86	0.00	0.00	100.14	CORE
MG3	0.00	1.24	13.81	45.78	8.25	23.56	0.00	7.72	0.00	0.00	100.36	RIM
MG3	0.00	1.32	13.78	45.94	8.23	23.64	0.00	7.78	0.00	0.00	100.69	CORE

Code	SiO_2	TiO_2	Al_2O_3	Cr_2O_3	Fe_2O_3	FeO	MnO	MgO	CaO	Na_2O	TOTAL	
MG4	0.00	0.67	18.33	42.93	0.00	21.05	0.00	9.45	0.00	0.00	92.43	RIM
MG4	0.00	0.80	18.19	42.77	7.61	21.38	0.00	9.27	0.00	0.00	100.02	CORE
MG4	0.00	0.83	17.93	42.62	0.00	21.25	0.00	9.36	0.06	0.00	92.05	RIM
MG4	0.00	0.82	18.09	42.84	7.81	21.43	0.00	9.29	0.00	0.00	100.28	CORE
MG4	0.00	0.79	18.03	42.57	8.02	21.32	0.00	9.28	0.00	0.00	100.01	RIM
MG4	0.00	0.77	18.08	42.71	0.00	21.29	0.00	9.39	0.00	0.00	92.24	CORE
MG4	0.00	0.84	18.21	42.43	0.00	21.07	0.00	9.53	0.00	0.00	92.08	RIM
MG4	0.00	0.75	18.23	42.68	8.12	21.11	0.00	9.49	0.00	0.00	100.38	CORE
MG4	0.00	0.68	18.26	41.77	7.85	21.08	0.00	9.14	0.00	0.00	98.78	RIM
MG4	0.00	0.81	18.16	42.45	0.00	21.22	0.00	9.22	0.00	0.00	91.86	CORE
MG4	0.00	0.82	18.41	42.13	7.88	20.95	0.00	9.48	0.05	0.00	99.72	RIM
MG4	0.00	0.76	18.16	42.74	7.99	21.01	0.00	9.51	0.00	0.00	100.17	CORE
MG4	0.00	0.79	18.16	42.72	0.00	20.95	0.00	9.54	0.00	0.00	92.16	RIM
MG4	0.00	0.79	18.48	42.66	7.91	21.20	0.00	9.52	0.00	0.00	100.56	CORE
MG4	0.00	0.79	18.42	42.90	0.00	21.27	0.00	9.42	0.00	0.00	92.80	RIM
MG4	0.00	0.82	18.37	42.95	0.00	21.26	0.00	9.50	0.00	0.00	92.90	CORE
MG4	0.00	0.86	18.37	42.83	8.06	21.40	0.00	9.52	0.00	0.00	101.04	RIM
MG4	0.00	0.78	18.32	42.75	0.00	21.09	0.00	9.48	0.00	0.00	92.42	CORE
MG4	0.05	0.83	18.28	42.83	7.80	21.21	0.00	9.56	0.00	0.00	100.56	RIM
MG4	0.00	0.86	18.13	42.82	7.50	21.06	0.00	9.47	0.00	0.00	99.84	CORE
MG4	0.00	0.84	18.12	42.87	0.00	21.23	0.00	9.37	0.00	0.00	92.43	RIM
MG4	0.00	0.78	18.15	42.98	0.00	21.35	0.00	9.30	0.00	0.00	92.56	CORE
MG4	0.00	0.83	18.34	43.39	7.54	21.64	0.00	9.36	0.00	0.00	101.10	RIM
MG4	0.00	0.82	18.47	43.11	0.00	21.41	0.00	9.52	0.00	0.00	93.33	CORE
MG4	0.00	0.84	18.14	43.46	0.00	21.25	0.00	9.58	0.00	0.00	93.27	RIM
MG4	0.00	0.89	18.17	43.22	0.00	21.42	0.00	9.42	0.00	0.00	93.12	CORE
MG4	0.00	0.80	17.75	43.07	0.00	20.97	0.00	9.51	0.00	0.00	92.10	RIM
MG4	0.00	0.78	18.24	43.40	0.00	21.45	0.00	9.39	0.00	0.00	93.26	CORE
MG4	0.00	0.86	18.18	43.09	7.36	21.25	0.00	9.42	0.00	0.00	100.16	RIM
MG4	0.00	0.84	18.00	42.95	0.00	21.29	0.00	9.34	0.00	0.00	92.42	CORE

Code	SiO_2	TiO_2	Al_2O_3	Cr_2O_3	Fe_2O_3	FeO	MnO	MgO	CaO	Na_2O	TOTAL	
MG4a	0.00	0.77	17.23	43.77	7.60	21.86	0.00	8.85	0.00	0.00	100.08	RIM
MG4a	0.00	0.88	16.97	43.72	0.00	21.55	0.00	9.05	0.00	0.00	92.17	CORE
MG4a	0.00	0.89	17.30	43.54	0.00	21.84	0.00	9.01	0.00	0.00	92.58	RIM
MG4a	0.00	0.85	17.46	43.20	0.00	21.82	0.00	8.99	0.00	0.00	92.32	CORE
MG4a	0.00	0.90	17.35	43.39	0.00	21.96	0.00	8.91	0.00	0.00	92.51	RIM
MG4a	0.00	0.82	17.32	42.60	8.24	21.54	0.00	8.97	0.00	0.00	99.49	CORE
MG4a	0.05	0.86	17.31	42.61	8.33	21.68	0.00	9.02	0.00	0.00	99.86	RIM
MG4a	0.00	0.87	17.32	41.81	8.59	21.43	0.00	8.96	0.00	0.00	98.98	CORE
MG4a	0.00	0.77	17.17	42.75	0.00	21.31	0.00	9.01	0.05	0.00	91.06	RIM
MG4a	0.00	0.81	17.18	42.95	0.00	21.52	0.00	9.02	0.00	0.00	91.48	CORE
MG4a	0.00	0.84	17.26	43.49	7.77	21.64	0.00	8.99	0.05	0.00	100.04	RIM
MG4a	0.00	0.91	16.94	43.39	7.51	21.60	0.00	8.90	0.00	0.00	99.25	CORE
MG4a	0.00	0.67	17.63	43.15	7.97	21.27	0.00	9.12	0.07	0.00	99.88	RIM
MG4a	0.00	0.70	17.25	43.50	0.00	21.49	0.00	8.97	0.00	0.00	91.91	CORE
MG4a	0.00	0.85	16.92	43.42	0.00	21.70	0.00	8.89	0.07	0.00	91.85	RIM
MG4a	0.00	0.87	16.84	42.97	0.00	21.17	0.00	8.92	0.00	0.00	90.77	CORE
MG4a	0.00	0.80	17.16	43.21	7.94	21.49	0.00	9.00	0.00	0.00	99.60	RIM
MG4a	0.00	0.82	16.98	42.94	8.05	21.32	0.00	9.00	0.00	0.00	99.11	CORE
MG4a	0.00	0.80	16.72	43.80	7.93	21.36	0.00	8.93	0.17	0.00	99.71	RIM
MG4a	0.00	0.84	17.10	43.79	0.00	21.64	0.00	9.03	0.00	0.00	92.40	CORE
MG4a	0.00	0.84	17.21	43.12	8.00	21.35	0.00	9.13	0.00	0.00	99.65	RIM
MG4a	0.00	0.86	16.98	43.33	0.00	21.50	0.00	8.93	0.00	0.00	91.60	CORE
MG4a	0.00	0.71	17.15	43.89	0.00	21.53	0.00	9.10	0.07	0.00	92.45	RIM
MG4a	0.00	0.86	17.23	43.71	0.00	21.73	0.00	9.07	0.00	0.00	92.60	CORE
MG4a	0.00	0.67	17.30	43.87	0.00	21.34	0.00	9.13	0.06	0.00	92.37	RIM
MG4a	0.00	0.58	17.84	44.13	7.56	21.41	0.00	9.24	0.00	0.00	100.76	CORE
MG4a	0.00	0.84	16.76	42.12	0.00	21.01	0.00	8.98	0.00	0.00	89.71	RIM
MG4a	0.00	0.79	16.61	42.37	8.38	21.01	0.00	8.93	0.00	0.00	98.09	CORE
MG4a	0.00	0.82	16.57	42.27	0.00	20.98	0.00	9.00	0.00	0.00	89.64	RIM
MG4a	0.00	0.82	16.70	42.57	8.31	21.08	0.00	8.99	0.00	0.00	98.47	CORE

Appendix F. Electron Microprobe Data of the LG6, MG1 - MG3 Chromitite Seams, western Bushveld.

Rustenburg section

Code	SiO_2	TiO_2	Al_2O_3	Cr_2O_3	Fe_2O_3	FeO	MnO	MgO	CaO	Na_2O	TOTAL
LG6	0.00	0.78	17.05	47.02	3.78	21.72	0.00	8.77	0.00	0.00	99.12
LG6	0.00	0.80	16.80	47.65	4.73	22.16	0.00	8.85	0.00	0.00	100.99
LG6	0.00	0.83	17.68	46.87	5.06	22.40	0.00	8.97	0.00	0.00	101.82
LG6	0.00	0.84	16.94	47.14	4.99	22.65	0.00	8.60	0.00	0.00	101.16
LG6	0.00	0.85	17.19	47.44	4.92	22.62	0.00	8.79	0.00	0.00	101.81
LG6	0.00	0.80	17.17	46.83	4.80	22.48	0.00	8.62	0.00	0.00	100.70
LG6	0.00	0.78	17.48	47.18	4.76	22.50	0.00	8.79	0.00	0.00	101.49
LG6	0.00	0.84	17.65	46.90	4.98	23.03	0.00	8.60	0.00	0.00	102.00
LG6	0.00	0.74	16.78	46.67	4.87	22.90	0.00	8.14	0.00	0.00	100.11
LG6	0.00	0.80	16.95	46.89	4.68	22.83	0.00	8.32	0.00	0.00	100.47
LG6	0.00	0.82	17.45	46.36	5.32	23.79	0.00	8.02	0.00	0.00	101.75
LG6	0.00	0.78	17.53	45.96	5.15	22.58	0.00	8.54	0.00	0.00	100.55
LG6	0.00	0.83	17.46	46.59	5.02	22.50	0.00	8.74	0.00	0.00	101.14
LG6	0.00	0.91	17.41	45.46	5.31	22.73	0.00	8.45	0.00	0.00	100.27
LG6	0.00	0.83	17.21	47.15	3.73	23.03	0.00	8.17	0.00	0.00	100.12

Rustenburg section

Code	SiO_2	TiO_2	Al_2O_3	Cr_2O_3	Fe_2O_3	FeO	MnO	MgO	CaO	Na_2O	TOTAL
MG1	0.00	1.19	18.39	45.38	3.37	23.51	0.00	8.17	0.00	0.00	100.01
MG1	0.00	1.21	18.49	46.08	3.37	22.97	0.00	8.72	0.00	0.00	100.84
MG1	0.00	1.27	18.51	46.78	2.90	23.29	0.00	8.67	0.00	0.00	101.42
MG1	0.00	1.35	17.95	44.66	3.66	22.76	0.00	8.46	0.00	0.00	98.84
MG1	0.00	1.17	18.38	46.27	2.19	23.35	0.00	8.17	0.00	0.00	99.53
MG1	0.00	1.24	18.19	45.88	3.16	23.17	0.00	8.41	0.00	0.00	100.05
MG1	0.00	1.31	18.27	46.72	2.79	23.10	0.00	8.68	0.00	0.00	100.87
MG1	0.00	1.27	18.63	44.84	3.32	22.88	0.00	8.69	0.00	0.00	99.74
MG1	0.00	1.23	18.20	45.45	3.18	22.26	0.00	8.81	0.00	0.00	99.13
MG1	0.00	1.27	19.03	42.85	4.32	22.09	0.00	8.87	0.00	0.00	98.42
MG1	0.00	1.28	17.88	46.99	2.42	22.58	0.00	8.77	0.00	0.00	99.92
MG1	0.00	1.31	18.45	46.30	2.70	22.79	0.00	8.79	0.00	0.00	100.34
MG1	0.00	1.24	18.38	46.12	3.10	22.70	0.00	8.80	0.00	0.00	100.34
MG1	0.00	1.28	18.80	46.10	3.12	23.08	0.00	8.79	0.00	0.00	101.17
MG1	0.00	1.26	18.69	46.58	3.04	23.12	0.00	8.81	0.00	0.00	101.50

Rustenburg section

Code	SiO_2	TiO_2	Al_2O_3	Cr_2O_3	Fe_2O_3	FeO	MnO	MgO	CaO	Na_2O	TOTAL
MG2	0.00	1.42	18.03	45.26	3.37	24.27	0.00	7.80	0.00	0.00	100.15
MG2	0.00	1.32	18.33	45.10	3.42	24.36	0.00	7.74	0.00	0.00	100.27
MG2	0.00	1.26	18.03	44.97	2.97	24.24	0.00	7.48	0.00	0.00	98.95
MG2	0.00	1.21	18.54	45.28	2.28	24.41	0.00	7.44	0.00	0.00	99.16
MG2	0.00	1.23	17.65	45.14	2.45	23.85	0.00	7.43	0.00	0.00	97.74
MG2	0.00	1.22	17.99	44.84	2.74	23.99	0.00	7.47	0.00	0.00	98.24
MG2	0.00	1.20	18.05	45.12	2.88	24.24	0.00	7.44	0.00	0.00	98.93
MG2	0.00	1.23	18.53	45.06	3.00	24.43	0.00	7.57	0.00	0.00	99.82
MG2	0.00	1.22	17.54	45.32	3.75	24.05	0.00	7.64	0.00	0.00	99.52
MG2	0.00	1.30	17.54	45.01	3.48	24.10	0.00	7.54	0.00	0.00	98.97
MG2	0.00	1.29	18.06	45.21	3.20	24.19	0.00	7.67	0.00	0.00	99.62
MG2	0.00	1.36	18.05	45.49	3.22	24.25	0.00	7.78	0.00	0.00	100.15
MG2	0.00	1.26	17.58	45.23	2.95	23.96	0.00	7.52	0.00	0.00	98.51
MG2	0.00	1.29	17.68	45.40	3.11	24.27	0.00	7.50	0.00	0.00	99.25
MG2	0.00	1.34	17.70	45.19	3.46	23.81	0.00	7.85	0.00	0.00	99.35

Rustenburg section

Code	SiO_2	TiO_2	Al_2O_3	Cr_2O_3	Fe_2O_3	FeO	MnO	MgO	CaO	Na_2O	TOTAL
MG3	0.00	1.46	18.17	44.60	2.77	23.33	0.00	8.10	0.00	0.00	98.43
MG3	0.00	1.33	18.91	44.97	3.18	23.72	0.00	8.24	0.00	0.00	100.35
MG3	0.00	1.15	18.95	44.63	3.58	23.45	0.00	8.24	0.00	0.00	100.00
MG3	0.00	1.02	19.52	44.79	2.99	23.46	0.00	8.22	0.00	0.00	100.00
MG3	0.00	1.07	19.35	45.29	2.56	23.17	0.00	8.39	0.00	0.00	99.84
MG3	0.00	0.94	18.82	45.70	3.21	22.98	0.00	8.39	0.00	0.00	100.09
MG3	0.00	1.05	19.21	45.84	2.52	23.10	0.00	8.49	0.00	0.00	100.21
MG3	0.00	1.14	19.33	45.80	2.41	23.42	0.00	8.41	0.00	0.00	100.51
MG3	0.00	1.08	18.86	45.51	2.84	22.54	0.00	8.69	0.00	0.00	99.52
MG3	0.00	1.10	19.39	44.96	2.51	22.86	0.00	8.51	0.00	0.00	99.33
MG3	0.00	1.04	18.99	45.84	3.01	23.00	0.00	8.57	0.00	0.00	100.45
MG3	0.00	1.10	18.95	45.97	2.74	23.08	0.00	8.54	0.00	0.00	100.38
MG3	0.00	0.92	19.79	46.06	2.46	23.30	0.00	8.52	0.00	0.00	101.05
MG3	0.00	1.00	19.46	45.71	2.45	23.02	0.00	8.53	0.00	0.00	100.16
MG3	0.00	1.04	19.95	45.06	2.89	22.71	0.00	8.88	0.00	0.00	100.53

Rustenburg/Marikana section

Code	SiO_2	TiO_2	Al_2O_3	Cr_2O_3	FeO	MnO	MgO	CaO	Na_2O	TOTAL
LG6	0.0240	0.7409	14.8042	47.6244	25.8234	0.00	9.8462	0.0197	0.00	98.8829
LG6	0.0108	0.7708	14.4707	46.8798	25.9888	0.00	9.7535	0.0095	0.00	97.8839
LG6	0.0000	0.7661	14.8599	47.6879	26.1777	0.00	10.1342	0.0208	0.00	99.6466
LG6	0.0000	0.7231	14.6047	47.0771	26.1411	0.00	9.9136	0.0000	0.00	98.4596
LG6	0.0074	0.7603	14.5714	47.0891	26.3607	0.00	9.9011	0.0332	0.00	98.7233
LG6	0.0013	0.7890	14.7439	44.7521	25.7478	0.00	9.9216	0.0146	0.00	95.9703
LG6	0.0094	0.7614	14.6502	47.1938	26.1631	0.00	9.4456	0.0006	0.00	98.2241
LG6	0.0000	0.7041	14.9158	46.8810	26.2562	0.00	9.4472	0.0118	0.00	98.2162
LG6	0.0132	0.6819	15.0190	47.7492	26.1451	0.00	10.1593	0.0051	0.00	99.7728
LG6	0.0363	0.6901	14.7166	46.3094	25.6622	0.00	9.9671	0.0000	0.00	97.3817
LG6	0.0118	0.7300	14.8992	47.0779	26.1894	0.00	10.0525	0.0000	0.00	98.9609
LG6	0.0027	0.7144	14.4813	46.7490	25.9085	0.00	9.8453	0.0000	0.00	97.7011
LG6	0.0037	0.8144	14.9085	48.0872	26.0231	0.00	9.8770	0.0000	0.00	99.7139
LG6	0.0108	0.6803	14.8497	47.1825	25.9153	0.00	10.1727	0.0000	0.00	98.8113
LG6	0.0000	0.7640	14.6878	47.3548	25.9937	0.00	9.9549	0.0113	0.00	98.7665

Marikana/Brits section

Code	SiO_2	TiO_2	Al_2O_3	Cr_2O_3	FeO	MnO	MgO	CaO	Na_2O	TOTAL
MG1	0.0095	0.7166	15.5056	45.9293	27.5260	0.00	9.7983	0.0124	0.00	99.4977
MG1	0.0078	0.7642	15.8038	46.0267	26.8455	0.00	9.8539	0.0248	0.00	99.3267
MG1	0.0204	0.7993	15.4969	45.8581	26.4910	0.00	9.7100	0.0000	0.00	98.3267
MG1	0.0252	0.7628	15.5806	45.5637	26.6986	0.00	9.9625	0.0000	0.00	98.5933
MG1	0.0051	0.8147	15.4483	46.4462	26.7085	0.00	10.0434	0.0000	0.00	99.4662
MG1	0.0061	0.7568	15.6250	45.3961	27.0105	0.0095	9.8688	0.0051	0.00	98.6778
MG1	0.0085	0.7968	15.8389	45.9331	26.6629	0.00	9.8487	0.0000	0.00	99.0888
MG1	0.0184	0.7800	15.6331	46.4576	26.7195	0.00	9.8413	0.0000	0.00	99.4499
MG1	0.0037	0.7094	15.5043	46.1671	26.7879	0.00	10.0076	0.0147	0.00	99.1947
MG1	0.0000	0.7421	14.9470	45.3694	26.7934	0.0253	9.7889	0.0000	0.00	97.6662
MG1	0.0074	0.8182	15.5771	45.7851	26.5381	0.00	9.8461	0.0000	0.00	95.5721
MG1	0.0169	0.7573	15.5366	45.7368	27.0713	0.00	9.7837	0.0118	0.00	98.9144
MG1	0.0054	0.7156	15.6085	45.5121	26.7180	0.00	9.8590	0.0011	0.00	99.4197
MG1	0.0000	0.8376	15.4835	46.0078	26.7766	0.00	9.8232	0.0085	0.00	98.9372
MG1	0.0412	0.6900	15.0336	45.7917	26.8422	0.00	9.6898	0.0051	0.00	98.0935

Marikana/Brits section

Code	SiO_2	TiO_2	Al_2O_3	Cr_2O_3	FeO	MnO	MgO	CaO	Na_2O	TOTAL
MG2	0.0000	0.8972	15.8056	43.8605	29.6191	0.0016	8.7007	0.0000	0.0000	98.8846
MG2	0.0082	0.9800	15.8256	44.0689	29.2870	0.0000	9.0253	0.0000	0.0000	99.1950
MG2	0.0318	1.0130	15.8826	43.5326	28.8166	0.0000	9.0390	0.0000	0.0000	98.3155
MG2	0.0215	0.9072	15.9234	43.7992	29.3558	0.0000	9.0917	0.0000	0.0000	99.0989
MG2	0.0000	0.9814	15.7668	43.5614	28.7873	0.0350	9.1085	0.0278	0.0000	98.2682
MG2	0.0031	0.9775	15.8901	43.5254	29.0525	0.0000	8.8640	0.0323	0.0000	98.3449
MG2	0.0055	0.9812	15.9634	43.2466	28.7674	0.0000	9.1412	0.0000	0.0000	98.1052
MG2	0.0014	0.9035	15.6992	42.8459	28.7843	0.0000	8.9985	0.0000	0.0000	97.2328
MG2	0.0113	0.8696	15.8275	44.1010	28.5256	0.0000	8.7522	0.0301	0.0000	98.1173
MG2	0.0117	0.9046	16.4757	43.7292	29.1682	0.0000	9.1273	0.0000	0.0000	99.4166
MG2	0.0109	0.8708	15.8056	43.3672	28.4568	0.0000	8.5306	0.0000	0.0000	97.0418
MG2	0.0000	0.9609	15.8755	43.4106	28.8208	0.0095	8.8164	0.0000	0.0000	97.8938
MG2	0.0181	0.9199	15.8301	44.0136	28.4963	0.0000	8.9609	0.0170	0.0000	98.2559
MG2	0.0181	0.9480	15.9338	43.6581	28.8221	0.0032	9.0339	0.0352	0.0000	98.4524
MG2	0.0000	1.0157	16.0314	43.6483	29.1063	0.0000	8.9950	0.0000	0.0000	98.7967
MG2	0.0136	1.0215	16.0583	43.8923	29.1097	0.0000	9.1275	0.0000	0.0000	99.2229
MG2	0.0000	0.9641	16.4056	43.3581	28.9113	0.0000	9.2089	0.0000	0.0000	98.8479
MG2	0.0292	0.9157	15.9313	44.0775	29.1635	0.0000	8.9623	0.0000	0.0000	99.0795

Marikana/Brits section

Code	SiO_2	TiO_2	Al_2O_3	Cr_2O_3	FeO	MnO	MgO	CaO	Na_2O	TOTAL
MG3	0.0041	0.7456	14.6450	47.5753	25.6298	0.0000	9.5372	0.0203	0.0000	98.1573
MG3	0.0000	0.7185	14.7429	47.0113	26.0666	0.0000	9.4609	0.0299	0.0000	98.0301
MG3	0.0216	0.7052	14.8036	47.5017	26.4766	0.0000	9.4633	0.0214	0.0000	98.9921
MG3	0.0138	0.7242	14.6471	46.6389	26.5653	0.0000	9.4318	0.0000	0.0000	98.0424
MG3	0.0169	0.7337	14.7299	47.4651	25.8324	0.0000	9.5628	0.0000	0.0000	98.3409
MG3	0.0179	0.7690	14.7026	47.9422	26.5016	0.0000	9.4031	0.0000	0.0000	99.3364
MG3	0.0109	0.7626	15.1791	47.5045	26.6178	0.0000	9.5751	0.0000	0.0000	99.6498
MG3	0.0348	0.6386	14.7039	47.8017	26.6098	0.0000	9.3299	0.0180	0.0000	99.1367
MG3	0.0169	0.8075	14.9771	48.0370	26.2620	0.0000	9.6908	0.0000	0.0000	99.7913
MG3	0.0115	0.7998	14.8324	47.5448	26.5543	0.0000	9.7449	0.0000	0.0000	99.4876
MG3	0.0027	0.6760	14.5785	47.4692	26.3848	0.0189	9.5625	0.0000	0.0000	98.6926
MG3	0.0074	0.6591	14.5538	46.8622	26.4096	0.0000	9.5105	0.0000	0.0000	98.0027
MG3	0.0000	0.7448	14.4372	48.0608	25.3406	0.0000	9.2373	0.0342	0.0000	97.8550
MG3	0.0111	0.7047	14.8800	47.2711	25.6471	0.0000	9.1662	0.0051	0.0000	97.6853
MG3	0.0067	0.7349	14.4524	47.3565	25.8738	0.0000	9.4713	0.0118	0.0000	97.8975

Appendix G. Standards Used for the Electron Microprobe Analysis.

Tiebaghi Mine, New Caledonia

Jarosewich, Smithsonian USNM 117075

Al_2O_3	9.92
Cr_2O_3	60.50
FeO	13.04
MnO	0.11
MgO	15.20
CaO	0.12
Total	98.89

Appendix H. Structural Logs of Trenches, Spruitfontein Upfold.

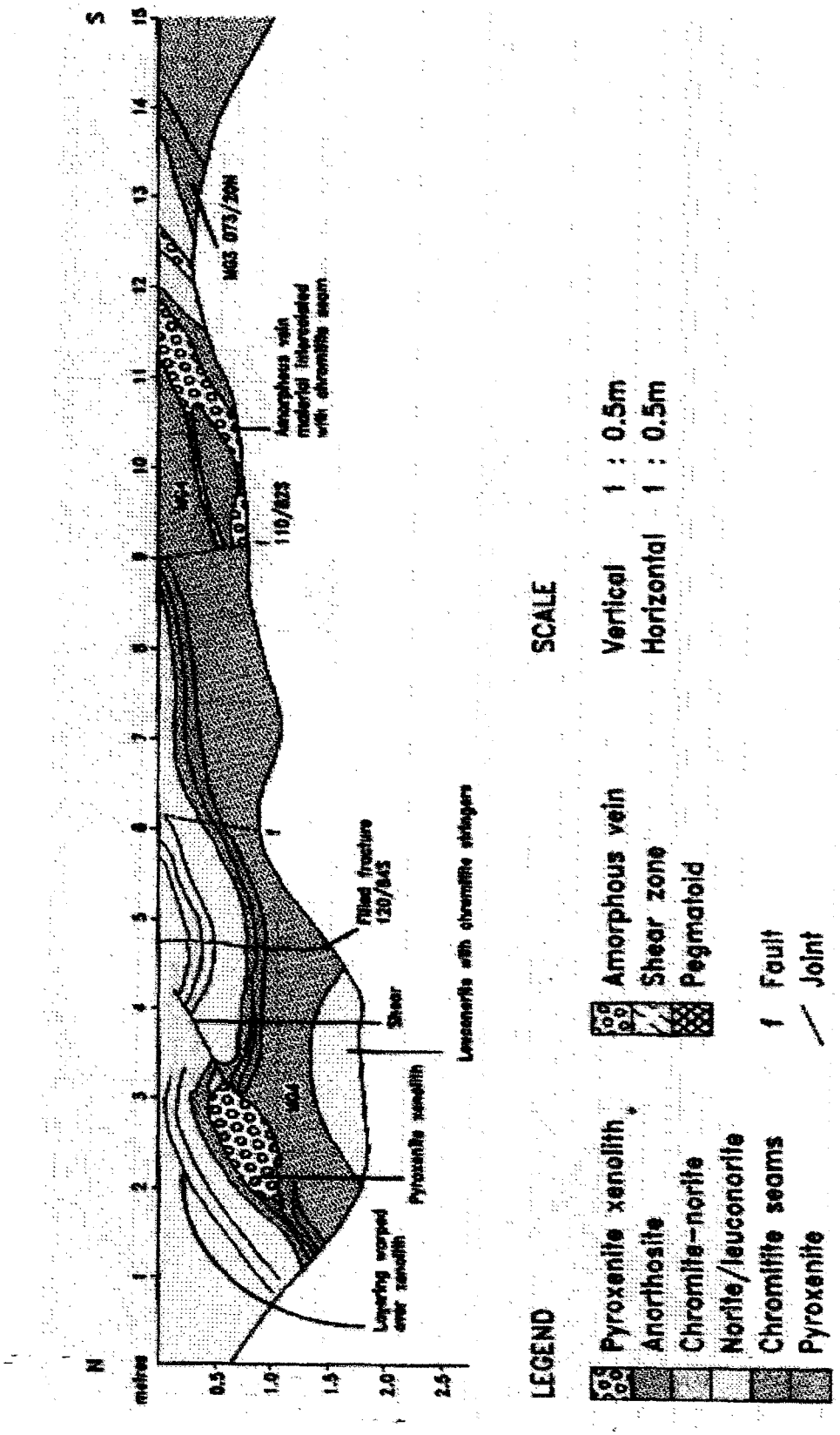

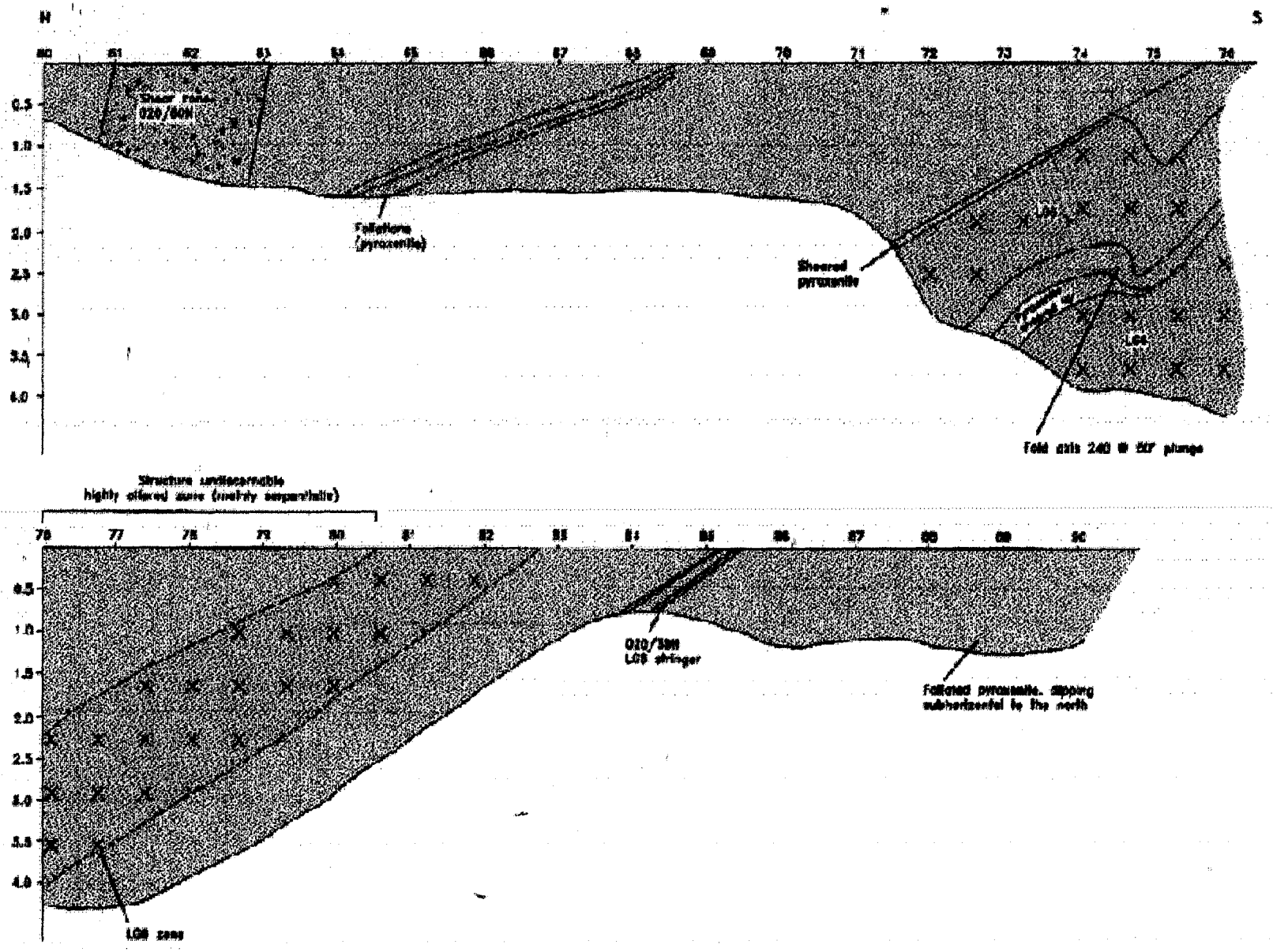
N
S
Sheared pyroxenite
Folded pyroxenite, dipping subhorizontal to the north
LGS zone

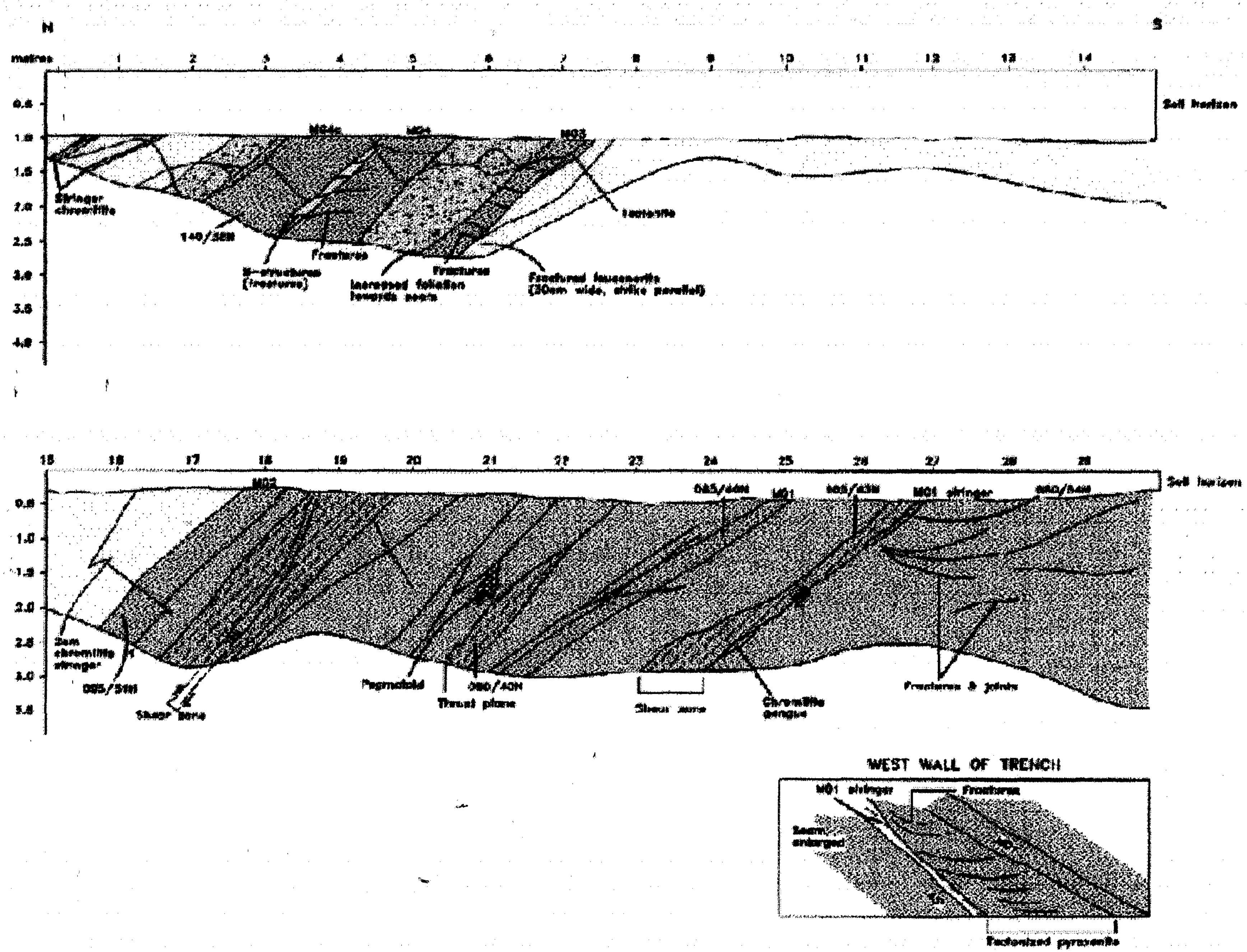
N
S
metres
Soil horizon
Stringer chromitite
140/32N
S-structures (fractures)
Fractures
Increased foliation towards seam
Fractured lauxenerite (30cm wide, strike parallel)
MO4a
MO4
MO3
Soil horizon
MO2
Seam chromitite stringer
085/31N
Shear zone
Pegmatoid
Thrust plane
080/40N
Shear zone
Chromitite gangue
Fractures & joints
085/44N
MO1
MO1 stringer
WEST WALL OF TRENCH
MO1 stringer
Fractures
Seam, enlarged
Tectonized pyroxenite

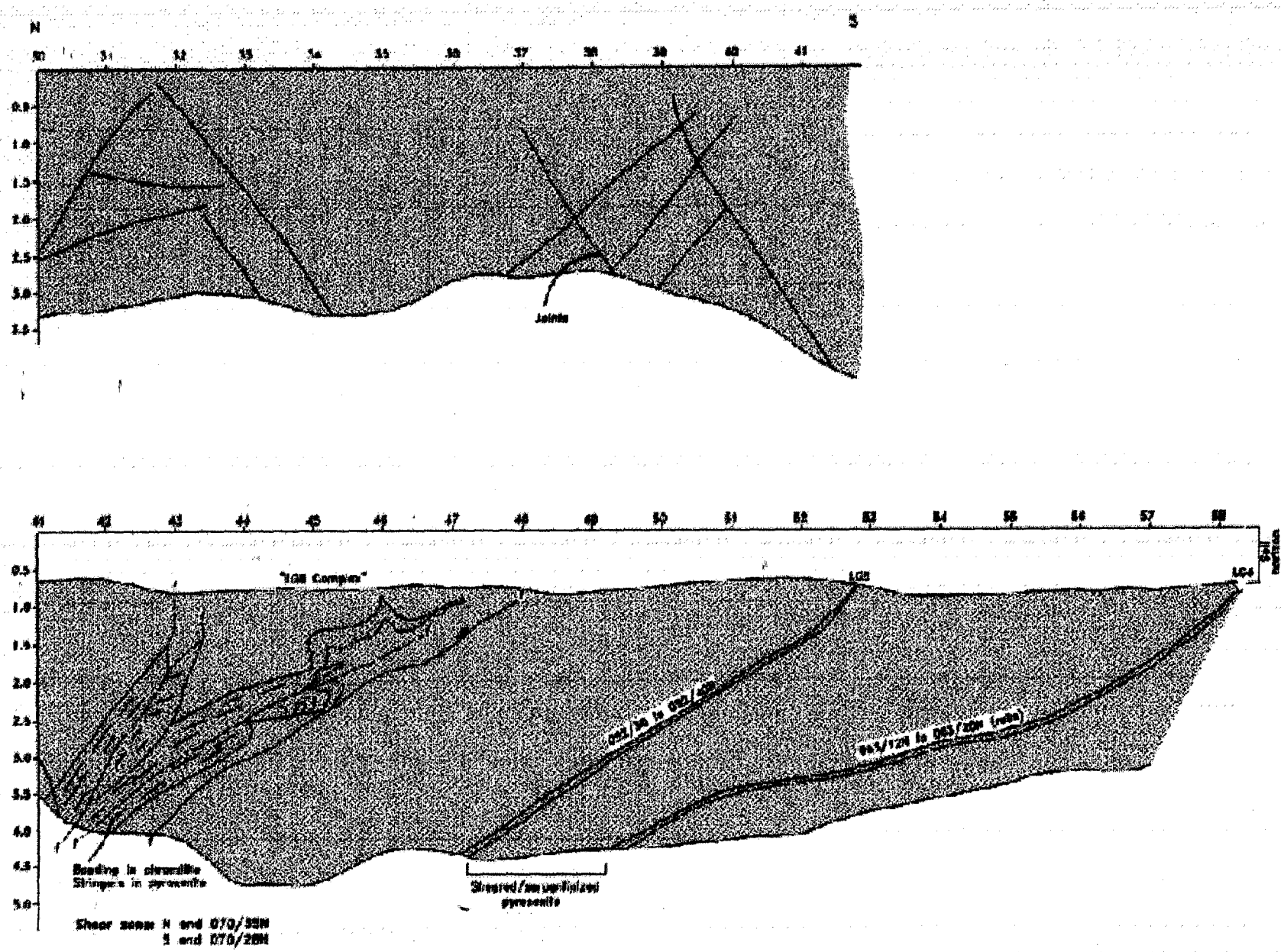
N
S
Joints
"IGR Complex"
LG5
LG4
Bedding in chromitite
Stringers in pyroxenite
Sheared/recrystallized pyroxenite
Shear zones N end 010/35N
S end 070/20N

Appendix I. A portion of the western Lobe of the Bushveld, with the location of the sampling points (from the 1:250 000 geological series, sheet 2526).

Appendix J. Standard Deviation Values for the Average Compositions of the Chromite Grains, LG1 - MG4a, Ruighoek Section.

	Cr_2O_3	Al_2O_3	FeO	TiO_2
MG4a	0.619	0.311	0.228	0.082
MG4	0.240	0.139	0.145	0.038
MG3	0.269	0.137	0.224	0.125
MG2	0.692	0.189	0.211	0.026
MG1	0.431	0.144	0.227	0.085
LG6a	0.375	0.189	0.272	0.061
LG6	0.287	0.111	0.164	0.023
LG5	0.341	0.156	0.254	0.037
LG4	0.536	0.492	0.357	0.044
LG3	0.364	0.134	0.207	0.032
LG2	0.262	0.154	0.253	0.052
LG1	0.507	0.116	0.257	0.036

Appendix K. Standard Deviation Values for the Average Compositions of the Chromite Grains, LG6 - MG3, Rustenburg and Marikana/Brits Sections.

Rustenburg	Cr_2O_3	Al_2O_3	FeO	TiO_2
MG3	0.460	0.332	0.328	0.093
MG2	0.151	0.380	0.187	0.066
MG1	0.643	0.205	0.372	0.047
LG6	0.691	0.271	0.432	0.049

Marikana/Brits	Cr_2O_3	Al_2O_3	FeO	TiO_2
MG3	0.237	0.199	0.128	0.065
MG2	0.234	0.253	0.210	0.051
MG1	0.350	0.133	0.262	0.043
LG6	0.363	0.139	0.172	0.045

Appendix. L. Stratigraphic Log of the Drill Core Sampled for Electron-Microprobe Analysis (Section 7.7.4)

BOREHOLE CC1